

F.W. Klaiber, T.J. Wipf, M.J. Nahra,  
J.S. Ingersoll, A.G. Sardo, X. Qin

# Field and Laboratory Evaluation of Precast Concrete Bridges

November 2001

Sponsored by the  
Iowa Department of Transportation  
Highway Division and  
the Iowa Highway Research Board

Iowa DOT Project TR-440



Iowa Department  
of Transportation

# ***FINAL REPORT***

IOWA STATE UNIVERSITY  
OF SCIENCE AND TECHNOLOGY

Department of Civil and Construction Engineering

The opinions, findings, and conclusions expressed in this publication are those of the authors and not necessary those of the Iowa Department of Transportation.

F.W. Klaiber, T.J. Wipf, M.J. Nahra,  
J.S. Ingersoll, A.G. Sardo, X. Qin

# Field and Laboratory Evaluation of Precast Concrete Bridges

November 2001

Sponsored by the  
Iowa Department of Transportation  
Highway Division and  
the Iowa Highway Research Board

Iowa DOT Project TR-440

---

## ***FINAL REPORT***

---

IOWA STATE UNIVERSITY  
OF SCIENCE AND TECHNOLOGY



Iowa Department  
of Transportation

Department of Civil and Construction Engineering

## ABSTRACT

Recent data compiled by the National Bridge Inventory revealed 29% of Iowa's approximate 24,600 bridges were either structurally deficient or functionally obsolete. This large number of deficient bridges and the high cost of needed repairs create unique problems for Iowa and many other states. The research objective of this project was to determine the load capacity of a particular type of deteriorating bridge – the precast concrete deck bridge – which is commonly found on Iowa's secondary roads. The number of these precast concrete structures requiring load postings and/or replacement can be significantly reduced if the deteriorated structures are found to have adequate load capacity or can be reliably evaluated.

Approximately 600 precast concrete deck bridges (PCDBs) exist in Iowa. A typical PCDB span is 19 to 36 ft long and consists of eight to ten simply supported precast panels. Bolts and either a pipe shear key or a grouted shear key are used to join adjacent panels. The panels resemble a steel channel in cross-section; the web is orientated horizontally and forms the roadway deck and the legs act as shallow beams. The primary longitudinal reinforcing steel bundled in each of the legs frequently corrodes and causes longitudinal cracks in the concrete and spalling.

The research team performed service load tests on four deteriorated PCDBs; two with shear keys in place and two without. Conventional strain gages were used to measure strains in both the steel and concrete, and transducers were used to measure vertical deflections. Based on the field results, it was determined that these bridges have sufficient lateral load distribution and adequate strength when shear keys are properly installed between adjacent panels. The measured lateral load distribution factors are larger than AASHTO values when shear keys were not installed. Since some of the reinforcement had hooks, deterioration of the reinforcement has a minimal affect on the service level performance of the bridges when there is minimal loss of cross-sectional area.

Laboratory tests were performed on the PCDB panels obtained from three bridge replacement projects. Twelve deteriorated panels were loaded to failure in a four point bending arrangement. Although the panels had significant deflections prior to failure, the experimental capacity of eleven panels exceeded the theoretical capacity. Experimental capacity of the twelfth panel, an extremely distressed panel, was only slightly below the theoretical capacity. Service tests and an ultimate strength test were performed on a laboratory bridge model consisting of four joined panels to determine the effect of various shear connection configurations. These data were used to validate a PCDB finite element model that can provide more accurate live load distribution factors for use in rating calculations. Finally, a strengthening system was developed and tested for use in situations where one or more panels of an existing PCDB need strengthening.

## TABLE OF CONTENTS

LIST OF FIGURES .....	ix
LIST OF TABLES .....	xiii
1 . INTRODUCTION .....	1
1.1 . Background.....	1
1.2 . Objective and Scope .....	2
2 . LITERATURE REVIEW .....	5
2.1 . Typical PCDB Cross-Section .....	5
2.1.1 . Type I PCDB Panels .....	5
2.1.2 . Type II PCDB Panels.....	7
2.2 . Deterioration of Reinforced Concrete.....	9
2.3 . Replacement of PCDBs .....	11
2.4 . Questionnaire Results .....	11
3 . FIELD TESTING.....	13
3.1 . General Field Testing Procedures.....	13
3.1.1 . Instrumentation .....	13
3.1.2 . Loading Procedure .....	16
3.2 . Bridge 1: Butler County Bridge.....	18
3.2.1 . Bridge Description .....	18
3.2.2 . Test Setup.....	21
3.2.3 . Test Vehicle and Load Positions.....	21
3.2.4 . Discussion of Results .....	25
3.3 . Bridge 2: Delaware County Dairy Bridge .....	30
3.3.1 . Bridge Description .....	30
3.3.2 . Test Setup.....	32
3.3.3 . Test Vehicle and Load Positions.....	34
3.3.4 . Discussion of Results .....	34
3.4 . Bridge 3: Delaware County Trout Bridge.....	38

3.4.1 . Bridge Description .....	38
3.4.2 . Test Setup.....	41
3.4.3 . Test Vehicle and Load Positions.....	43
3.4.4 . Discussion of Results .....	46
3.5 . Bridge 4: Story County Bridge .....	48
3.5.1 . Bridge Description .....	48
3.5.2 . Test Setup.....	50
3.5.3 . Test Vehicle and Load Positions.....	52
3.5.4 . Discussion of Results .....	52
3.6 . Load Rating.....	55
3.6.1 . Bridge 1 Load Rating.....	57
3.6.2 . Bridge 2 Load Rating.....	58
3.6.3 . Bridge 3 Load Rating.....	59
3.6.4 . Bridge 4 Load Rating.....	59
3.6.5 . PCDB Load Rating Recommendations .....	60
4 . LABORATORY TESTING OF INDIVIDUAL PCDB PANELS .....	63
4.1 . Individual PCDB Panel Load Testing Program.....	63
4.1.1 . Instrumentation .....	63
4.1.2 . Loading Setup .....	64
4.1.3 . Test Procedure .....	66
4.1.4 . Material Properties.....	66
4.2 . Test Results.....	67
4.2.1 . Overview.....	67
4.2.2 . Cedar County Panels.....	69
4.2.2.1 . Cedar 1 .....	69
4.2.2.2 . Discussion of Results for Cedar 1-3 and Cedar 8 Load Tests .....	74
4.2.3 . Butler County Panels .....	75
4.2.3.1 . Discussion of Results for Butler 1-4 Load Tests .....	76
4.2.4 . Black Hawk County Panels .....	79
4.2.4.1 . Discussion of Results for Black Hawk 1-4 Load Tests .....	79

5 . TESTING OF FOUR PANEL LABORATORY PCDB .....	83
5.1 . Laboratory PCDB Setup .....	83
5.1.1 . Configuration .....	83
5.1.2 . Instrumentation .....	85
5.2 . Joint Configuration Testing Program .....	85
5.2.1 . Load Setup .....	85
5.2.2 . Test Procedure .....	87
5.2.3 . Discussion of Results .....	87
5.2.3.1 . Comparison of Strain and Deflection Data .....	88
5.2.3.2 . Magnitude of load .....	91
5.2.3.3 . Joint Configuration .....	91
5.3 . Ultimate Strength Testing Program .....	93
5.3.1 . Load Setup .....	93
5.3.2 . Test Procedure .....	96
5.3.3 . Discussion of Results .....	96
6 . STRENGTHENING OF PANELS .....	101
6.1 . Strengthening System Design and Installation .....	101
6.2 . Strengthening System Testing Program .....	104
6.3 . Discussion of Results .....	106
6.3.1 . Post-Tensioning Force Distribution .....	106
6.3.2 . Service Load Testing on Strengthened Laboratory PCDB .....	107
6.3.3 . Ultimate Strength Testing of a Strengthened PCDB Panel .....	108
6.4 . Strengthening Variations .....	109
7 . STRUCTURAL MODELING AND ANALYSIS .....	113
7.1 . Modeling of Individual PCDB Panels .....	113
7.1.1 . Solid45 - Link8 model .....	113
7.1.2 . Solid73 - Pipe16 model .....	115
7.1.3 . Discussion of Results .....	117
7.1.4 . Summary of models .....	120

7.2 . Modeling of the Laboratory PCDB .....	120
7.2.1 . Modeling of Bolt Connections.....	120
7.2.1.1 . Mechanism of Load Transfer Through Bolts.....	120
7.2.1.2 . Selection of Bolt Model Element.....	121
7.2.1.3 . Node Connection Sensitivity Study.....	123
7.2.1.4 . Discussion of Results.....	123
7.2.2 . Modeling of Pipe Connections.....	125
7.2.2.1 . Mechanism of Load Transfer through Pipes.....	125
7.2.2.2 . Selection of Pipe Model Elements.....	126
7.2.3 . Modeling of PCDBs with Bolt and Pipe Connections.....	127
7.2.4 . Summary of Models.....	128
7.3 . Modeling of Field PCDBs .....	128
7.3.1 . Bridge 1: Butler County Bridge.....	128
7.3.1.1 . Model Description .....	128
7.3.1.2 . Discussion of Results.....	128
7.3.2 . Bridge 2: Delaware County Dairy Bridge .....	132
7.3.2.1 . Model Description .....	132
7.3.2.2 . Results and Discussion .....	132
7.3.3 . Conclusions.....	135
8 . SUMMARY AND CONCLUSIONS .....	137
8.1 . Summary.....	137
8.2 . Conclusions.....	138
9 . ACKNOWLEDGMENTS .....	141
10 . REFERENCES .....	143
APPENDIX A.....	145
APPENDIX B.....	149

## LIST OF FIGURES

Figure 2.1. Type I PCDB panel cross-section.....	6
Figure 2.2. Hooked ends of lower reinforcing bars. ....	7
Figure 2.3. Type II PCDB panel cross-section. ....	8
Figure 2.4. Deterioration damage common to PCDBs. ....	9
Figure 3.1. Bonded steel strain gage.....	14
Figure 3.2. Fabricated metal truss supporting multiple displacement transducers.....	15
Figure 3.3. Test vehicle tracking entirely on two panels. ....	16
Figure 3.4. Bridge 1 (looking east).....	18
Figure 3.5. Plan view of Bridge 1.....	19
Figure 3.6. Close-up of Bridge 1 corrosion damage.....	20
Figure 3.7. Location of strain gages and displacement transducers for Bridge 1.....	22
Figure 3.8. Bridge 1 test vehicle.....	23
Figure 3.9. Bridge 1 load positions.....	24
Figure 3.10. Bridge 1 deflection data.....	27
Figure 3.11. Bridge 1 steel strain data. ....	29
Figure 3.12. Bridge 2 (looking north).....	30
Figure 3.13. Plan view of Bridge 2.....	31
Figure 3.14. Location of strain gages and displacement transducers on Bridge 2.....	33
Figure 3.15. Bridge 2 test vehicle.....	35
Figure 3.16. Bridge 2 load positions.....	36
Figure 3.17. Bridge 2 service test data.....	37
Figure 3.18. Bridge 3 (looking south).....	39
Figure 3.19. Plan view of Bridge 3.....	40
Figure 3.20. Bridge 3 corrosion damage.....	41
Figure 3.21. Location of strain gages and displacement transducers on Bridge 3.....	42
Figure 3.22. Bridge 3 test vehicle.....	44
Figure 3.23. Bridge 3 load positions.....	45
Figure 3.24. Steel strain profile for load position 3-LP46.B. ....	46
Figure 3.25. Midspan deflection plot for Bridge 3. ....	47

Figure 3.26. Bridge 4 (looking east).....	48
Figure 3.27. Plan view of Bridge 4.....	49
Figure 3.28. Location of strain gages and displacement transducers on Bridge 4.....	50
Figure 3.29. Typical BDI gage installation.....	51
Figure 3.30. Bridge 4 test vehicle.....	53
Figure 3.31. Bridge 4 load positions.....	54
Figure 3.32. Midspan deflection plot for Bridge 4.....	54
Figure 3.33. Rating vehicles: axle spacing and wheel line loads.....	56
Figure 4.1. Typical midspan at instrumentation.....	64
Figure 4.2. Side view of loading setup for individual panel tests.....	65
Figure 4.3. Cross-section view of loading setup for individual panel load tests.....	65
Figure 4.4. Photograph of loading setup for individual panel load tests.....	66
Figure 4.5. Line of ruptured concrete across the deck of Cedar 1.....	70
Figure 4.6. Vertical deflection along the length of Cedar 1.....	71
Figure 4.7. Steel strains along the length of Cedar 1.....	71
Figure 4.8. Midspan moment vs. midspan deflection for Cedar 1 ultimate strength test.....	72
Figure 4.9. Midspan moment vs. midspan steel strain for Cedar 1 ultimate strength test.....	73
Figure 4.10. Midspan moment vs. midspan concrete strain for Cedar 1 ultimate strength test.....	73
Figure 4.11. Midspan moment vs. midspan deflection for Cedar 1, 2, 3 and 8 ultimate strength tests.....	74
Figure 4.12. Failed curb on Cedar 8.....	76
Figure 4.13. Deck deterioration in Butler 3.....	77
Figure 4.14. Ultimate strength tests of Butler 1-4: midspan moment vs. midspan deflection.....	77
Figure 4.15. Modified loading setup.....	80
Figure 4.16. Black Hawk 3 at imminent failure.....	81

Figure 4.17. Midspan moment vs. midspan deflection for Black Hawk 1-4 ultimate strength tests.....	82
Figure 5.1. Plan view of laboratory PCDB.....	84
Figure 5.2. Photograph of the laboratory PCDB.....	84
Figure 5.3. Laboratory PCDB instrumentation at midspan. ....	85
Figure 5.4. Load setup for joint configuration tests.....	86
Figure 5.5. Load positions used in the joint configuration tests.....	87
Figure 5.6. Laboratory PCDB response curves at 28 kip for ‘tight bolts plus shear connectors’ joint configuration.....	89
Figure 5.7. Midspan deflection curves at various load increments with load applied at LP3.....	92
Figure 5.8. LP1 midspan deflection at 28 kip for all three joint configurations.....	93
Figure 5.9. Photograph of load setup used in the ultimate strength test of the laboratory PCDB.....	94
Figure 5.10. Details of load setup for ultimate strength test of the laboratory PCDB.....	95
Figure 5.11. Crack in deck of P3 at failure.....	97
Figure 5.12. Detail of shear failure on P3 (looking east).....	97
Figure 5.13. Failed concrete above shear connector in P3 (looking east). ....	97
Figure 5.14. Load/steel strain plot for laboratory PCDB ultimate strength test. ....	98
Figure 5.15. Midspan deflections at various loads for laboratory PCDB ultimate strength test.....	99
Figure 6.1. Strut developed for strengthening retrofit. ....	103
Figure 6.2. Photograph of strut installed on midspan diaphragm.....	103
Figure 6.3. Details of tensioning system.....	105
Figure 6.4. Tensioning system during tensioning of the strand.....	105
Figure 6.5. Deflection curves for post-tensioning force distribution testing. ....	107
Figure 6.6. Midspan steel strains for LP3 at 28 kip.....	108
Figure 6.7. Midspan moment vs. midspan deflection for Cedar 1 and 4 during the ultimate strength tests. ....	110
Figure 7.1. Solid45 element.....	114

Figure 7.2. Link8 element.....	114
Figure 7.3. Finite element models.....	115
Figure 7.4. Comparison between the beam theory and Solid45 – Link8 model.....	116
Figure 7.5. Pipe16 element [12].....	116
Figure 7.6. Comparison of results for Cedar 1.....	117
Figure 7.7. Comparisons of results for Butler 1.....	118
Figure 7.8. Mechanism of load transfer through bolts.....	120
Figure 7.9. Details of the Solid45 - Link8 and Solid73 - Pipe16 laboratory PCDB models.....	121
Figure 7.10. Comparison of the Solid45 – Link8 and Solid73 – Pipe16 models for LP2.....	122
Figure 7.11. Models of bolt connections.....	124
Figure 7.12. Comparison of node connections scenarios of bolt model for LP2.....	124
Figure 7.13. Effect of reinforcement and model on deflection.....	126
Figure 7.14. Mechanism of load transfer through pipe.....	126
Figure 7.15. Effect of translational stiffness of Combin7 element on deflection for LP2.....	127
Figure 7.16. Cross-section of the Solid73 – Pipe16 – Combin7 model.....	127
Figure 7.17. Comparison of deflection profiles for Bridge 1.....	129
Figure 7.18. Comparison of primary reinforcement strain profiles for Bridge 1.....	131
Figure 7.19. Comparison of deflection profiles for Bridge 2.....	133
Figure 7.20. Comparison of primary reinforcement strain profiles for Bridge 2.....	134

### LIST OF TABLES

Table 2.1. Type I primary reinforcement (H15 Loading).....	7
Table 2.2. Type II primary reinforcement. ....	8
Table 3.1. Bridge 1 maximum load fractions. ....	26
Table 3.2. Bridge 2 maximum load fractions. ....	36
Table 3.3. Bridge 3 maximum load fractions. ....	47
Table 3.4. Bridge 4 maximum load fractions. ....	55
Table 3.5. Bridge 1 rating factors. ....	57
Table 3.6. Bridge 2 rating factors. ....	58
Table 3.7. Bridge 3 rating factors. ....	59
Table 3.8. Bridge 4 rating factors. ....	60
Table 4.1. Ultimate strengths and stiffnesses for Cedar 1, 2, 3 and 8.....	75
Table 4.2. Ultimate strengths and stiffnesses of Butler 1-4.....	78
Table 4.3. Ultimate strengths and stiffnesses for Black Hawk 1-4.....	82
Table 5.1. Load fractions based on deflection, steel strain, and concrete strain data. ....	88
Table 5.2. Load fractions at various loads for LP3.....	91
Table 5.3. Load fractions at 28 kip for all load positions and joint configurations. ....	94
Table 6.1. Post-tensioning force distribution load fractions.....	106
Table 6.2. Maximum load fractions before and after strengthening.....	108
Table 6.3. Comparison of steel and concrete strains due to dead load and the strengthening system.....	109
Table 7.1. Element types and properties used in the analytical models. ....	122

# 1. INTRODUCTION

## 1.1. Background

Recent data compiled by the National Bridge Inventory revealed 29% of Iowa's approximate 24,600 bridges were either structurally deficient or functionally obsolete (1). A structurally deficient bridge contains deteriorated or damaged structural components and thus cannot carry legal vehicles. A functionally obsolete bridge contains older design features that render it incompatible with today's traffic volumes, vehicle sizes and weights. While not necessarily unsafe, the restriction placed upon these bridges still inconveniences the traveling public. Motorists can experience delays due to a volume-restricted bridge and trucks may need to use longer haul routes to avoid a posted bridge.

The public agencies responsible for Iowa's bridges, namely the Iowa Department of Transportation (Iowa DOT), county secondary road departments, and municipalities, have several options for rectifying a deficient bridge. First, the deficient bridge may be replaced with a new bridge. While quite effective, the high cost and lengthy road closure period deem this solution inappropriate in some instances. Another option is to repair or retrofit the deficient bridge. The cost of this alternative, while less than the replacement cost, varies greatly with the amount of repair work required and could approach the replacement cost in extreme cases. The effectiveness of a repair can also vary from one that adds only a few years of serviceability to one that increases the life of the bridge essentially indefinitely.

This research focused on an approach for rectifying a deficient bridge. A service load test can be performed on a deficient bridge and the results used to accurately evaluate the bridge's load capacity. Bridge rating engineers typically apply the American Association of State Highway and Transportation Officials (AASHTO) code provisions to simplified models for rating a given bridge. The conservative assumptions made during this process inherently lead to a bridge evaluation that frequently underestimates the actual bridge capacity. A service load test provides accurate values for many of the assumed properties, and the subsequent evaluation of the bridge better represents the actual capacity of the bridge.

One particular type of bridge commonly found deficient on Iowa's secondary road system is the precast concrete deck bridge (PCDB). The superstructure of a PCDB is

composed of multiple precast reinforced concrete panels connected longitudinally with shear connectors and bolts. The panels frequently exhibit signs of deterioration due to corrosion of the main reinforcing steel in each stem of the channel-shaped panels. Concern over the structural adequacy of the deteriorated bridges has prompted many county engineers to place load restrictions on these bridges. Frequently the load restrictions are set somewhat arbitrarily due to a lack of information on the actual capacity of the deteriorated elements in the PCDB.

## **1.2. Objective and Scope**

The primary objective of this investigation was to evaluate the adequacy of PCDBs. Components of this investigation include a literature review, a PCDB related questionnaire, field service tests of four existing PCDBs, and laboratory tests on deteriorated PCDB panels and a four panel PCDB.

The literature review was conducted to gather information on the PCDB. Topics of interest were the Iowa PCDB specifications, research performed on similar types of bridges, and effects of corrosion on reinforced concrete. The literature review is presented in Chapter 2.

A questionnaire was sent to each Iowa county engineer to determine the number and condition of the PCDBs in their county. Counties were also asked about their willingness to have the research team perform service load tests on one of their PCDBs and if any of their PCDBs were scheduled for replacement within the coming year. A synopsis of the questionnaire responses is also presented in Chapter 2.

Service load tests were performed on four PCDBs to determine their response to a loaded vehicle. During these tests, strains and deflections were measured and recorded at various critical locations. Results of the field load test, such as lateral load distribution, helped validate a PCDB analytical model. Presented in Chapter 3 is a description of each service load test and an analysis of the test data.

Laboratory tests were carried out on sixteen PCDB panels exhibiting varying levels of deterioration. Service and ultimate strength tests were performed on individual panels and on a laboratory bridge consisting of four joined panels. The flexural capacity of deteriorated panels and the failure mode of an overloaded bridge were two of the very useful pieces of

information gained from the laboratory testing. The laboratory test procedures and results are presented in Chapters 4 and 5.

In addition to testing the bridges and individual panels in their existing condition, an investigation was made into a possible method for increasing the strength of the deteriorated bridges. The research team devised a post-tensioning system and fitted the system to each of the four panels in the laboratory bridge. Service load tests were then performed on the retrofitted laboratory bridge. An individual post-tensioned panel was also tested for ultimate strength. Details of the strengthening retrofit and test results are given in Chapter 6.

Data from both the field and laboratory tests were used to develop and validate an analytical model of the PCDB. One benefit of this model is its ability to accurately model the lateral distribution of load for a particular PCDB. With the analytical results, theoretical load fractions can be calculated and used for rating purposes in place of the AASHTO values. The development of the model as well as a comparison of the analytical results with test data are presented in Chapter 7.



## 2. LITERATURE REVIEW

A thorough search for literature documenting past research on deteriorated multibeam bridges composed of reinforced concrete channel panels (PCDBs) resulted in very little useful information. Research involving bridges of this type focused mostly on the transverse distribution of load and the effectiveness of the shear connectors. No information on the adequacy of deteriorated PCDBs was found. This lack of past research can possibly be due to the fact that these bridges make up only a small percent of the total number of bridges in the United States. Reinforced concrete is an extremely common structural material; this plus the fact that bridges on low volume roads are usually short span has resulted in minimal research.

Therefore, the intent of this chapter is mainly to present background information on the PCDBs in Iowa. Two types of PCDB panels exist in Iowa and each is thoroughly described within this chapter. Included in these descriptions are cross-sectional details useful for analysis of these panels. A general discussion on reinforced concrete deterioration is also included in this chapter to help the reader better understand the factors involved in the deterioration of these panels. Concluding the chapter is a summary of the responses to a questionnaire sent to all Iowa county engineers.

### 2.1. Typical PCDB Cross-Section

Two separate yet geometrically similar PCDB panel designs were investigated in this study. The primary difference between the two designs was the details of the shear key connection.

#### 2.1.1. *Type I PCDB Panels*

Type I PCDB panels conform to the Iowa State Highway Commission's J-10 Standard Design for Precast Concrete Bridges (2). The panels were designed to withstand H15 loading as specified by the 1953 American Association of State Highway Officials (AASHTO) Specification. The standard design included three out-to-out panel lengths: 19 ft, 25 ft, and 31 ft. The size and number of reinforcing bars and the number and locations of midspan diaphragms varied with the span length while the overall cross-sectional dimensions remained constant.

Details of the typical Type I PCDB panel are shown in Figure 2.1. The panels were 39 in. wide with a 5 in. thick deck. Each stem of the panel extended down 14 in. below the top surface of the deck. Four or five reinforcing bars (the primary reinforcing steel) were bundled and placed near the bottom of each stem. At the panel ends, the lower two reinforcing bars terminated in large hooks similar to the ones shown in Figure 2.2. The other primary reinforcing bars terminated at various cut-off points within the span. The size and number of the primary reinforcing bars is tabulated for each panel length in Table 2.1. For use in flexural capacity calculations, the total area of primary reinforcement ( $A_s$ ) per panel and distance from the extreme compression fiber to the centroid of the primary reinforcement ( $d$ ) are also presented in this table. Shear reinforcement consisted of #3 stirrups in each stem. Spacing of the stirrups range from 3 in. near the panel ends to 8 in. at midspan.

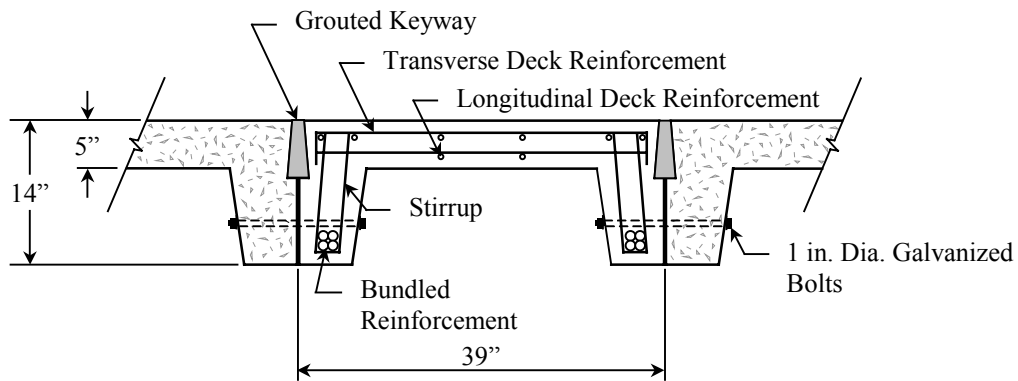


Figure 2.1. Type I PCDB panel cross-section.

The longitudinal connection between panels consisted of 1 in. diameter galvanized bolts for holding adjacent panels together and a tapered grouted shear key. The shear key distributed load transversely to the adjacent panels. Each shear key was 6 in. deep and 1 in. wide at the top and 2 in. wide at the bottom. Grout specifications called for a portland cement mortar consisting of 1 part portland cement and 2½ parts sand.

Each end of a Type I PCDB panel was anchored to either an abutment or pier. A 1 in. diameter dowel bar extended up from the abutment into a 6 in. diameter vertical hole at the end of each panel. Following erection of the bridge panels, each hole was filled with concrete.

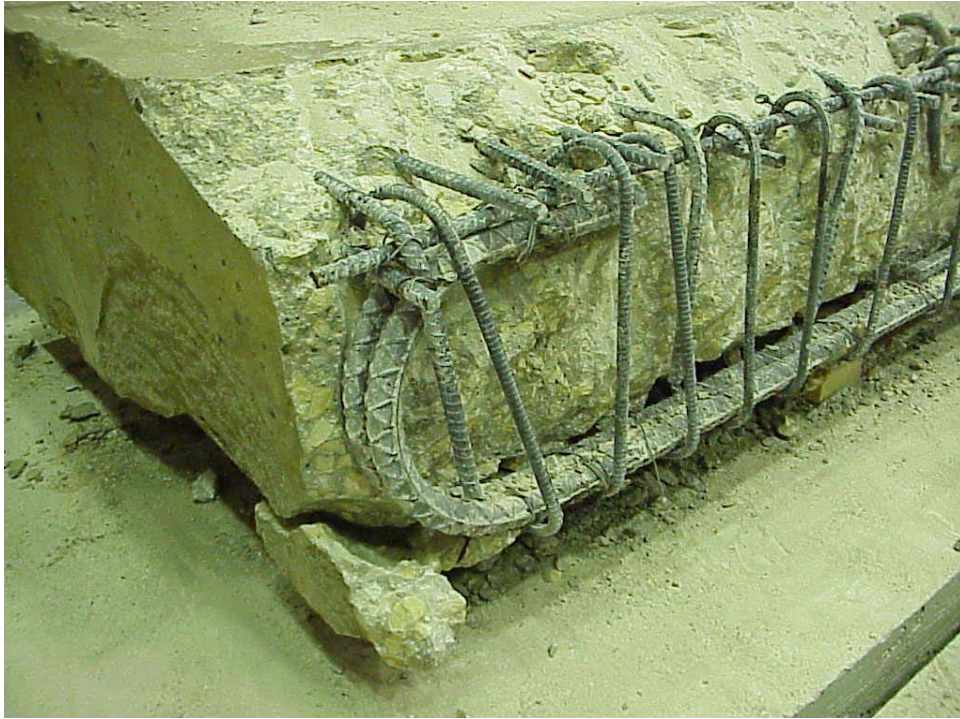


Figure 2.2. Hooked ends of lower reinforcing bars.

Table 2.1. Type I primary reinforcement (H15 Loading).

Variable	Out-to-Out Length (ft)		
	19	25	31
Primary reinforcement per panel	8-#6	4-#7 4-#8	2-#6 8-#9
$A_s$ (in <sup>2</sup> )	3.52	5.56	7.20
d (in.)	12.00	11.85	11.58

### 2.1.2. Type II PCDB Panels

In 1954, Iowa Concrete Products Company (ICPC) submitted a revised PCDB panel design to the Iowa State Highway Commission (3). The new panels, hereafter referred to as Type II panels, were geometrically and dimensionally similar to the Type I panels but utilized a new shear key design. The revised PCDB panel design included details for panels design for both the AASHO H15 loading and the heavier AASHO H20 loading. Also, a 36 ft long panel capable of withstanding AASHO H15 loading was added.

The revised shear key design consisted of a longitudinal half-circle groove cast into each side of a panel that mated with a 2 in. inside diameter galvanized pipe filled with concrete. The pipe between adjacent Type II panels restrained differential vertical movement between the panels. To facilitate installation, the pipe was installed in several short sections with foot long gaps between the ends. Again, as with the Type I panels, 7/8 in. diameter galvanized bolts held adjacent panels together. Details of the Type II panels are presented in Figure 2.3; the size and number of primary reinforcement bars, area of primary reinforcement per panel, and distance,  $d$ , are presented in Table 2.2 for each loading and panel length. The lower reinforcing bars were again terminated in the panel ends with large hooks and the upper bars terminated at specified cut-off points within the span. Also, shear reinforcement in both panel designs was essentially identical.

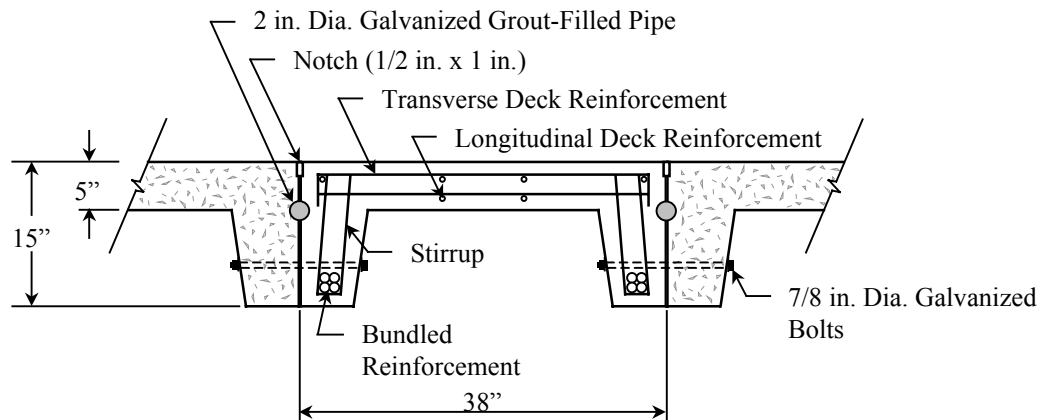


Figure 2.3. Type II PCDB panel cross-section.

Table 2.2. Type II primary reinforcement.

Variable	Loading						
	H-15				H-20		
	Out-to-Out Length (ft)				Out-to-Out Length (ft)		
	19	25	31	36	19	25	31
Primary reinforcement per panel	6-#6 2-#7	4-#7 4-#8	2-#8 6-#9	6-#11	4-#6 4-#7	2-#7 6-#8	8-#9
$A_s$ (in <sup>2</sup> )	3.84	5.56	7.58	9.36	4.16	5.94	8.00
$d$ (in.)	12.82	12.72	12.54	12.45	12.84	12.67	12.50

Another detail unique to the Type II PCDB panels was a notch (1/4 in. wide x 1 in. deep) cast into both top corners on each panel. These notches formed a groove (1/2 in. wide x 1 in. deep) between adjacent panels that was filled with a crack sealing compound. This prevented water from entering the joint between adjacent panels. Also, unlike the Type I panels, the Type II panels were not connected to the abutments or piers. The panels simply rested directly on these elements.

## 2.2. Deterioration of Reinforced Concrete

Many PCDBs throughout Iowa were found to be in a deteriorated state. Common damage included corrosion of the primary reinforcing steel and spalled concrete cover. In areas of intact concrete cover, a longitudinal crack running parallel to the primary reinforcement was often observed. The extent of the deterioration varied from bridge to bridge. Some PCDBs were found in excellent condition while others were severely deteriorated. Bridges with over half of the primary reinforcement exposed or with longitudinal cracks in most of the stems were considered severely damaged. An example of such deterioration is shown in Figure 2.4.



Figure 2.4. Deterioration damage common to PCDBs.

In sound concrete, the alkalinity of the concrete covering the reinforcement prevents the reinforcement from corroding (4). This protection is permanently reduced when chlorides or acid gases penetrate the concrete. In Iowa, common sources of these pollutants are deicing chemicals used to thaw ice and snow and carbon dioxide in the air. Exposure to these pollutants will vary with the location of the bridge. Bridges on paved roads are most severely exposed since deicing chemicals are applied directly to them in the wintertime. Bridges on unpaved roads usually are not treated with deicing chemicals, however there is some exposure from vehicles that previously traveled on treated roads. The length of time from when the concrete is exposed to these pollutants to when the reinforcement begins to corrode varies with the thickness of the concrete cover and the permeability of the concrete.

Inadequate cover was a factor that led to the deterioration of the PCDB panels. Current recommendations for the thickness of concrete cover are greater than those required at the time these panels were produced. Concrete cover thickness as specified by the J-10 Standard was 1 in.; the current AASHTO Standard Specification recommends 2.5 in. for elements exposed to deicing chemicals. One inch of concrete cover was simply not enough to protect the reinforcement from corrosive deicing chemicals. Furthermore, for some panels, improper placement of the stirrups in the stems during construction resulted in essentially no concrete cover over the stirrups.

Harmful levels of chlorides can also be introduced into the concrete during its production. During the 1960s and early 1970s, a construction boom occurred and high demand forced increased production from the precast concrete companies (4). Admixtures containing calcium chloride were frequently used to shorten curing time. Mixing water and aggregate are also possible sources of chlorides.

Once the alkalinity of the concrete is sufficiently reduced, the reinforcement will begin to corrode. Outward signs of corroding reinforcement include rust stains on the surface of the member and cracks running parallel to the reinforcement. Iron oxide, or rust, occupies many times the volume of the original steel. This expansion results in tensile stresses in the concrete covering the reinforcement, which leads to cracks in the concrete cover. A relatively small amount of corrosion will cause a crack to form and the crack width

will increase as the underlying reinforcement continues to corrode. Eventually, the concrete cover will spall and the reinforcement will be directly exposed to the environment.

Corrosion of reinforcement can jeopardize the load carrying capacity of a reinforced concrete member in two ways. First, corrosion will reduce the cross sectional area of reinforcement which in turn reduces the load carrying capacity of the steel. Second, the bond between the reinforcement and concrete is weakened. Reduction in bond limits the amount of force that can be transferred between the concrete and steel and prevents the full capacity of the reinforcement from being developed. A deteriorating, load carrying reinforced concrete member will eventually fail. Fortunately though, the corrosion process is quite slow and the process produces several visible signs of distress, such as staining, cracking and spalling.

### **2.3. Replacement of PCDBs**

Currently, PCDB channel shaped panels are no longer manufactured for use in Iowa. A similar product, the quad tee, is currently used in situations where PCDBs were previously utilized. Quad tees have approximately the same overall dimensions as the PCDB panels but have four stems instead of two. The prestressed panels are designed for HS20 loading and can span up to 50 ft (5). Intermittent welded shear connectors and a continuous grouted shear key connect the adjacent panels. It is assumed that improved design (i.e. elimination of bundled reinforcement), detailing and construction practices have corrected the problems that led to the deterioration of the channel shaped PCDBs.

### **2.4. Questionnaire Results**

During the preliminary stages of this investigation, the research team found that bridge inspectors were using a variety of codes for the PCDB. Several consultants who frequently inspect and rate secondary road bridges stated that at least ten codes were used. The Iowa DOT inventory showed 5,985 bridges were listed for these ten codes. Obviously, this count does not give an accurate estimate of the number of PCDBs in Iowa since several other types of bridges are undoubtedly included. Therefore, the research team sent a questionnaire to all Iowa county engineers asking about the PCDBs in their county. If the county engineer did have such bridges in their county, they were also asked to provide information on the condition, method of rating, if any were scheduled for replacement, and

their willingness to allow the research team to perform either field or laboratory tests on their PCDBs. The questionnaire is presented in Appendix A.

The questionnaire received a good response with 77 of Iowa's 99 counties returning a completed questionnaire (i.e. 78% response). The results revealed that 58 of the 77 responding counties have at least one PCDB and the total number of PCDBs in the reporting counties was 598. Of these bridges, 28% were posted and 14 counties were planning to replace a PCDB in the next two years. Comments on deterioration noted longitudinal cracks in the stems, spalling of the primary reinforcing steel cover, and severe corrosion of the exposed reinforcement. This damage is consistent with the findings of the research team. Other types of deterioration not associated with the superstructure, such as piling and pier cap damage, were also occasionally noted.

Sixteen counties indicated willingness to allow the research team to load test a PCDB scheduled for replacement. Three deteriorated bridges were selected for testing from these counties based on extent of damage and location. A fourth bridge, which was not scheduled for replacement and was in relatively good condition, was also load tested for comparison. This bridge was selected from the 30 counties who indicated a willingness to allow testing of a bridge not scheduled for replacement.

### 3. FIELD TESTING

Service load field tests were performed on four PCDBs. Test results were used to determine the condition and transverse load distribution in each bridge and to validate an analytical model. In this chapter, general test procedures are presented first followed by a summary of each field test. General test procedures were essentially the same for all bridges and include the instrumentation, loading methods, and test execution. A bridge description, instrumentation and load position diagrams, and a discussion of the test results are included in each field test summary. Load ratings of the four PCDBs tested are also given at the end of this chapter.

#### 3.1. General Field Testing Procedures

##### 3.1.1. Instrumentation

Electrical resistance strain gages (henceforth referred to as strain gages) were used to measure strains in both the reinforcing steel and concrete. Reinforcing steel strain gages were general purpose (1/2 in. gage length, 120 ohm) strain gages manufactured by Measurements Group, Inc., Micro-Measurements Division, Raleigh, North Carolina. Concrete strain gages were specialty (2.4 in. gage length, 120 ohm) strain gages manufactured by Precision Measurement Co., Ann Arbor, Michigan. The longer gage length was as per the manufacturer's recommendation for measurement of the concrete strains and was based on the aggregate diameter.

Prior to bonding the strain gages, both the concrete and reinforcing steel surfaces required special preparation. For the concrete strain gages, the concrete surface was first ground smooth. A two-part epoxy compound was then applied and allowed to properly cure. Use of the epoxy 'patch' ensured all voids in the concrete surface were filled. Subsequent light sanding of the patch resulted in a smooth, uniform surface to which the strain gage could adequately bond.

The first step in instrumenting the reinforcing steel involved removing the concrete cover with an electric chipping hammer. A grinding disk was then used to grid a flat area approximately 1 in. long and 1/2 in. wide on each reinforcing bar. Lastly, gouges left by the grinding wheel in the flattened area were removed with a small belt sander. This preparation

resulted in a flat, polished surface ideal for strain gage installation. Both the concrete and steel strain gages were bonded using the recommended adhesives. An example of a bonded steel strain gage is shown in Figure 3.1.



Figure 3.1. Bonded steel strain gage.

A butyl rubber patch was applied over all the bonded strain gages to prevent contamination from moisture and/or dirt. Foil tape applied over the butyl rubber patch provided physical protection. Also, to protect the concrete strain gages and wires mounted on the bridge deck from vehicle contact, plywood ‘shells’ were constructed and held in place over the strain gages with concrete anchor screws.

Celesco PT-101 potentiometers (displacement transducers) were used to measure deflections. Cables extending from the displacement transducers were connected to the ‘anchor points’ that were attached to the PCDB with epoxy. Each anchor point consisted of a small wooden block and an eyelet. Care was taken to ensure that each cable was ‘plumb’.

In the first two field tests, each displacement transducer was supported approximately 4 ft above the ground on a surveyor’s tripod. A large number of tripods were needed for each test due to the need to measure displacements at many points. Installation of this many tripods was cumbersome and time consuming. In the remaining two field tests, setup time

was reduced by the use of metal truss sections and 'T' posts. Each truss was 8 ft long, approximately 8 in. deep, and was fabricated from two 1 in. square tubes and 1/4 in. diameter bar stock. A 'T' post was used to support each end of the truss. Less time was needed to setup the displacement transducers since many displacement transducers could be mounted on a single truss as shown in Figure 3.2.



Figure 3.2. Fabricated metal truss supporting multiple displacement transducers.

Tape switches that were activated whenever a tire contacted them were used to accurately record the longitudinal position of the test vehicle. The speed and longitudinal position of the test vehicle was calculated using the recordings from two switches spaced a known distance apart.

All strain gages, deflection transducers, and tape switches were connected to a Megadac 3415AC computer controlled data acquisition system (DAS). The data collection frequency was 20 Hz for the slow rolling static tests.

### 3.1.2. Loading Procedure

The county engineer in whose county the PCDB was being tested provided the test vehicle. Tandem axle dump trucks were used in three of the field load tests and a truck tractor-semitrailer combination was used in the fourth test. Each vehicle was loaded to the Iowa legal load for that particular vehicle. The exact axle weights and truck geometry of each test vehicle are presented in the subsequent sections.

For all four test vehicles, the distance between the center of each wheel line was approximately the same as the width of two PCDB panels. Also, the width of each wheel line was less than the width of a single PCDB panel. Due to this geometry, two unique methods of transversely positioning the truck were possible. First, the test vehicle could be positioned so that each wheel line of the test vehicle would track entirely on a single panel, as shown in Figure 3.3. For this transverse position, care was taken to ensure that the centerline of each wheel line was as close to the centerline of each panel as possible. Secondly, the test vehicle could be positioned so that each wheel line tracked directly over the joints between adjacent panels.



Figure 3.3. Test vehicle tracking entirely on two panels.



place of the transverse position numbers signify that the longitudinal position is fixed and the transverse position is variable.

Longitudinal position is denoted with three letters: A, B, or C. Letters 'A' and 'C' signify that the reference point of the test vehicle was located at the near or far quarter point, respectively. The letter 'B' signifies that the test vehicle reference point was located at the center of the bridge. The test vehicle reference point is shown in the test vehicle diagrams presented in subsequent sections. A single 'x' in place of the longitudinal position letter signifies that the transverse position is fixed and the longitudinal position is variable.

### **3.2. Bridge 1: Butler County Bridge**

#### ***3.2.1. Bridge Description***

Bridge 1 was a single span PCDB located in north central Jefferson Township of Butler County, Iowa. The bridge was initially constructed in 1952 and widened to its final width in 1972. As shown in Figure 3.4, Bridge 1 carried secondary county road T-47 across a small stream. The two-lane paved highway was a farm-to-market route and served an average of 660 vehicles daily. Although the percentage of trucks using the highway was unavailable, the truck traffic was assumed significant due to a nearby gravel quarry. The highway was initially paved the same year the bridge was widened.



Figure 3.4. Bridge 1 (looking east).

At the time of the service load test, Bridge 1 consisted of ten Type II (H20) PCDB panels. The overall length of each panel was 31 ft - 0 in. and the total width of the bridge from inside of the curb to the inside of curb was 30 ft - 4 in., as shown in Figure 3.5. Galvanized bolts secured the panels longitudinally and galvanized concrete-filled pipe was properly installed in each longitudinal joint. The panels rested on the reinforced cast-in-place concrete abutments supported by timber piling. Each abutment was 2 ft wide and crowned to provide proper roadway drainage.

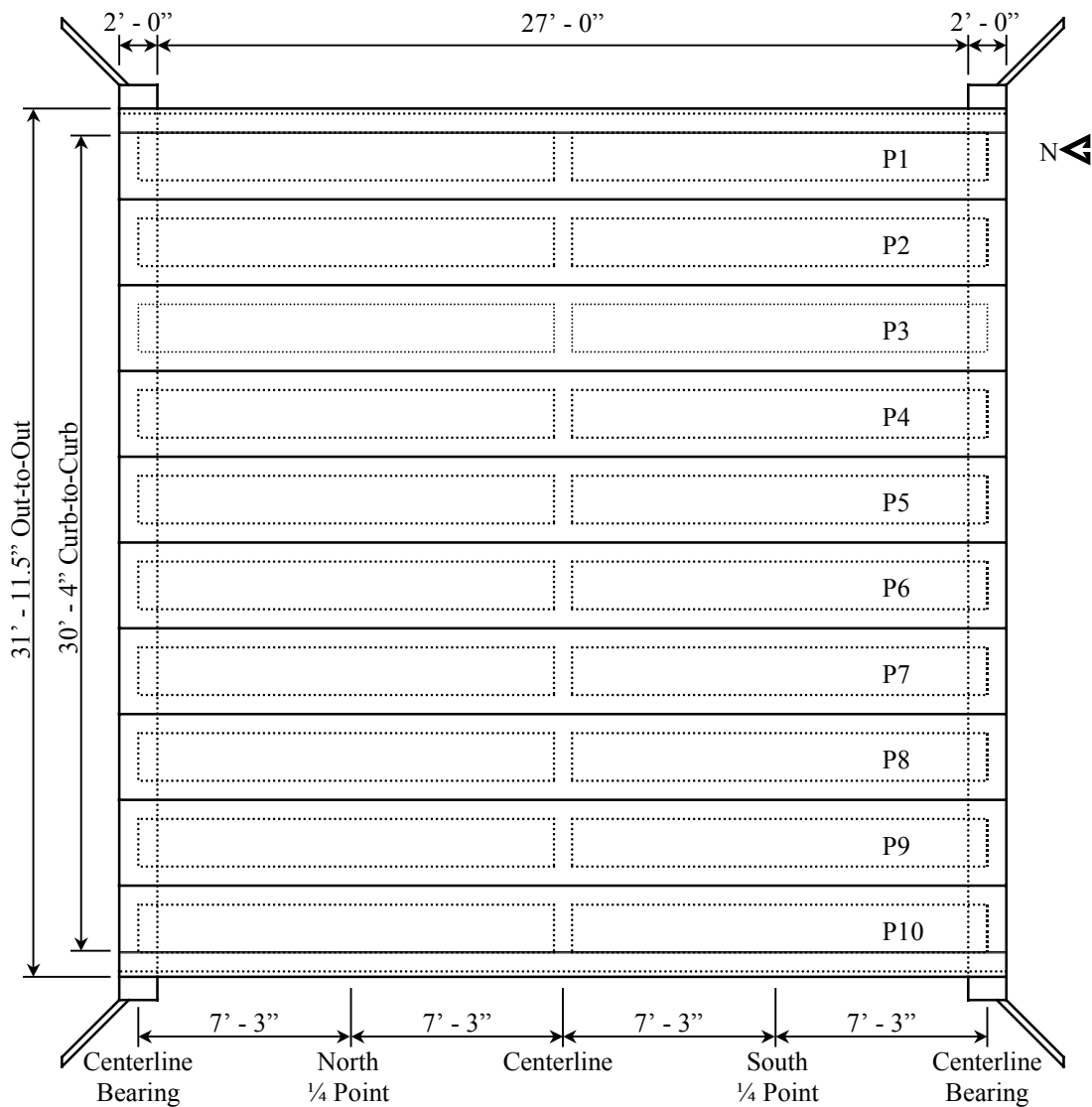


Figure 3.5. Plan view of Bridge 1.

The railing along each side of Bridge 1 consisted of a single 6 in. square steel tube supported by steel posts. Each post was rigidly bolted to the exterior PCDB panel and welded to the steel tube. Exterior panels 1 and 10 (P1 and P10) included a monolithically cast concrete curb approximately 11 in. deep and 10 in. wide.

The PCDB panels in Bridge 1 had significant deterioration. All panels had longitudinal cracks along the bottom face of the stems and the bundled longitudinal reinforcement was exposed on significant portions of eight of the ten PCDB panels, as shown in Figure 3.6. Bridge 1 also exhibited another form of deterioration less common to PCDBs. The deck surface of two panels had delaminated and spalled; efflorescence was visible on the underside of these panels. The delamination was likely caused by corrosion of the deck reinforcement. An asphalt cement concrete (ACC) patch had been used to replace the missing concrete.



Figure 3.6. Close-up of Bridge 1 corrosion damage.

Bridge 1 was most recently inspected in 1999. The engineer conducting the inspection did not perform a load rating analysis but did recommend the bridge be load posted. The engineer also advised the county to closely monitor the panels and to schedule

the bridge for replacement. In accordance with the inspecting engineer's advise, Bridge 1 was removed and replaced with a reinforced concrete box culvert in July 2000, shortly after the service load test. The research team obtained four PCDB panels from Bridge 1 and transported them to the Town Engineering Structures Laboratory for further testing (see Section 4.2.3).

### **3.2.2. Test Setup**

Bridge 1 was instrumented with strain gages and deflection transducers to monitor response to the loaded test vehicle. The longitudinal position of the test vehicle was recorded with tape switches. The midspan location of Bridge 1, as shown in Figure 3.7, was instrumented to measure the maximum strains and deflections that will occur near this location as the test vehicle travels across the bridge. Steel strain gages were bonded to the bundled reinforcing bars at midspan of the five eastern panels (P1-P5). One gage was attached to the underside of one reinforcing bar in each stem of the five panels for a total of ten steel strain gages. Due to symmetry, strain gages were installed on only one half of Bridge 1. A steel strain gage was also attached in a similar fashion to a lower reinforcing bar in each stem of P3 near the north abutment to monitor the amount of support rotational restraint. An additional steel strain gage was installed on the top surface of the eastern steel tube railing at midspan of Bridge 1 to monitor the amount of load carried by the railing. One displacement transducer was attached to each stem of each panel for a total of 20 deflection measurements; the layout of the displacement transducers is also shown in Figure 3.7.

### **3.2.3. Test Vehicle and Load Positions**

A truck tractor-semitrailer combination was used as the test vehicle. The test vehicle as well as the vehicle's dimensions and weight distribution (Gross Vehicle Weight (GVW) = 80.18 kip) are shown in Figure 3.8. The test vehicle moved north across Bridge 1 in three different transverse positions, shown in Figure 3.9. Load positions 1-LP24.x and 1-LP79.x corresponded approximately to the northbound and southbound travel lanes, respectively. In these two positions, the test vehicle was tracking entirely on two panels. For load position 1-LP56.x, the test vehicle was transversely centered on Bridge 1 and was tracking over panel joints between P4 and P5 and P6 and P7.

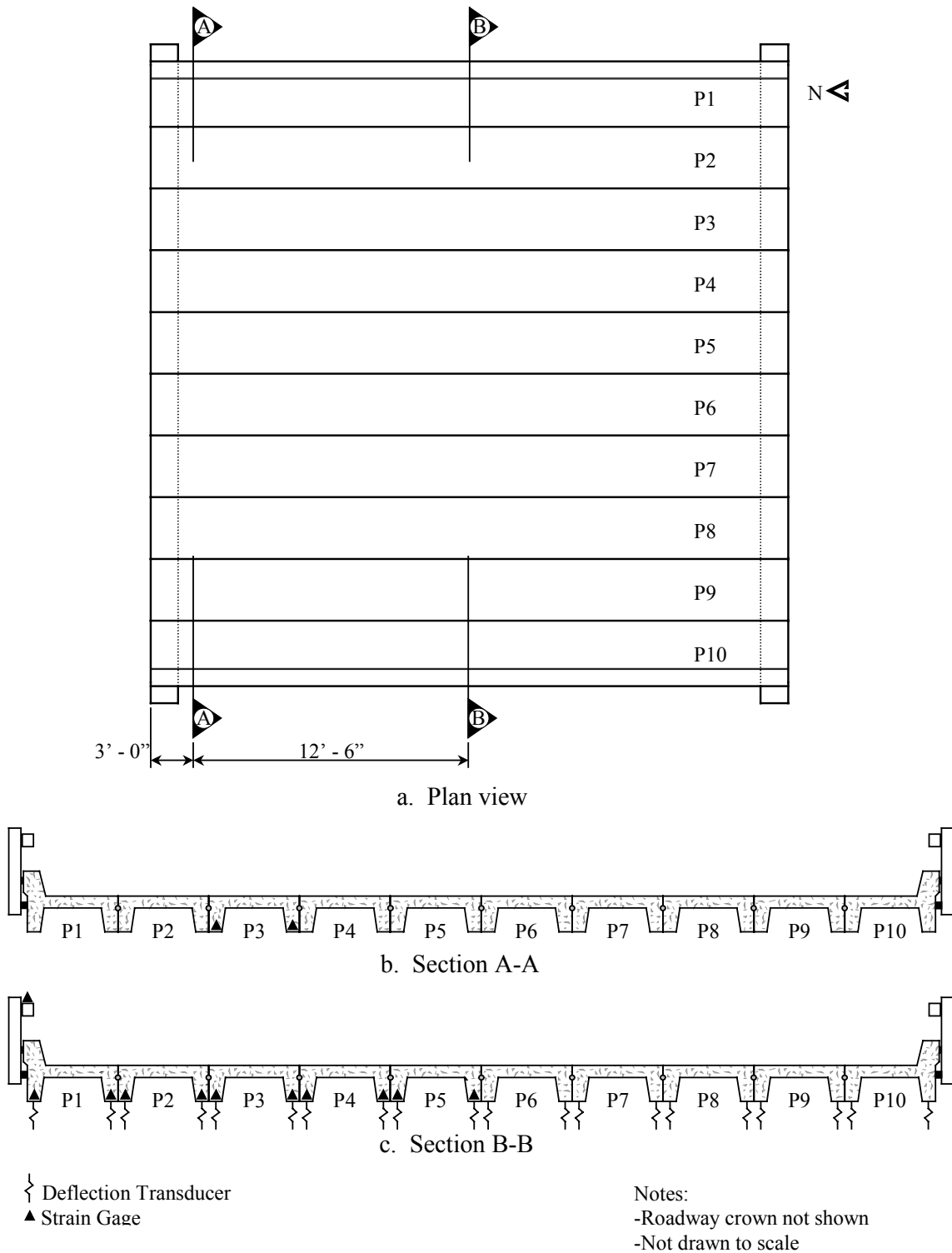
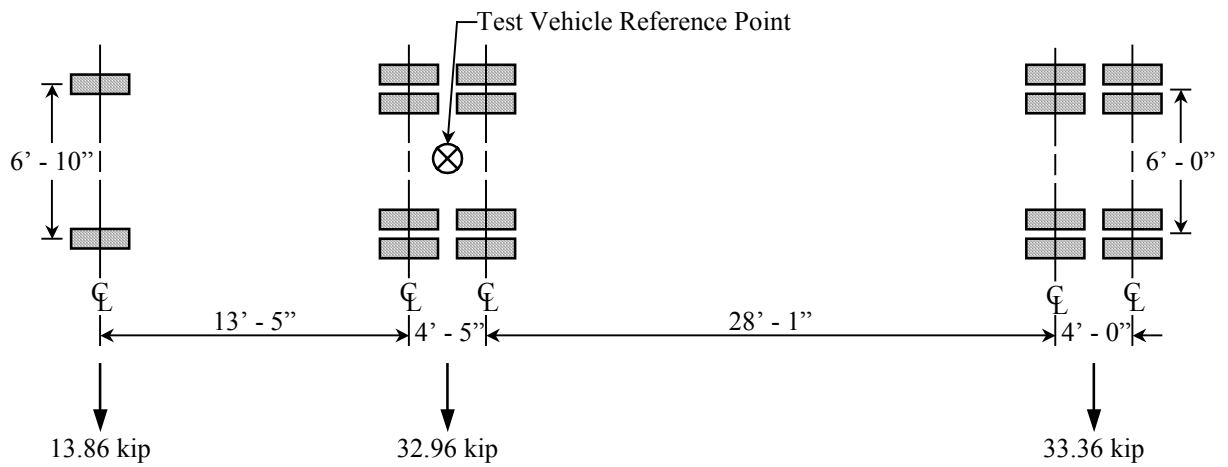


Figure 3.7. Location of strain gages and displacement transducers for Bridge 1.

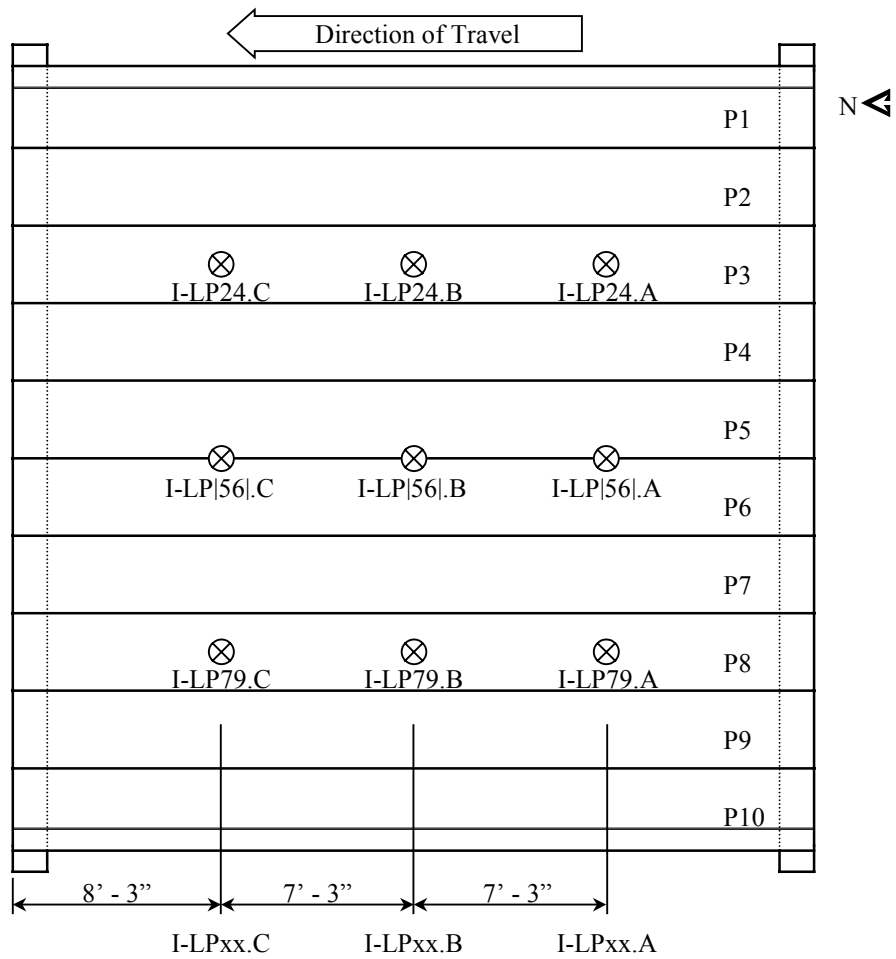


a. Photograph of test vehicle

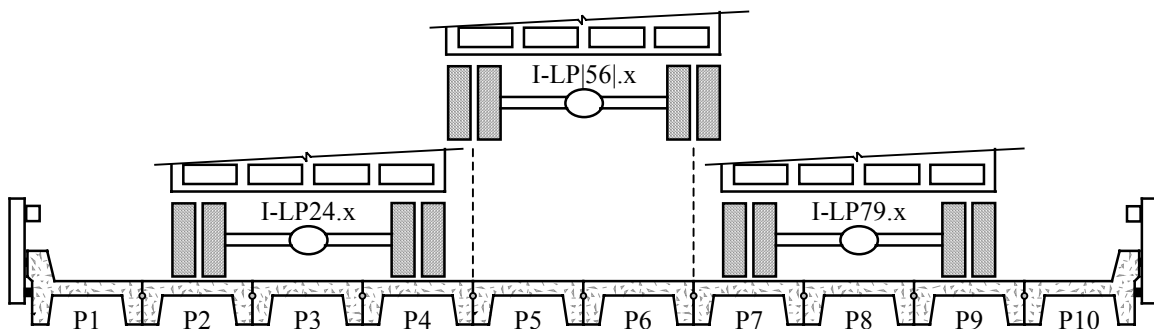


b. Wheel configuration and weight distribution of test vehicle

Figure 3.8. Bridge 1 test vehicle.



a. Load position locations



b. Transverse positioning of test vehicle (looking North)

Figure 3.9. Bridge 1 load positions.

### 3.2.4. Discussion of Results

In general, the field load tests were performed to determine how PCDBs respond to load and to obtain useful information that can be used to modify the theoretical rating calculations for deteriorated PCDBs. One particularly useful result of this testing was the transverse distribution of load. AASHTO (6) outlines a procedure to theoretically determine load fractions (LFs) based on the bridge dimensions and individual panel geometry. The load fraction is essentially the percentage of a wheel line load carried by an individual panel. Remaining load is distributed transversely, via the shear connection between PCDB panels, to adjacent panels. The AASHTO equations are general in that they can be used for several types of multibeam bridges; load fractions from these equations are likely conservative due to this generality. A bridge rating based on these theoretical load fractions usually produces a conservative bridge rating. Data from the field load tests can be used to determine experimental load fractions, and a rating calculation based on these will give a better estimate of the bridge strength (i.e. rating).

Experimental load fractions can be calculated from either strain or deflection data. Field and laboratory testing confirmed that load fractions calculated from strain data (both concrete and steel) and deflection data are nearly identical. Deflection transducers are relatively easier to install across a bridge cross-section than strain gages and therefore deflection data were used to calculate actual load fractions for all load tests. Equation 1 was used to calculate the experimental load fractions.

$$LF_i = \alpha \cdot \frac{\Delta_i}{\sum_{j=1}^n \Delta_j} \quad (1)$$

where:

$LF_i$  = Load fraction for  $i^{th}$  panel

$\alpha$  = 2 (for one lane LF); 4 (for two lane LF)

$\Delta_i$  = Deflection of  $i^{th}$  panel

$\Delta_j$  = Deflection of  $j^{th}$  panel

$n$  = Number of panels in PCDB

The two stem deflections were averaged for each panel to give the panel deflection, and a load fraction was calculated for every panel for each load position. For the two lane load fractions, deflection data were generated by superposition. Deflection data from a left lane load position were added to the deflection data from the corresponding right lane load position to give two lane deflection data that theoretically corresponds to simultaneously loading both lanes of the bridge.

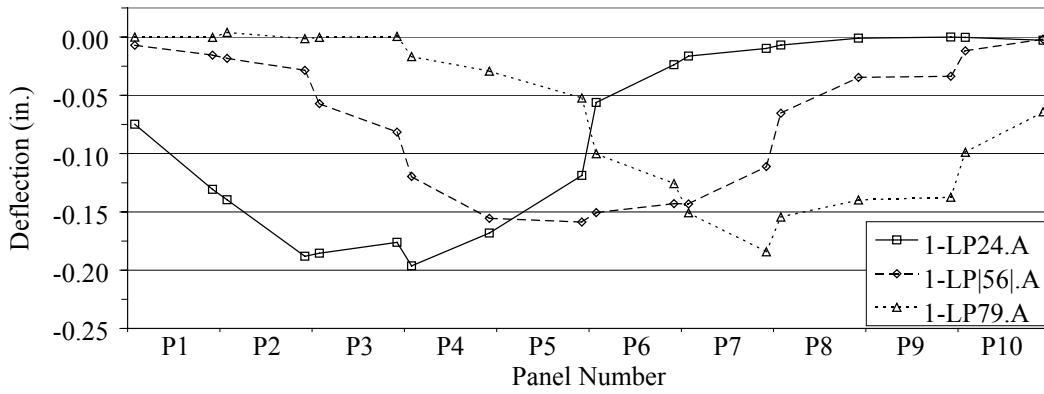
The largest experimental load fraction for each load position for Bridge 1 is shown in Table 3.1. Typically, when the test vehicle tracked entirely on two panels, the panel supporting the wheel line closest to the center of the bridge had the largest load fraction. In a few instances, the panel between the two loaded panels had the highest load fraction. Also, as expected, the largest load fraction was somewhat smaller when the test vehicle tracked on four panels (i.e. on the joint between adjacent panels) as opposed to only tracking on two panels. Two lane load fractions were consistently larger than the one lane load fractions.

As shown in Table 3.1, the highest one and two lane experimental load fractions for all load positions was 0.49 and 0.54, respectively. For comparison, the one lane theoretical load fraction from AASHTO for Bridge 1 was 0.57, or 16% greater than the one lane experimental load fraction. The theoretical two lane load fraction, 0.59, was 9% greater than the experimental two lane load fraction.

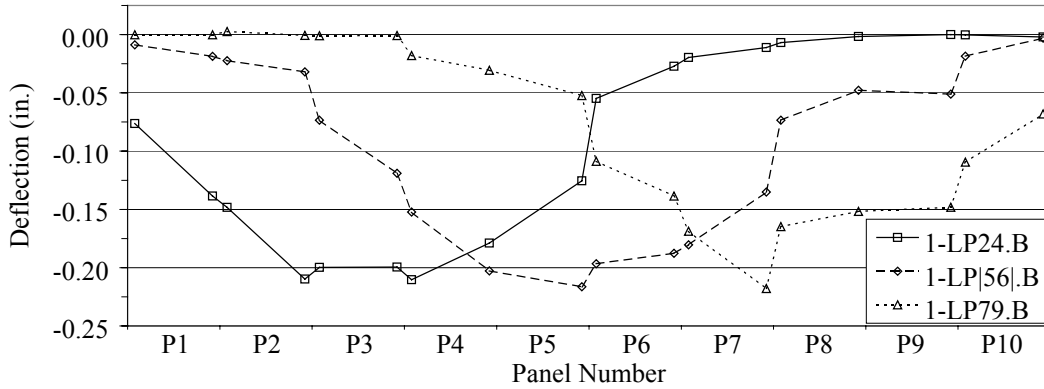
Table 3.1. Bridge 1 maximum load fractions.

Longitudinal Load Position	Transverse Load Position			
	1-LP24.x	1-LP 56 .x	1-LP79.x	Two Lane
1-LPxx.A	0.45	0.41	0.46	0.53
1-LPxx.B	0.46	0.43	0.49	0.53
1-LPxx.C	0.47	0.43	0.47	0.54

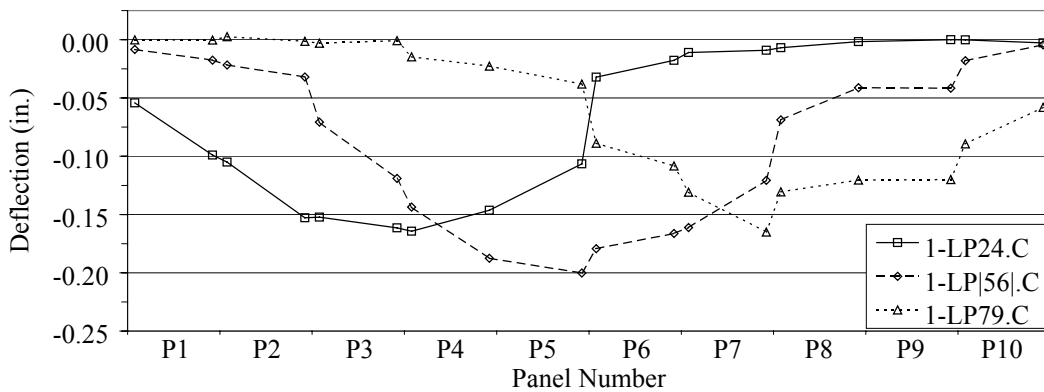
The displacement measurements from which the experimental load fractions were calculated are plotted in Figure 3.10. These plots are also useful in determining whether Bridge 1 responded symmetrically to corresponding symmetrically placed loads. Structural inadequacies, such as a panel weakened by corrosion or a failing shear connection, would be indicated by an unsymmetrical response. As shown in Figure 3.10, some minor variation exists between 1-LP24.x and 1-LP79.x but overall the data are reasonably symmetric and no



a. Deflection data for 1-LPxx.A



b. Deflection data for 1-LPxx.B



c. Deflection data for 1-LPxx.C

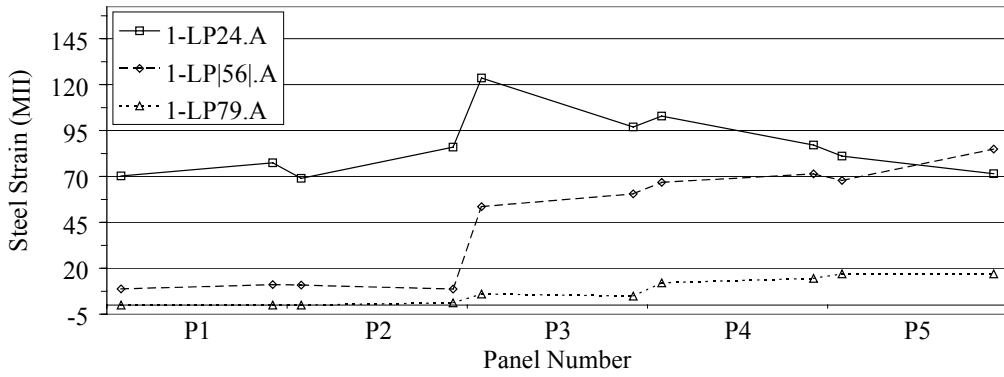
Figure 3.10. Bridge 1 deflection data.

inadequacies are apparent. Excessive deflection can be another indication of a deficient panel or panels. Maximum measured deflection for any load position was 0.22 in. or  $L/1582$  ('L' is the span length of the bridge in inches). In design, maximum allowable deflection is often taken as  $L/800$  (6). Therefore, deflection of Bridge 1 is well within allowable limits.

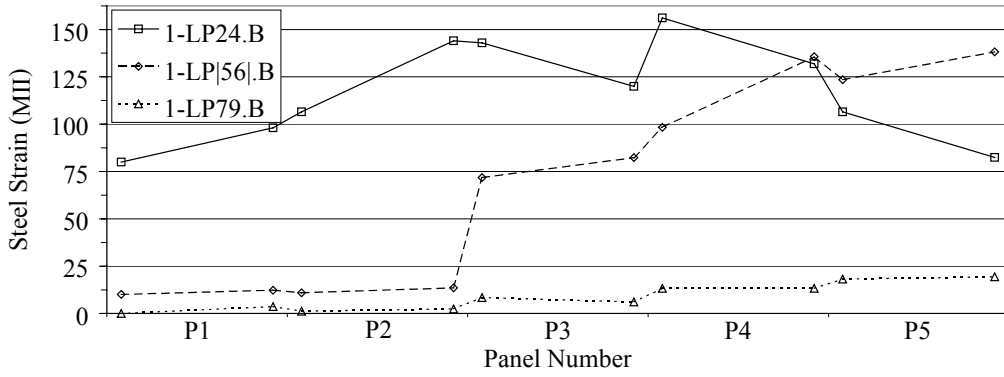
Strain data can be used to calculate stress in a particular component using Young's modulus of elasticity, provided the stress in the component is within the elastic range. Steel strain data for each load position are plotted in Figure 3.11. The highest measured steel strain was 156 microstrain (MII) and the corresponding steel stress was calculated to be 4,520 psi (assuming Young's modulus,  $E_s$ , for the reinforcing steel is 29,000,000 psi). The J-10 standard plans specify Grade 40 reinforcing steel and an allowable stress of 20,000 psi. Thus, the highest 'measured' stress was only 23% of the allowable stress, indicating the reinforcement in Bridge 1 was adequate to carry legally loaded vehicles.

A simplified bridge model with simply supported beams would typically be used in rating a PCDB. This model does not incorporate edge stiffening effects or support restraint due to construction details. Railings and curbs also add stiffness to the outer panels but the amount added is difficult to predict. Without field measurements, support rotational restraint is difficult to predict. A level of conservatism is added to the bridge rating when these two characteristics are neglected since both of these characteristics decrease midspan bending moments.

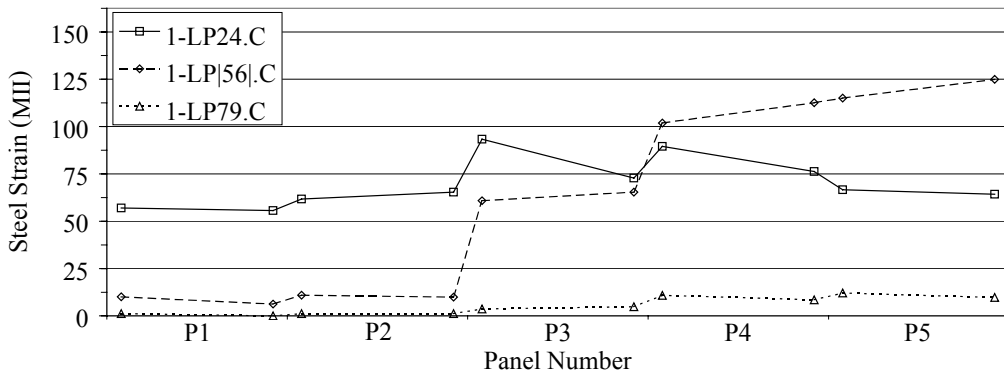
Strain and deflection data collected during a service load test can be used to determine edge stiffening or support restraint. In the case of Bridge 1, strain data from a steel strain gage attached to the railing showed that indeed the rail was taking some load and therefore causing an increase in the edge panel stiffness. Compressive strains were greatest when the test vehicle was closest to the railing. They ranged from 39 MII (1,130 psi) for 1-LP24.B to 0 MII for 1-LP79.B. Edge stiffening was also detected by the deflection measurements and is shown by the deflection plots in Figure 3.10. For example, in 1-LP24.B, P1 and P5 were adjacent to the loaded panels (P2 and P4). Average deflection for P1 was approximately 30% less than the average deflection of P5, indicating that P1 was stiffer than P5.



a. Steel strain data for 1-LPxx.A



b. Steel strain data for 1-LPxx.B



c. Steel strain data for 1-LPxx.C

Figure 3.11. Bridge 1 steel strain data.

Potential support restraint was measured by two steel strain gages mounted near the face of one abutment. If there is support restraint, a negative moment region will exist near the abutment and compressive steel strains will be detected in the reinforcement. For Bridge 1, tensile steel strains near the abutments ranged from 3 MII to 68 MII. No compressive strains were measured for any load positions investigated. This indicated that the supports did not restrict rotation of the panel ends (assuming the other panels acted in a similar manner as the instrumented panel).

### **3.3. Bridge 2: Delaware County Dairy Bridge**

#### ***3.3.1. Bridge Description***

Bridge 2 was located on a dead end gravel road in the Union Township of Delaware County, Iowa. The single span PCDB was constructed of salvaged PCDB panels of unknown origin in 1997 and served approximately 20 vehicles a day. A dairy farm was located at the end of the road (hence the bridge name) and the majority of the traffic crossing Bridge 2 was either farm vehicles or milk trucks. Concerns due to panel deterioration and to the type of vehicles (i.e., heavily loaded milk trucks) using Bridge 2 prompted the service load test. Also, the unique geometry of Bridge 2, as detailed below, was a source for additional concern. This bridge crossed a small stream as shown in Figure 3.12.



Figure 3.12. Bridge 2 (looking north).

Bridge 2 consisted of eight Type II (H15) PCDB panels, and the overall length of each panel was 36 ft – 0 in. As shown in Figure 3.13, the outer face of each abutment was several feet in from the panel ends. This geometry was unique to Bridge 2 and cause for some concern since loads placed on the cantilevered panel ends cause negative bending in the panels. The J-10 Standards are only for simple span bridge configurations and the panels were likely not designed to withstand negative bending.

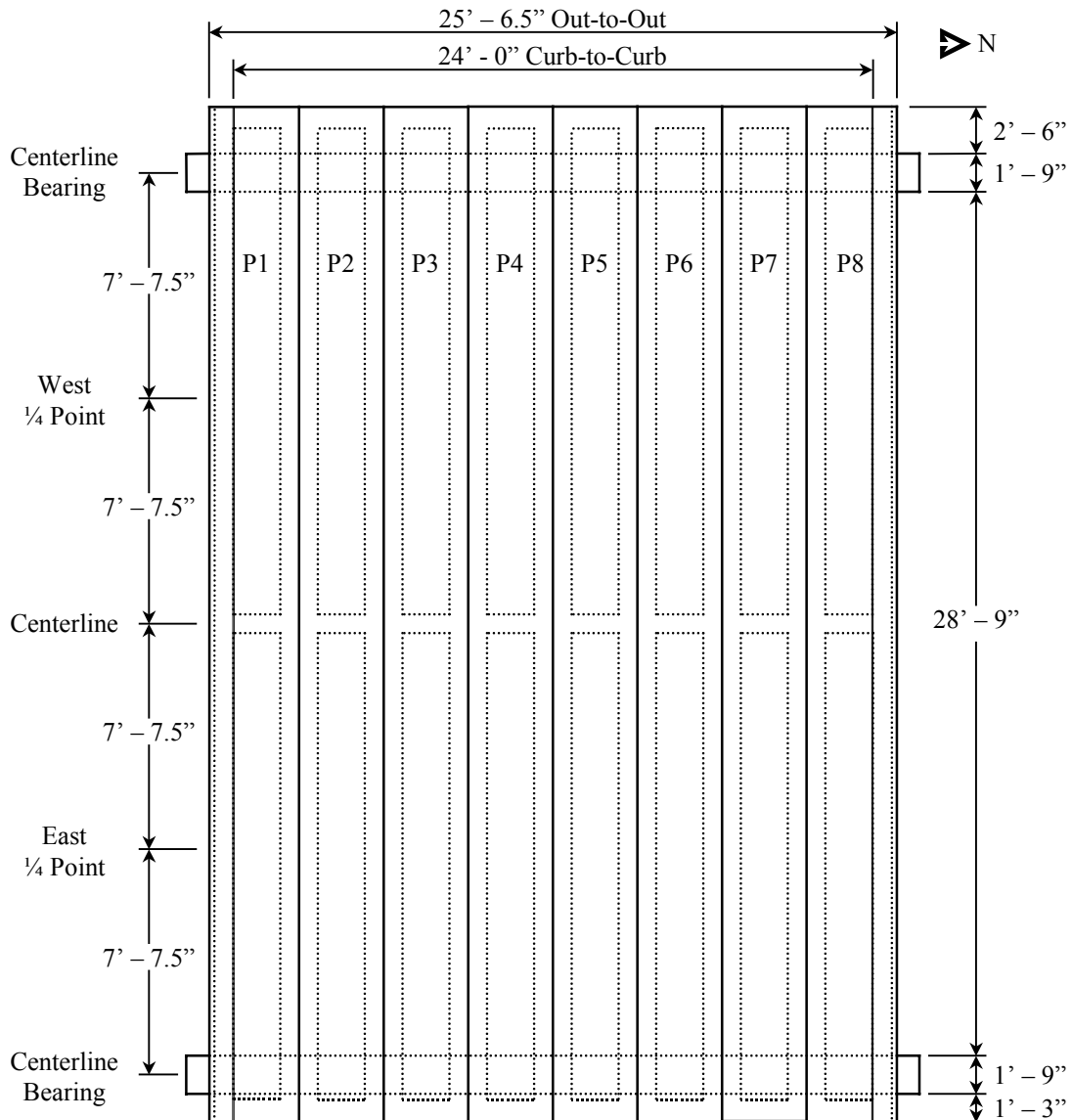


Figure 3.13. Plan view of Bridge 2.

Curb-to-curb width of Bridge 2 was 24 ft – 0 in. and the overall width was 25 ft – 6.5 in., as shown in Figure 3.13. Span length, measured between the abutment centerlines, was 30 ft – 0 in. Each abutment was 1 ft – 9 in. wide and consisted of a steel wide flange beam laid flat-wise (i.e., web parallel with ground) on steel piles. The abutments were not crowned and therefore Bridge 2 lacked proper roadway drainage. A concrete curb approximately 11 in. deep and 10 in. wide was cast monolithically on the exterior panels (P1 and P8). Railings consisted of standard ‘W’ guardrail supported by concrete posts. Galvanized bolts were used to fasten the concrete posts to exterior panels P1 and P8.

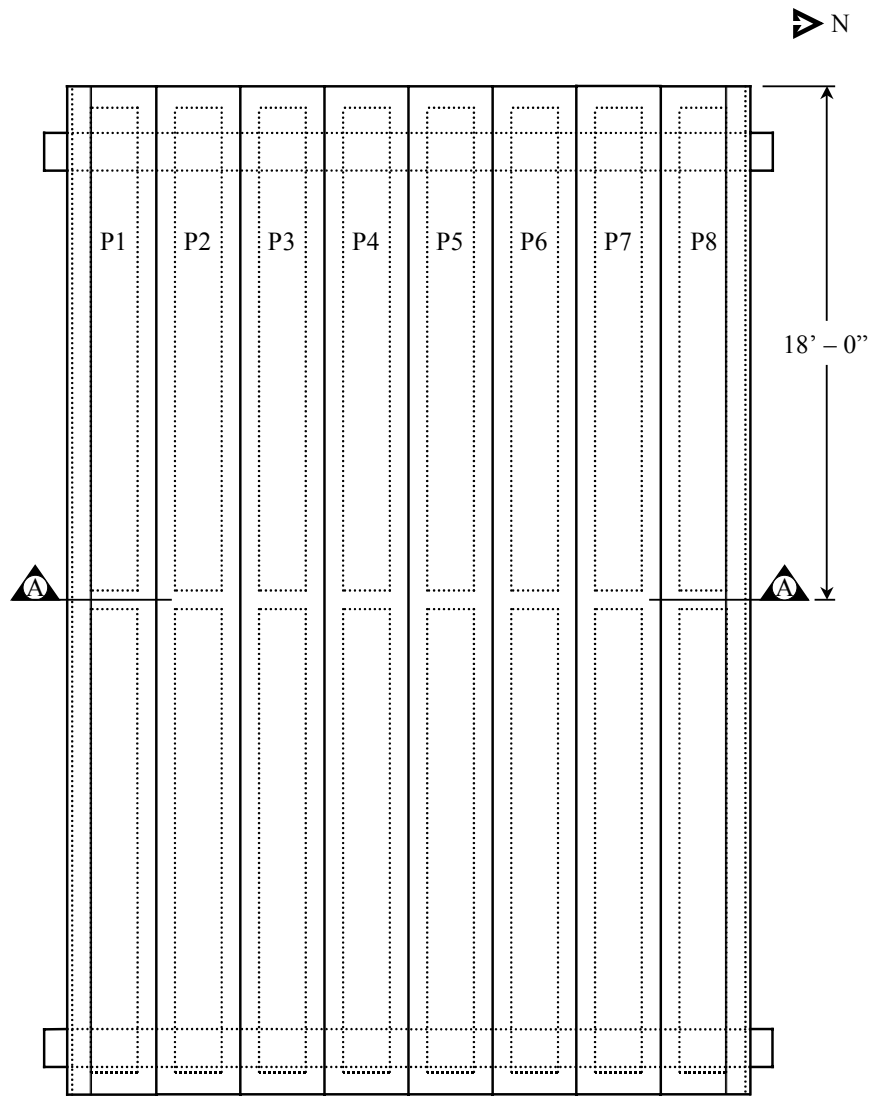
Galvanized bolts were also used to hold adjacent panels together. Although the bolts were properly installed, the concrete-filled galvanized pipes that form a continuous shear connection between the adjacent panels were missing. Lack of proper shear connection and its effect on the transverse distribution of load was cause for additional concern over the adequacy of Bridge 2. The effect of missing shear connectors (i.e., pipes) was further studied in laboratory tests (see Chapter 5).

Most of the PCDB panels in Bridge 2 were in good condition and exhibited no deterioration. Concrete covering the primary reinforcing steel had spalled in only three discrete locations and the exposed reinforcing was moderately corroded. A cement patching compound had been used to repair one location. Also, several flexural cracks appeared in the deck at the cantilevered ends. Bridge 2 was scheduled for replacement in 2001.

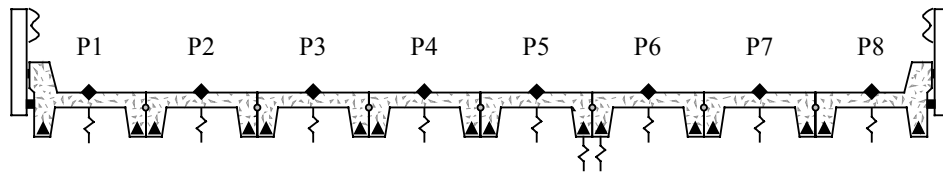
### ***3.3.2. Test Setup***

Bridge 2 was instrumented with sixteen steel strain gages, eight concrete strain gages, and ten deflection transducers. The location of the instrumentation is presented in Figure 3.14. At midspan, one steel strain gage was bonded to a reinforcing bar in each stem of all eight PCDB panels and a concrete strain gage was bonded to the deck surface at the center of each panel. Deflection transducers attached to the center of each panel measured panel deflection. Two additional transducers were attached to adjacent stems of Panels 5 and 6 (P5 and P6) to measure differential deflection across a joint. Tape switches were used to determine the longitudinal position of the test vehicle.

The western cantilevered ends of P5 and P6 were instrumented to investigate how these elements reacted to loaded vehicles. A steel strain gage was bonded to a longitudinal



a. Plan view



b. Section A-A

- ⌋ Deflection Transducer
- ▲ Steel Strain Gage
- ◆ Concrete Strain Gage

Figure 3.14. Location of strain gages and displacement transducers on Bridge 2.

deck reinforcing bar in each panel and a deflection transducer was attached to the end of each panel. Rain during the service load test caused the two steel strain gages to malfunction thus no useful strain data were acquired. Measured deflections were quite small ( $<0.05$  in.) and also appeared somewhat erroneous. Therefore, due to these complications, the data from these instruments are not presented in this report.

### **3.3.3. Test Vehicle and Load Positions**

A tandem axle dump truck provided by the Delaware County Engineer was used for the test vehicle. Vehicle dimensions and axle weights (GVW = 46.36 kip) are presented in Figure 3.15.

The test results of three load positions, shown in Figure 3.16, are presented in the following section. For load positions 2-LP24.B and 2-LP57.B, the transverse location of the test vehicle corresponded to east and west bound lanes, respectively. For load position 2-LP45.B, the test vehicle was transversely centered on Bridge 2. The reference point of the test vehicle was longitudinally located at midspan for all three load positions (see Figure 3.16a).

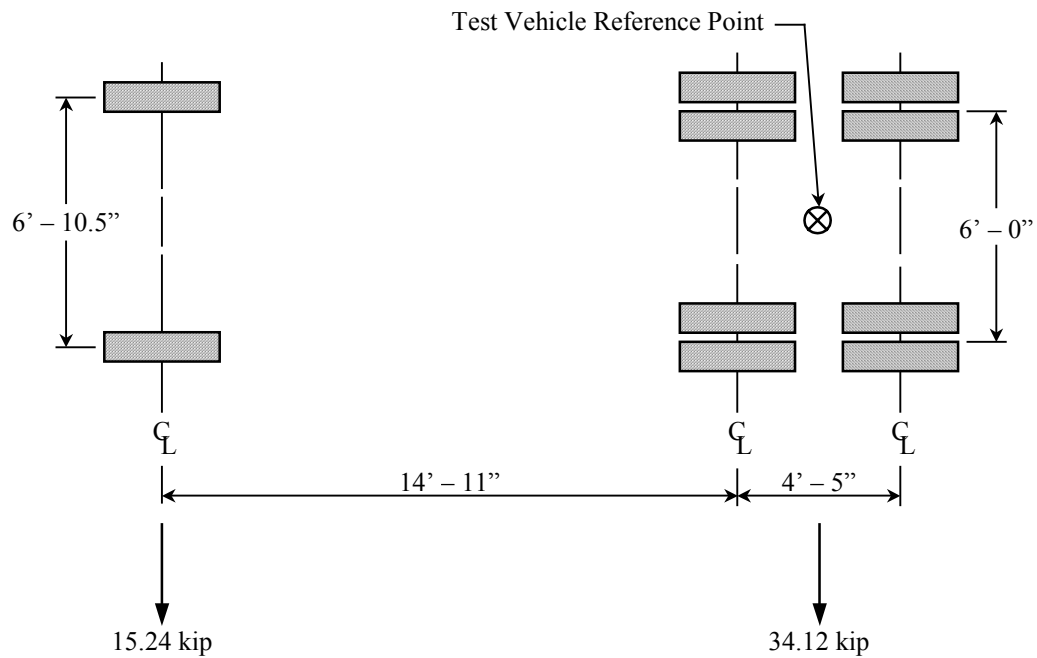
### **3.3.4. Discussion of Results**

Deflection data from the Bridge 2 service load test were used in Equation 1 to calculate experimental load fractions for each load position. The largest load fractions for each load position are presented in Table 3.2. Overall, the largest one lane load fraction for Bridge 2 was 0.68. By comparison, the largest one lane load fraction for Bridge 1 was 0.49. The large variation from Bridge 1 to Bridge 2 was due to the substantial difference between these two bridges. While both bridges were constructed with Type II PCDB panels, only Bridge 1 had the concrete-filled galvanized pipe shear connectors. These critical elements were not installed in Bridge 2 and, as a result, the bridge's ability to transversely distribute load was greatly reduced.

Load transfer between adjacent panels in Bridge 2 relied solely upon the bolts connecting adjacent panels. These bolts were intended to only hold adjacent panels together and thus functioned poorly for transfer of shear. Oversized holes (1 1/8 in. diameter) facilitated bolt installation but also allowed for relative displacement across panel joints.



a. Photograph of test vehicle



b. Wheel configuration and weight distribution of test vehicle

Figure 3.15. Bridge 2 test vehicle.

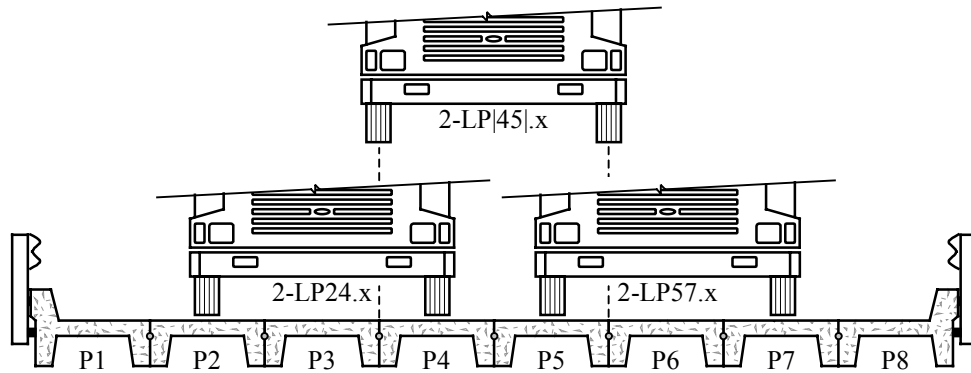
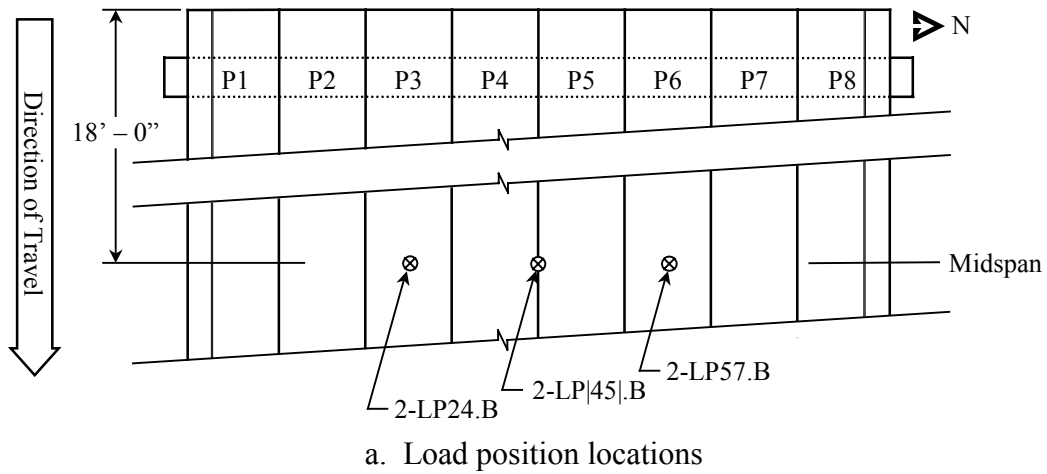
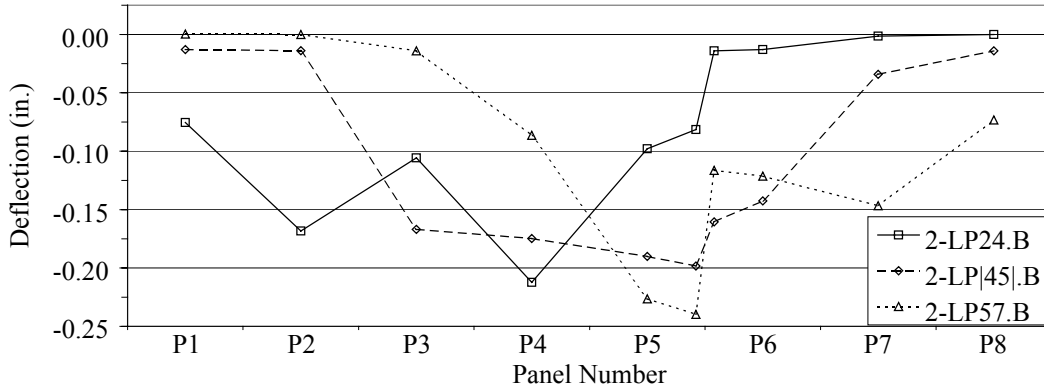


Figure 3.16. Bridge 2 load positions.

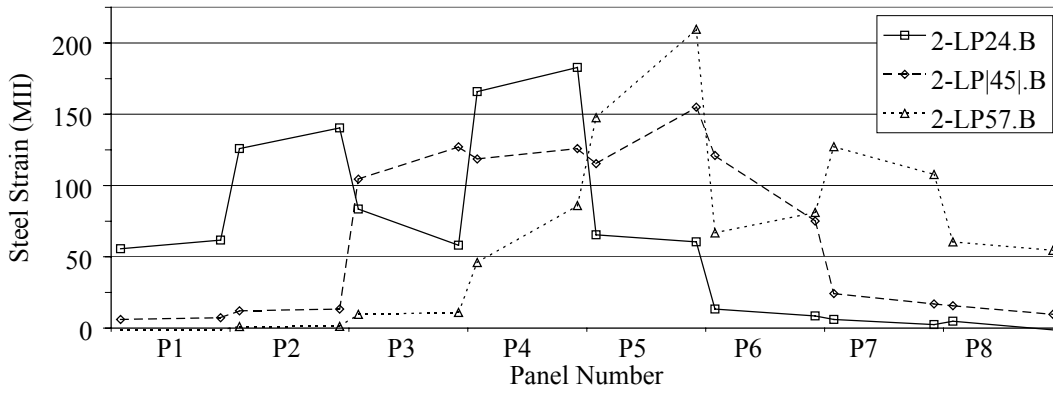
Table 3.2. Bridge 2 maximum load fractions.

Load Position			
2-LP24.B	2-LP45 .B	2-LP57.B	Two Lane
0.63	0.51	0.68	0.97

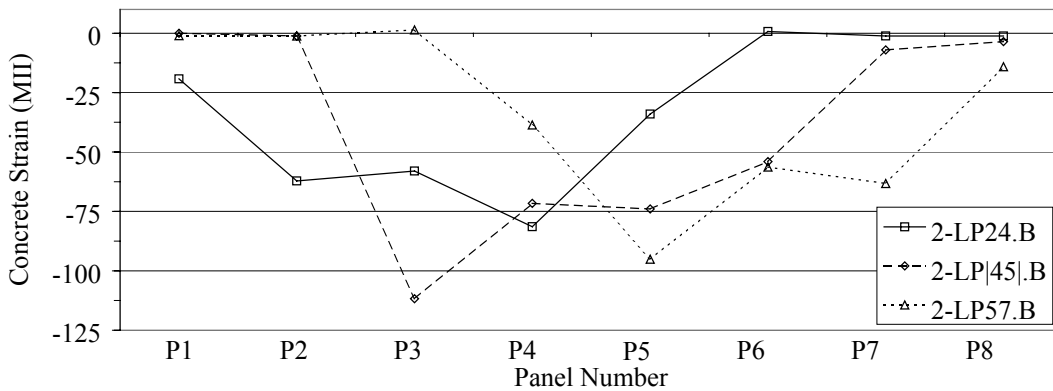
This can easily be seen in the deflection plot shown in Figure 3.17a. For load position 2-LP57.B, approximately 0.12 in. of relative displacement occurred across the joint between P5, which was supporting a wheel line, and P6, an unloaded panel. For comparison, the largest relative displacement across a joint in Bridge 1 was 0.07 in. Visual inspection of the



a. Midspan deflection plot



b. Midspan primary reinforcing steel strain



c. Midspan concrete deck strain

Figure 3.17. Bridge 2 service test data.

deflection plots for Bridge 1 and Bridge 2 reveals that the panels in Bridge 1 deflected together as a unit and the panels in Bridge 2 deflected more independently. Maximum deflection was 0.24 in. ( $L/1525$ ) and is well within acceptable limits.

The AASHTO one lane load fraction for Bridge 2 is 0.56, or 18% less than the experimental one lane load fraction. Moreover, the theoretical two lane load fraction, 0.58, is 40% less than the experimental two lane load fraction. If a rating calculation were performed using the theoretical values, as would be the typical procedure, the calculated capacity of Bridge 2 would exceed its actual capacity (assuming other variables are correctly known). This is reason for concern and adjustments must be made in the rating calculations when the proper shear connectors are not used in a PCDB.

Steel and concrete strain data plots are shown in Figures 3.17b and 3.17c, respectively. Similar to the deflection data plot, both strain plots indicate a degree of independent panel behavior. The highest measured steel strain was approximately 208  $\mu\text{in/in}$ . Corresponding steel stress was 6,032 psi and was significantly less than the allowable value (20,000 psi). Likewise, the highest measured concrete strain was 110  $\mu\text{in/in}$ . Assuming Young's modulus for the concrete was 4,031,000 psi (normal weight concrete and  $f'_c = 5,000$  psi) (7), the corresponding concrete stress was 443 psi. This 'measured' stress was only 22% of the allowable value (2,000 psi).

The railing on Bridge 2 appeared less stiff than the railing on Bridge 1 and consequently, Bridge 2 displayed less edge stiffening than Bridge 1. For load position 2-LP24.B, the measured strain and deflection values were nearly the same for P1 and P5, both of which were adjacent to loaded panels. Hence, P1 exhibited little or no signs of increased stiffness due to the curb and railing system.

### **3.4. Bridge 3: Delaware County Trout Bridge**

#### **3.4.1. Bridge Description**

Bridge 3 was located in north central Milo Township of Delaware County, Iowa. Shown in Figure 3.18, the two span PCDB carried county road X21 across a trout stream (hence the bridge name). The two lane paved highway was a farm-to-market route and served 1,260 vehicles on an average daily basis. Bridge 3 was constructed in 1965.

Each simple span of Bridge 3 consisted of nine Type I PCDB panels. A plan view of Bridge 3 with its geometrical dimensions is shown in Figure 3.19. Overall length of each panel was 31 ft – 0 in. and each span, measured between bearing centerlines, was 29 ft – 6 in. Curb-to-curb-width was 27 ft – 3 in. and out-to-out width was 29 ft – 3 in.

Both abutments and the pier were 2 ft – 0 in. wide and consisted of reinforced concrete caps on timber piles. All were crowned to provide proper roadway drainage. The 6 in. diameter holes in the panel ends were filled with concrete, and the dowel bars connecting the panels to the concrete caps were assumed to be in place. A standard ‘W’ guardrail supported by steel angles formed the railing along each side of Bridge 3. A concrete curb approximately 12 in. wide and 10 in. deep was cast onto the exterior panels (P1, P9, P10, and P18). Galvanized bolts that hold adjacent panels together were properly installed, as were the grouted shear keys.



Figure 3.18. Bridge 3 (looking south).

The PCDB panels of Bridge 3 had significant deterioration. As shown in Figure 3.20, much of the primary reinforcement was exposed and extensively corroded. In areas of intact concrete cover, longitudinal cracks were present on the underside of the panel stems and the concrete covering appeared to be on the verge of spalling. Minor deterioration damage also existed on the deck of Bridge 3. These areas had been repaired with an ACC patch.

A bridge inspection performed in 1999 noted “much spalling with exposed rebar”. The condition of the deck and superstructure received low ratings and based on a rating

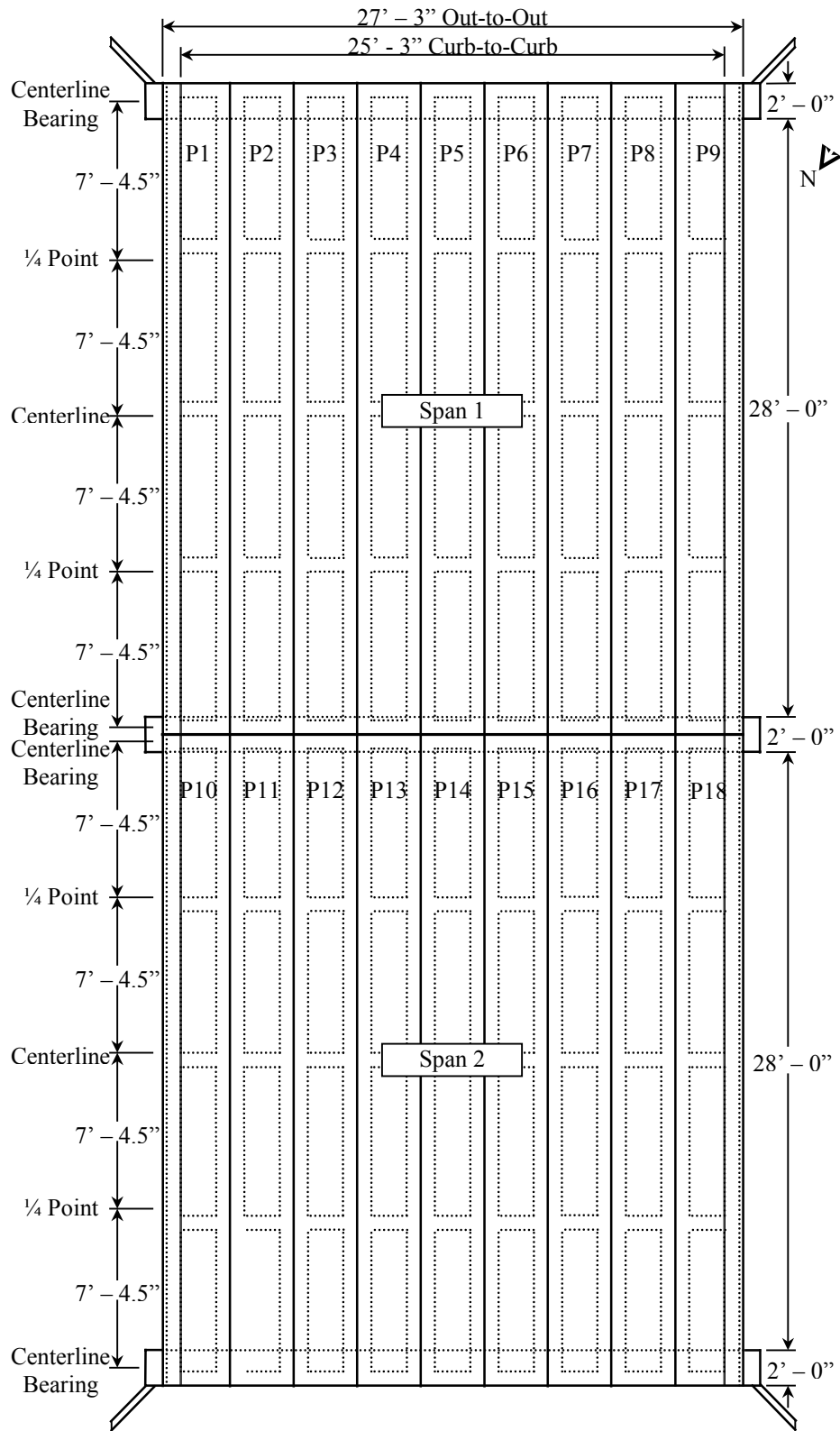


Figure 3.19. Plan view of Bridge 3.



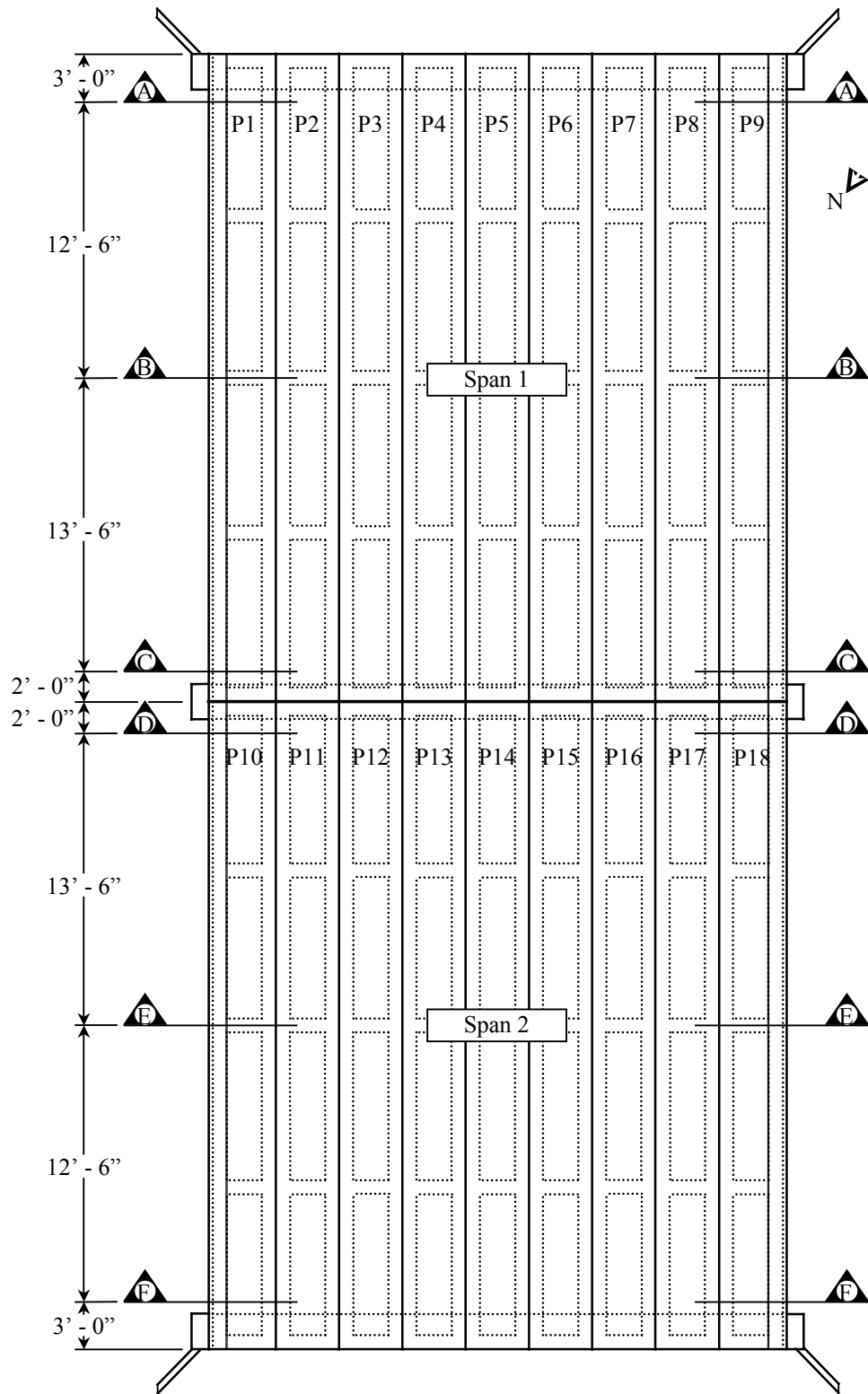
Figure 3.20. Bridge 3 corrosion damage.

calculation, Bridge 3 was posted 423, 535, and 642 (where the first digit refers to the vehicle type and the second two digits are the gross permitted vehicle weight in tons).

#### **3.4.2. Test Setup**

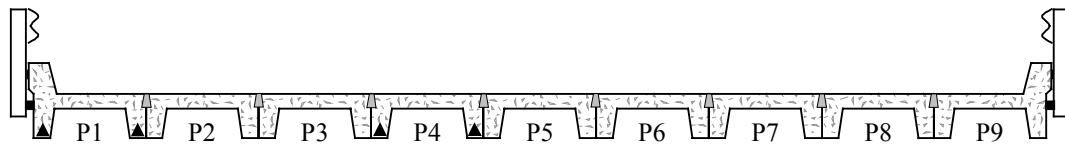
The majority of the instrumentation used during the Bridge 3 service field test was installed in Span 1. This span exhibited more deterioration than Span 2 and therefore was of more interest. The instrumentation layout for Bridge 3 is presented in Figure 3.21.

Steel strain gages were attached to P1 through P4 at the midpoint of Span 1. The gages were bonded to one reinforcing bar in each stem of these panels. Additional steel strain gages were attached in a similar fashion near both ends of P1, P4, and P13. These gages monitored both the amount of restraint provided by the abutments and the amount of continuity from Span 1 to Span 2. A concrete strain gage attached to the top surface of the P1 curb measured strain at this location. Deflection transducers were attached to each stem of each PCDB panel at the midpoint of Span 1. Two additional deflection transducers were attached to each stem of Panel 13 to detect continuity. Tape switches were used to indicate the longitudinal position of test vehicle.

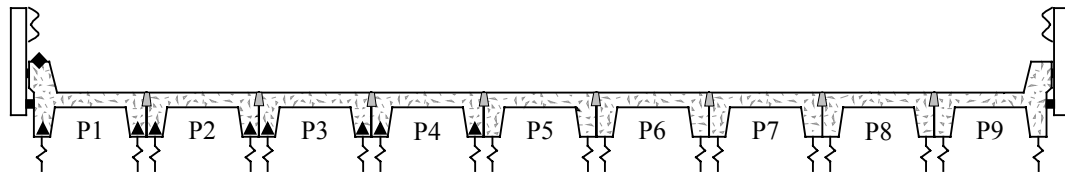


a. Plan view

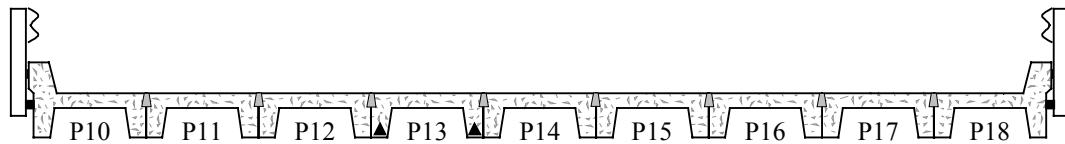
Figure 3.21. Location of strain gages and displacement transducers on Bridge 3.



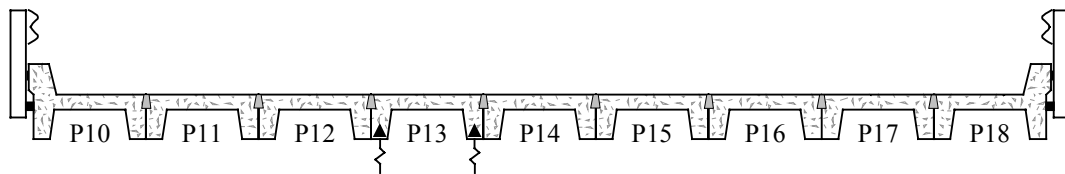
b. Section A-A, Section C-C



c. Section B-B



d. Section D-D, Section F-F



e. Section E-E

- ⌋ Deflection Transducer
- ▲ Steel Strain Gage
- ◆ Concrete Strain Gage

Notes:  
 -Roadway crown not shown  
 -Not drawn to scale

Figure 3.21. Continued.

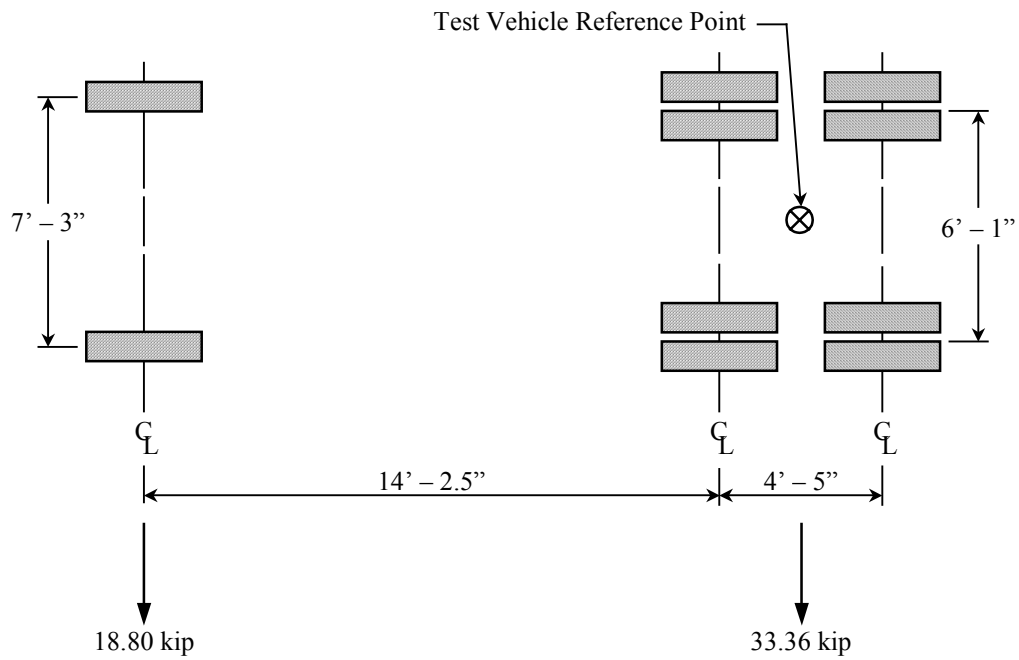
### 3.4.3. Test Vehicle and Load Positions

A tandem axle dump truck provided by the Delaware County Engineer served as the test vehicle for the Bridge 3 service load field test. Wheel configuration and weight distribution (GVW = 52.16 kip) for this vehicle are presented in Figure 3.22.

Three load positions, shown in Figure 3.23, were investigated for the Bridge 3 service load field test. For load positions 3-LP24.B and 3-LP68.B, the test vehicle was transversely located in the northbound and southbound lanes, respectively. For load position 3-LP46.B,

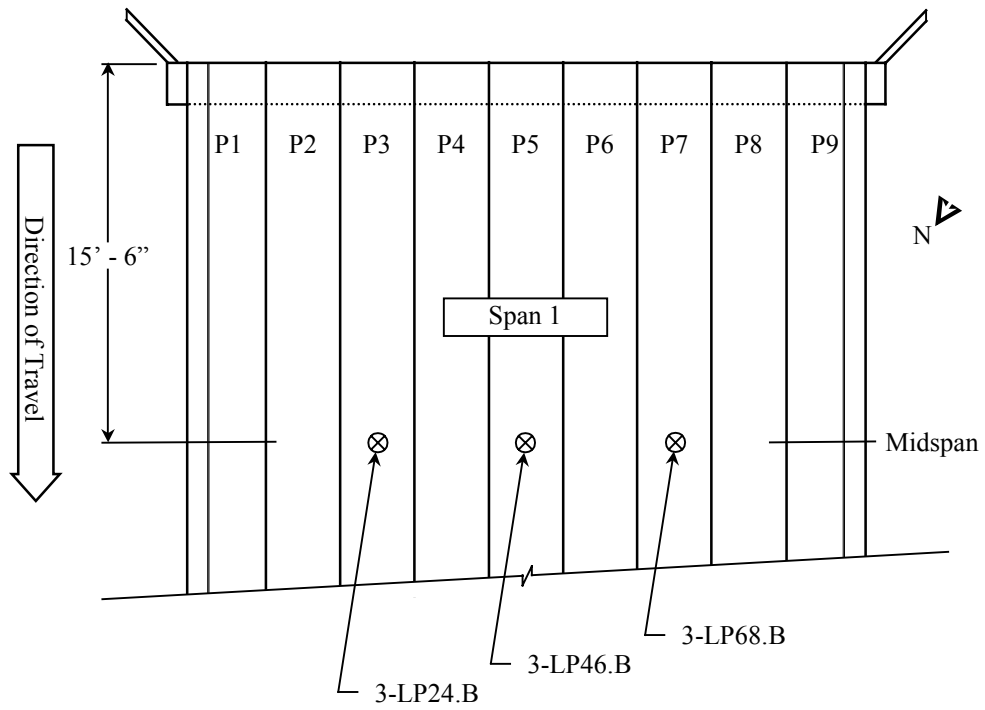


a. Photograph of test vehicle

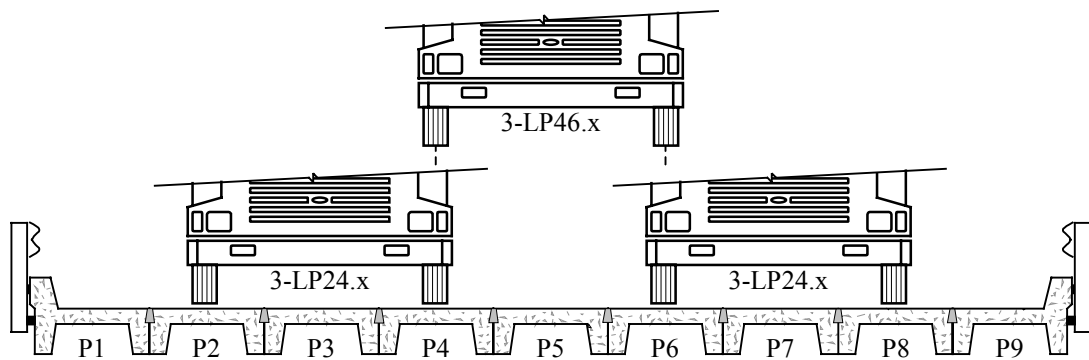


b. Wheel configuration and weight distribution of test vehicle

Figure 3.22. Bridge 3 test vehicle.



a. Load position locations



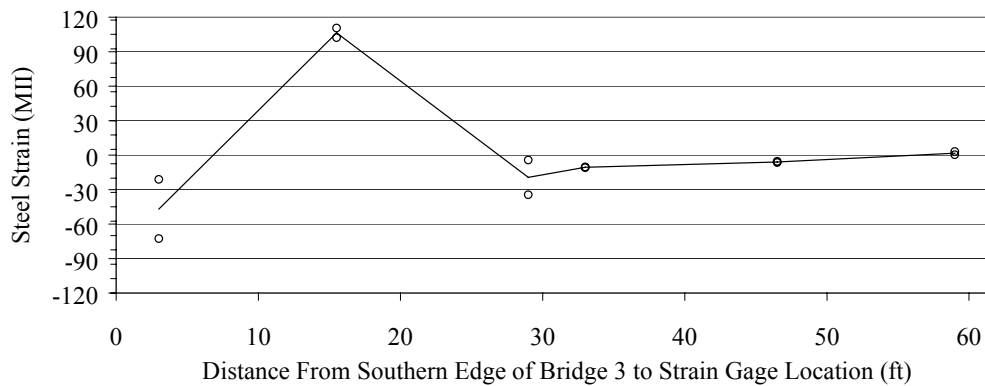
b. Transverse positioning of test vehicle (looking southeast)

Figure 3.23. Bridge 3 load positions.

the test vehicle was transversely centered on Bridge 3. The reference point of the test vehicle was longitudinally located at midspan of Span 1 for all load positions.

#### 3.4.4. Discussion of Results

Bridge 3 was the only multispan bridge service load tested by the research team. Additional strain gages and deflection transducers supplemented the typical midspan instrumentation and detected continuity and support restraint. In particular P4 and P13 were instrumented with steel strain gages on each stem at both the midspan locations and near all four end locations. The strain measurements from these gages for load position 3-LP46.B are presented in Figure 3.24. From this plot, both support restraint and continuity can easily be seen.



(Note: Strain gages on P4 and P13.)

Figure 3.24. Steel strain profile for load position 3-LP46.B.

For load position 3-LP46.B, average compressive strain at the southern abutment was 50 MII and average tensile strain at the midpoint of Span 1 was 100 MII. Comparison of these two values indicates significant support restraint. Such behavior can be attributed to the dowel bar connection between the panel and the abutment, a connection detail unique to Type I PCDB panels. Similar instrumentation on Bridge 1, which consisted of Type II panels, did not detect any support restraint.

Compressive strains, as shown in Figure 3.24, were measured by the four strain gages near the pier and by the two strain gages at the midpoint of Span 2. Small tensile strains (<5 MII) were measured by two gages near the northern abutment. This strain pattern

indicates continuity between the two spans. Similar to the source of the support restraint, the continuity between spans can be attributed to the dowel bar connection at the pier.

Deflection data shown in Figure 3.25 were used to calculate experimental load fractions, and the greatest load fraction for each load position is presented in Table 3.3. Bridge 3 displayed exceptional transverse load distribution. The largest one lane load fraction for all load positions, 0.42, was 28% less than the theoretical one lane load fraction (0.58). This performance can be attributed to the grouted shear keys. Adjacent panels were 'locked' together by the shear keys and a significant amount of load was transferred across the joint. As shown in Figure 3.25, the largest relative displacement across a panel joint was approximately 0.02 in. For comparison, in Bridge 1 the largest relative deflection across a panel joint was 0.07 in. and the largest experimental load fraction was 0.49. These values indicate that the concrete-filled pipe shear keys in Bridge 1 were less effective than the grouted shear keys in terms of shear transfer.

Similar to Bridge 1 and Bridge 2, the measured midspan deflections of Bridge 3 were much less than the maximum allowable values. The largest observed deflection for Bridge 3 was 0.16 in. ( $L/2213$ ).

Table 3.3. Bridge 3 maximum load fractions.

Load Position			
3-LP24.B	3-LP46.B	3-LP68.B	Two Lane
0.39	0.40	0.42	0.56

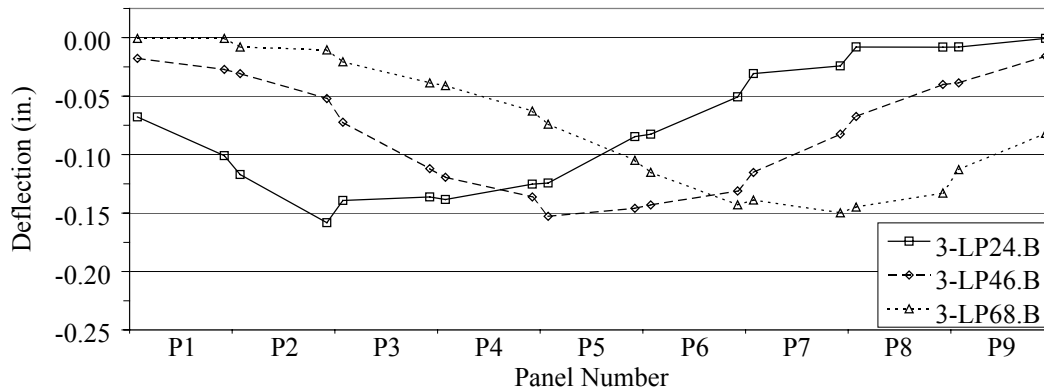


Figure 3.25. Midspan deflection plot for Bridge 3.

### 3.5. Bridge 4: Story County Bridge

#### 3.5.1. Bridge Description

Bridge 4, constructed in 1966, was located on a gravel road in central Fernald Township of Story County, Iowa. The farm-to-market route was a gravel road and served 95 vehicles on an average daily basis. A small stream, as shown in Figure 3.26, flowed beneath Bridge 4.



Figure 3.26. Bridge 4 (looking east).

Bridge 4 consisted of nine Type I PCDB panels. A plan view of Bridge 4 with its geometrical dimensions is presented in Figure 3.27. The overall length of each panel was 25 ft – 0 in. and the span length, measured between bearing centers, was 23 ft – 6 in. Curb-to-curb width was 25 ft – 3 in. and out-to-out width was 27 ft – 3 in.

Each abutment was 1' – 6" wide and consisted of a reinforced concrete cap supported by timber piles. The crowned abutments provided proper roadway drainage. A standard concrete curb approximately 12 in. wide and 10 in. deep was cast onto the exterior panels (P1 and P9). A 'W' guardrail and steel angle posts formed the railing along each side of Bridge 4 and was attached to the exterior panels. The shear keyways were found to be not properly packed with grout. Instead, they were found to contain only gravel and dirt from the 6 in.



### 3.5.2. Test Setup

As explained in Section 3.1.1, installation of the steel strain gages required removal of the concrete covering the reinforcing bar. For Bridges 1 and 3, much of the concrete cover had already spalled and removal of the additional cover did not cause further harm to the bridges. Bridge 2 was scheduled for replacement and therefore the county engineer allowed some concrete removal. Bridge 4, however, was in relatively good condition with only a small amount of spalling and was not scheduled for replacement in the near future. Steel strain gage installation would require an undesirable amount of concrete removal. Therefore, reusable strain gages manufactured by Bridge Diagnostics Incorporated (BDI) of Boulder, Colorado (henceforth referred to as BDI gages) were used in place of the steel strain gages.

Three BDI gages were installed on each PCDB panel; one on each stem and one on the underside of the panel. All gages were located at midspan as shown in Figure 3.28.

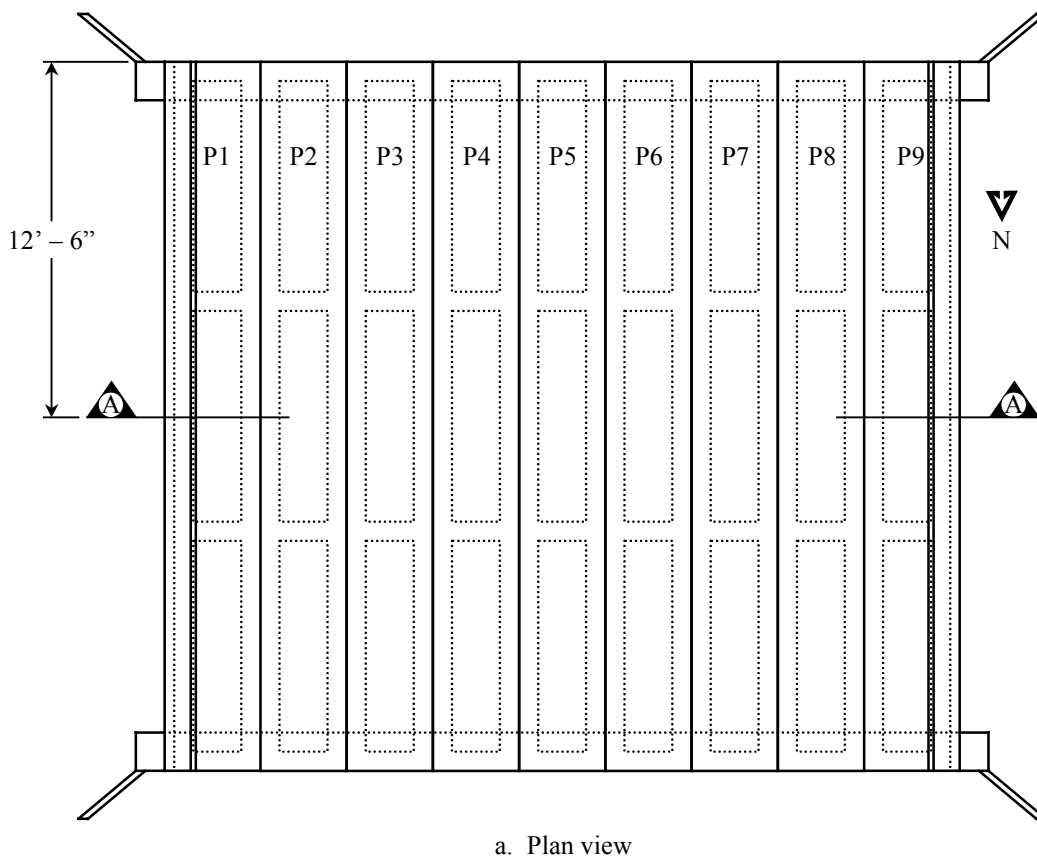


Figure 3.28. Location of strain gages and displacement transducers on Bridge 4.

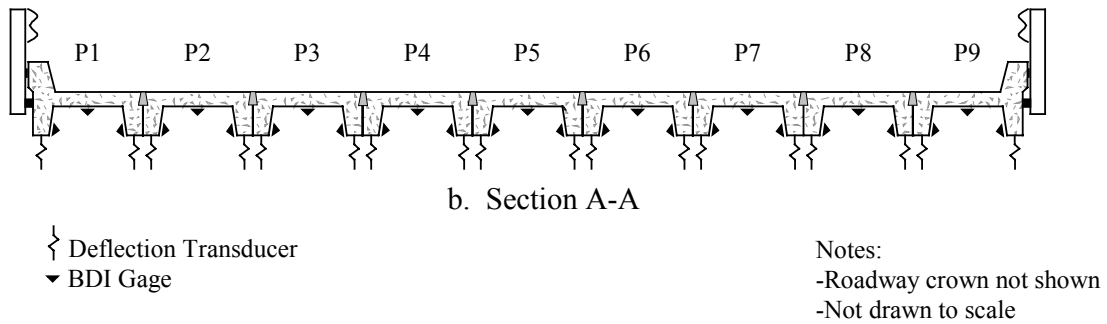


Figure 3.28. Continued.

Quick-setting epoxy was used to rigidly attach the gages to the concrete surface and each gage was orientated to measure longitudinal strain. A typical BDI gage installation is shown in Figure 3.29.

The BDI gages on the panel stems were approximately at the same elevation as the primary steel reinforcing. Therefore, assuming ‘perfect bond’ between the concrete and reinforcing steel, the strains measured by the BDI gages were assumed to equal the actual steel reinforcing strain. Laboratory testing validated this assumption.



Figure 3.29. Typical BDI gage installation.

Similar to the other field service tests, deflection transducers were attached to each panel stem at midspan. Deflection transducer locations are also shown in Figure 3.28. As with the other bridges, tape switches were used to determine the longitudinal position of the test vehicle on the bridge.

### **3.5.3. Test Vehicle and Load Positions**

The test vehicle was a tandem axle dump truck provided by the Story County Engineer. Weight distribution (GVW = 46.98 kip) and dimensions of the test vehicle are presented in Figure 3.30.

Three load positions were investigated in the Bridge 4 service test. Load position locations are shown in Figure 3.31. For load positions 4-LP24.B and 4-LP68.B, the test vehicle was transversely located in the southbound and northbound lanes, respectively. The test vehicle was transversely centered on Bridge 4 for load position 4-LP46.B. For all load positions, the test vehicle reference point was longitudinally located at midspan.

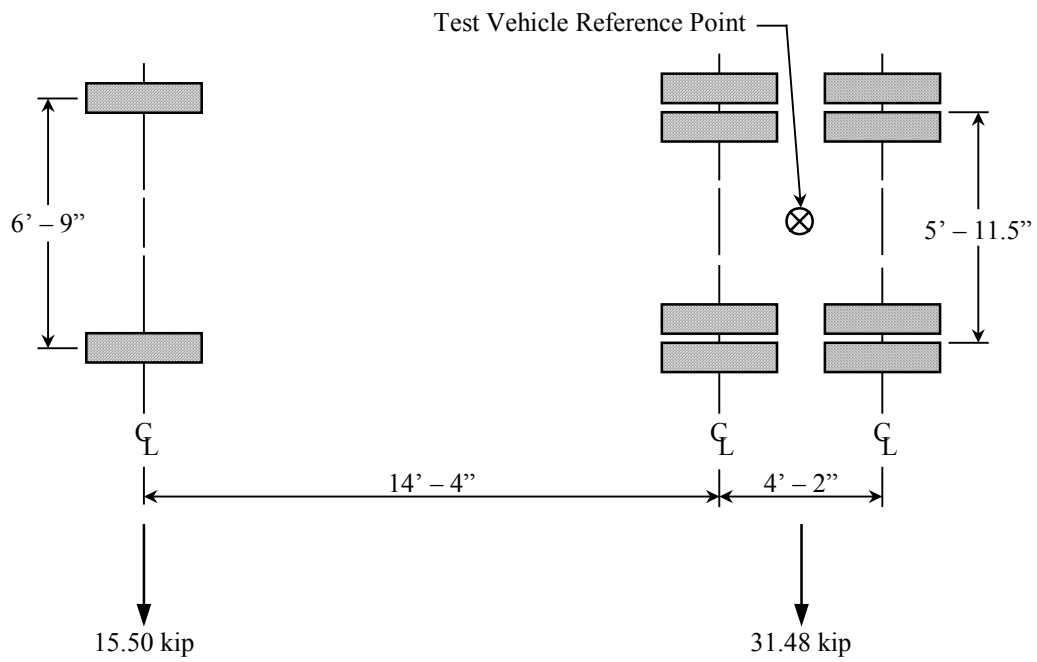
### **3.5.4. Discussion of Results**

Bridge 3 and Bridge 4 were very similar in that each span contained nine Type I PCDB panels and nearly identical load positions were used during testing. The primary performance affecting difference between these two bridges was the absence of grout in the shear keyways of Bridge 4. Comparison of Figure 3.24 and Figure 3.32 clearly reveals the importance of proper shear connection. Relative displacements between the adjacent panels in Bridge 4 were often four to seven times larger than the corresponding values for Bridge 3.

Deflection data shown in Figure 3.32 were used in Equation 1 to calculate experimental load fractions for Bridge 4. The greatest load fraction for each load position is presented in Table 3.4. In comparison to the load fractions for Bridge 3, the load fractions for Bridge 4 were approximately 150% higher. Experimental load fractions for Bridge 4 were, however, nearly equal to the theoretical load fractions. The theoretical one and two lane load fractions (0.59 and 0.61 respectively) are only slightly less than the corresponding experimental load fractions. Rock and dirt in the shear keyways apparently transferred enough load between adjacent panels to achieve satisfactory transverse load distribution.

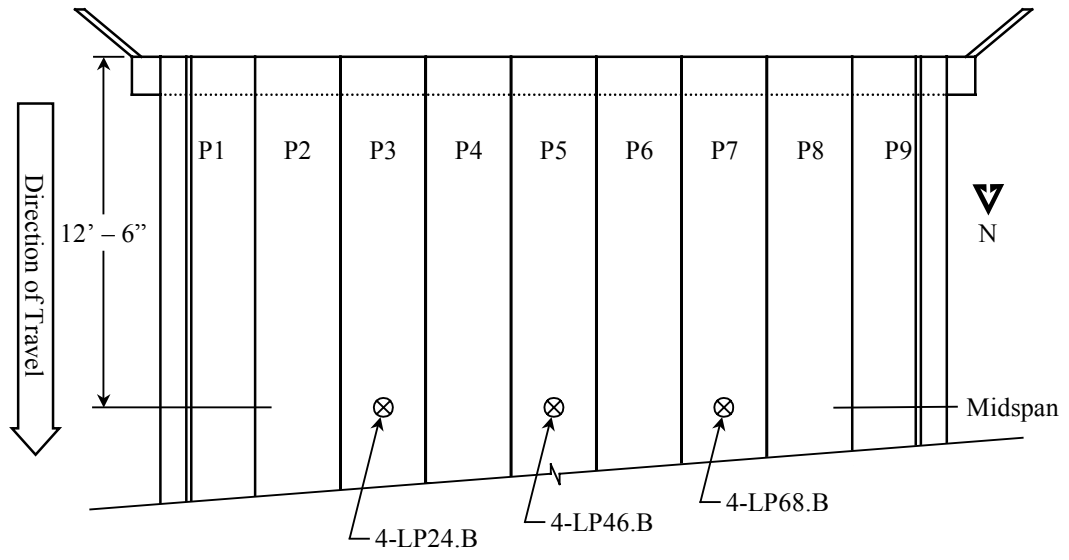


a. Photograph of test vehicle

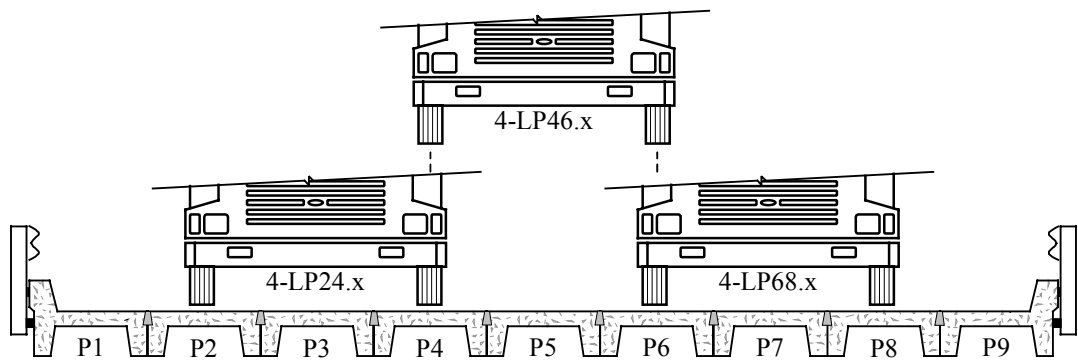


b. Wheel configuration and weight distribution of test vehicle

Figure 3.30. Bridge 4 test vehicle.



a. Load position locations



b. Transverse positioning of test vehicle (looking south)

Figure 3.31. Bridge 4 load positions.

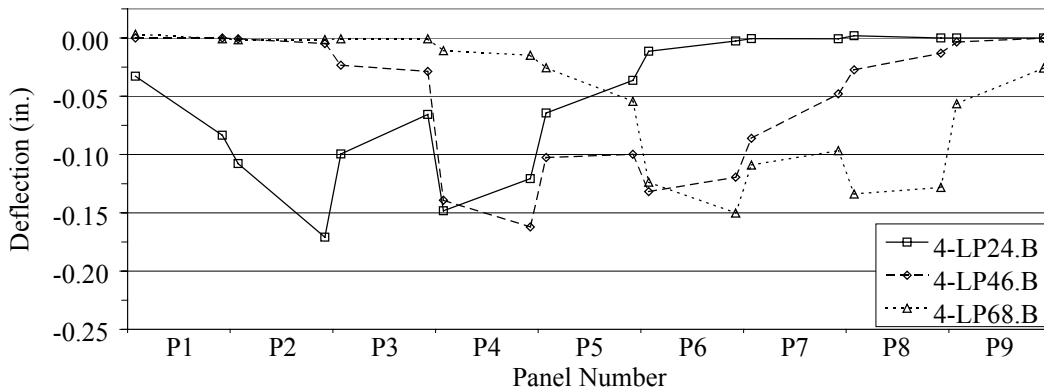


Figure 3.32. Midspan deflection plot for Bridge 4.

Table 3.4. Bridge 4 maximum load fractions.

Load Position			
4-LP24.B	4-LP46.B	4-LP68.B	Two Lane
0.59	0.61	0.59	0.63

Maximum measured deflection for Bridge 4 was 0.14 in. (L/1659). Again, as with the other three PCDBs test, this value is well below the maximum allowable deflection.

The largest strain measured by a BDI gage was 145 MII. Equivalent reinforcing steel stress is 4,205 psi and is far below the allowable steel stress (20,000 psi). Bridge 4, therefore, had sufficient capacity to support legal loads.

### 3.6. Load Rating

Load ratings were performed on Bridges 1 through 4 to determine the ability of each bridge to safely support legal loads. The end result of each rating calculation was a rating factor (RF). When the rating factor was greater than one, the bridge was considered capable of safely supporting the rating vehicle. The bridge was considered deficient when the rating factor was less than one.

There are several load rating methods available; the choice of which method to use for a bridge rating is left to the bridge owner. Available methods include allowable stress, load factor rating (LFR), and load and resistance factor rating (LRFR). The research team selected the load factor rating method of bridge rating based on the assumption that the owners of PCDBs (the respective county secondary road departments) would be most familiar with this method. The Manual for Condition Evaluation of Bridges 1994 (8) outlines the load factor rating method.

Each bridge was load rated at two different levels, inventory and operating, and for two different rating vehicles, HS20 truck and Type 3. Inventory level rating factors represent the ability of a bridge to safely carry the rating vehicle for an indefinite period of time. The ability of a bridge to safely carry a rating vehicle a limited number of times is represented by the operating level rating factor. Operating level is useful for determining if an overload permit vehicle may safely cross a particular bridge.

Rating vehicles were selected to represent traffic served by the PCDBs. The HS20 truck is a hypothetical truck used for bridge design and should induce stresses in a bridge that represent those produced by actual vehicles on the bridge. The Type 3 rating vehicle is similar to the tandem axle dump trucks used as the test vehicle for the field service load testing. Axle spacing and wheel line loads are presented for both rating vehicles in Figure 3.33. Also, for comparison, each bridge was rated for one and two lanes loaded. All four PCDBs tested were two lane bridges but the two bridges on gravel roads, Bridge 2 and Bridge 4, would practically function as one lane bridges.

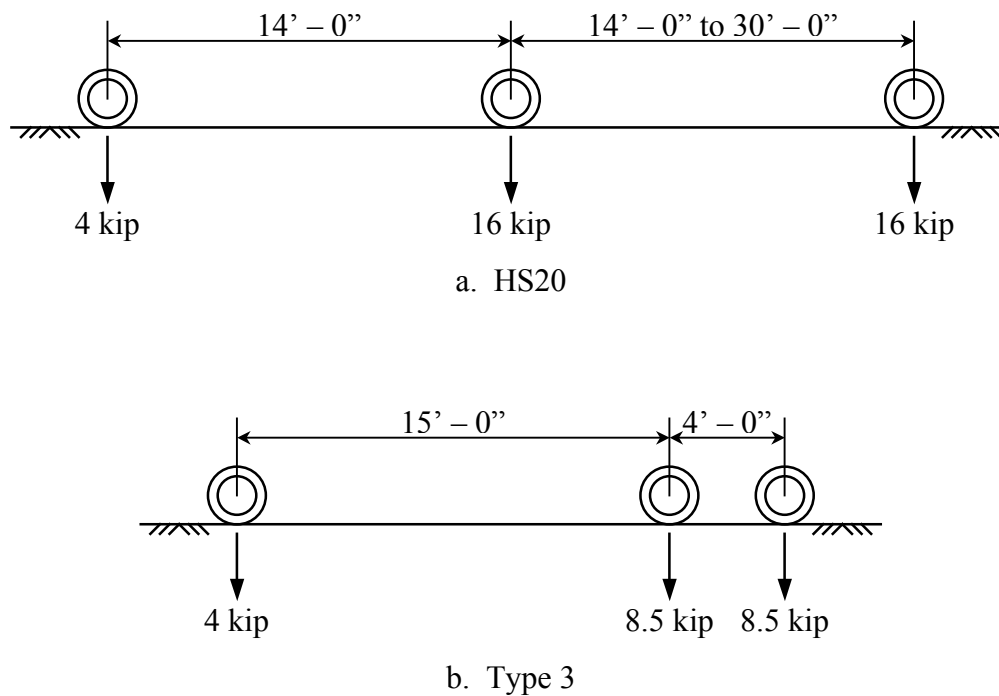


Figure 3.33. Rating vehicles: axle spacing and wheel line loads.

Two sets of rating calculations were performed for each bridge. The theoretical load rating replicates the procedure followed for a standard bridge rating. Calculations utilized load fractions from the AASHTO Standard Specification (6) equations for precast concrete multibeam bridges and the material strengths were taken from the J-10 Standard. The revised load ratings used load fractions calculated from field test data and actual material strengths when known. This dismissed many assumptions on the performance and strength

of the bridge and gave a more accurate bridge rating. For both sets of rating calculations, no reinforcement section loss was assumed. Laboratory testing verified that the amount of reinforcing steel corrosion commonly found on PCDBs does not significantly weaken the panels (see Chapter 4). Rating calculations for all four bridges are presented in Appendix B.

### 3.6.1. Bridge 1 Load Rating

Although the Type II PCDB panels in Bridge 1 were designed to withstand only H20 loading, the theoretical rating factors presented in Table 3.5 show that Bridge 1 can safely support the heavier HS20 loading. This is primarily due to the span length of the bridge in comparison to the length of the HS20 truck. These lengths were approximately equal and therefore one axle was off the bridge when the truck was positioned to induce the maximum possible bending moment in the bridge. Theoretical rating factors show that Bridge 1 could also safely support the Type 3 rating vehicle.

Table 3.5. Bridge 1 rating factors.

Level	Theoretical Rating Factor		Revised Rating Factor	
	HS20	Type 3	HS20	Type 3
One Lane				
Inventory	1.06	1.33	1.52	1.90
Operating	1.78	2.22	2.54	3.17
Two Lane				
Inventory	1.02	1.28	1.38	1.72
Operating	1.71	2.14	2.30	2.88

Bridge 1 had better than expected transverse load distribution and consequently the experimental load fractions were less than the theoretical load fractions. This, combined with actual material strengths that exceed the strengths given in the J-10 Standards, resulted in an increase in the revised rating factors. One lane revised rating factors were 43% greater than the theoretical rating factors and two lane revised rating factors were 25% greater than the theoretical rating factors. This demonstrates the positive benefits of a field service load test.

### 3.6.2. Bridge 2 Load Rating

Theoretical and revised rating factors for Bridge 2 are shown in Table 3.6. Similar to Bridge 1, theoretical rating factors show that Bridge 2 could also safely withstand loads heavier than those for which it was designed. Bridge 2 was constructed of Type II PCDB panels designed for H15 loading. These panels normally span 35 ft but abnormal geometry shortened the span to 30.5 ft. Therefore, the panels were over-designed for the 30.5 ft span and could safely support additional load. Theoretical rating factors for the Type 3 rating vehicle were also greater than one.

Bridge 2 was found to have poor transverse load distribution due to absent shear connectors. Experimental load fractions were greater than the theoretical load fractions. This caused a decrease in the revised rating factors. At inventory level, Bridge 2 was deficient for one and two lane HS20 loading and for two lane Type 3 loading. Deficient bridges are always a cause for concern but in the case of Bridge 2, some of this concern may be dismissed due to the location of this bridge. Located on a dead end gravel road, this bridge carries only a few vehicles per day and is unlikely to carry vehicles in both lanes simultaneously. Bridge 2 primarily serves farm vehicles and milk trucks similar to the Type 3 rating vehicle. As shown in Table 3.6, the revised rating factor for a single lane Type 3 loading is greater than one and therefore can safely support loads of this type for an indefinite period of time. All operating level rating factors were greater than one.

Table 3.6. Bridge 2 rating factors.

Level	Theoretical Rating Factor		Revised Rating Factor	
	HS20	Type 3	HS20	Type 3
One Lane				
Inventory	1.15	1.43	0.95	1.19
Operating	1.92	2.39	1.59	1.98
Two Lane				
Inventory	1.13	1.40	0.67	0.83
Operating	1.88	2.34	1.12	1.39

### 3.6.3. Bridge 3 Load Rating

Bridge 3 was constructed of Type I PCDB panels designed for H15 loading. HS20 loading is considerably greater than H15 loading and theoretical rating factors presented in Table 3.7 show that Bridge 3 cannot safely support the HS20 rating vehicle at inventory levels. For the Type 3 rating vehicle at inventory levels, theoretical rating factors were only slightly greater than one.

Grouted shear keys in Bridge 3 resulted in excellent transverse load distribution and the experimental load fractions were less than the theoretical load fractions. Consequently, revised rating factors were greater than the theoretical rating factors. Increased load distribution, however, did not raise all rating factors above one. Bridge 3 was found deficient for the two lane HS20 loading at inventory level. This is cause for concern since Bridge 3 was on a paved road and loaded vehicles could occupy both lanes simultaneously. All other revised rating factors were greater than one.

Table 3.7. Bridge 3 rating factors.

Level	Theoretical Rating Factor		Revised Rating Factor	
	HS20	Type 3	HS20	Type 3
One Lane				
Inventory	0.83	1.04	1.14	1.43
Operating	1.38	1.73	1.91	2.39
Two Lane				
Inventory	0.81	1.01	0.86	1.07
Operating	1.35	1.68	1.43	1.79

### 3.6.4. Bridge 4 Load Rating

Bridge 4 was similar to Bridge 3 in that both were constructed of Type I PCDB panels designed for H15 loading. As expected, theoretical rating factors for the heavier HS20 loading at inventory level were less than one. Theoretical rating factors for the Type 3 rating vehicle were nearly equal to one at inventory level. At operating level, all theoretical rating factors were greater than one. All rating factors are presented in Table 3.8.

The absence of grouted shear keys in Bridge 4 caused the experimental load fractions to be slightly more than the theoretical load fractions. Revised rating factors were therefore

approximately 2% - 4% less than the theoretical rating factors. At inventory level, all revised rating factors were less than one. All revised operating rating factors were again greater than one.

Table 3.8. Bridge 4 rating factors.

Level	Theoretical Rating Factor		Revised Rating Factor	
	HS20	Type 3	HS20	Type 3
One Lane				
Inventory	0.90	1.02	0.87	0.98
Operating	1.50	1.71	1.45	1.64
Two Lane				
Inventory	0.86	0.98	0.84	0.95
Operating	1.44	1.64	1.40	1.59

### 3.6.5. PCDB Load Rating Recommendations

The following recommendations are for county engineers and consultants use in the load rating of PCDBs. Use of these recommendations should be limited to bridges similar to those described and tested in this investigation – those constructed with Type I or Type II PCDB panels, with or without shear connectors in place, and with exposed and corroding primary reinforcing. Although the majority of PCDBs meet these criteria, an engineer may encounter PCDB panels with significantly more deterioration than the ones tested in this investigation, such as significant section loss in the reinforcement and/or substantial deck deterioration. In such cases, the following recommendations may not be applicable since very little testing was performed on severely deteriorated panels. As in any situation, the engineer is advised to exercise his/her best judgment in applying these recommendations.

- *Live load distribution* – For PCDBs with shear connectors in place, load fractions should be calculated in accordance with AASHTO Standard Specification [6] Equations (3-11 thru 3-14). It has been shown in this investigation that load fractions from these equations are consistently on the conservative side of the actual load fractions when shear connectors are in place. If the shear connectors are not properly installed, the recommended load fraction for one-lane loading is 0.7. Similarly, for two-lane loading, the recommended load fraction is 1.0.

- *Panel capacity* – A conservative value for nominal flexural strength ( $M_n$ ) may be obtained from the specified concrete and reinforcement strengths ( $f'_c=5,000$  psi and  $f_y=40,000$  psi) and cross sectional properties presented in Chapter 2. If known, the actual concrete strength may also be used. In the following chapter it will be shown that the actual strength of a typical deteriorated panel was consistently greater than the nominal strength calculated according to the above method. Additional capacity stemmed from actual material strengths that consistently exceed the specified material strengths. Furthermore, loss of reinforcement cross sectional area was found to have a negligible affect on panel strength. Thus, the full area of reinforcing steel may be used in the strength calculation.

Load rating calculations for all four field tested PCDBs are presented in Appendix B to further assist an engineer in load rating a PCDB.



#### **4. LABORATORY TESTING OF INDIVIDUAL PCDB PANELS**

A total of sixteen PCDB panels were tested in the Town Engineering Structures Laboratory. The panels were obtained from PCDB replacement projects in Cedar County, Butler County and Black Hawk County. All panels were Type II (H20) PCDB panels and were representative of the panels commonly found in deteriorated PCDBs. The primary purpose of the laboratory testing was to determine the behavior, the ultimate strength, and the failure mode of the deteriorated panels. Ultimate strength was useful for determining the reduction in strength due to deterioration and whether load rating reductions were necessary.

In this chapter, the testing program used in the load testing of individual PCDB panels is presented; load test results are also presented and are summarized according to the county of origin. Results from one load test, Cedar 1, are discussed in detail; these results are similar to those of all load tests performed.

##### **4.1. Individual PCDB Panel Load Testing Program**

In the following four sections, the general testing program for the individual PCDB panels is presented.

###### **4.1.1. Instrumentation**

The PCDB panels tested in the laboratory were instrumented in a manner similar to the bridges tested in the field. Electrical resistance strain gages were used to measure both concrete and reinforcing steel strains, and string potentiometer displacement transducers were used to measure vertical deflections. Strain and deflection measurements were recorded by a Hewlett-Packard 3852A computer controlled DAS.

The majority of the instrumentation was placed at midspan for all panels. A diagram of the “standard” instrumentation used for most load tests is shown in Figure 4.1. Steel strain gages were bonded to the lower pair of primary reinforcing bars and the concrete strain gages were bonded to the deck. Deflection transducers measured the vertical displacement of each stem.

Additional instrumentation was installed on several panels to further investigate reinforcement development and symmetry. Steel strain gages bonded to both the upper and

lower pairs of reinforcement bars at the quarterpoints indicated bond development. Deflection transducers positioned at the quarterpoints verified the symmetry.

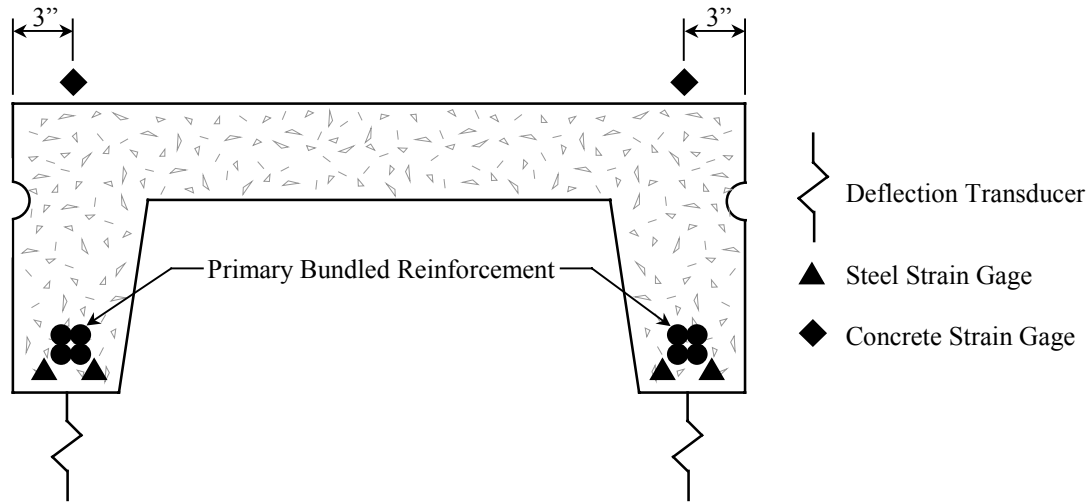


Figure 4.1. Typical midspan at instrumentation.

#### 4.1.2. Loading Setup

Each PCDB panel was loaded in a four point bending arrangement as shown in Figure 4.2. The main components of the load setup were two hydraulic actuators and a reaction frame. Hydraulic actuators were 100 ton hollow core double acting actuators. The two actuators were connected in parallel with hydraulic hoses to assure equal pressure to each actuator. Hydraulic pressure was supplied by either an electric or hand operated hydraulic pump. As shown in Figure 4.3, each actuator was positioned on a bearing pad, steel plate, and load cell. The elastomeric bearing pad (12 in. x 12 in. x 1 in.) and steel plate (12 in. x 12 in. x 1 in.) evenly distributed load to the PCDB panel, and the load cell electronically measured the magnitude of load applied. To create a pure bending region between the actuators, they were centered transversely and longitudinally (6 ft apart) on the panel.

The reaction frame (see Figure 4.3) consisted of two structural tubes (12 in. x 6 in. x 3/8 in.) and post-tensioning tendons (1 in. Dywidag Threadbar) which transferred the applied load to the structural tie down floor. Two smaller steel bracing tubes (6 in. x 6 in. x 1/4 in.) prevented the reaction frame from deflecting parallel to the panel during testing.

Each end of the PCDB panel rested on elastomeric bearing pads (8 in. wide x 1/4 in. thick) positioned on steel abutments that were fabricated from two stiffened W21 x 83 sections. Length of bearing was 8 in. One end of the specimen had a pin support while the other end had a roller support. An overall view of the test setup is shown in Figure 4.4.

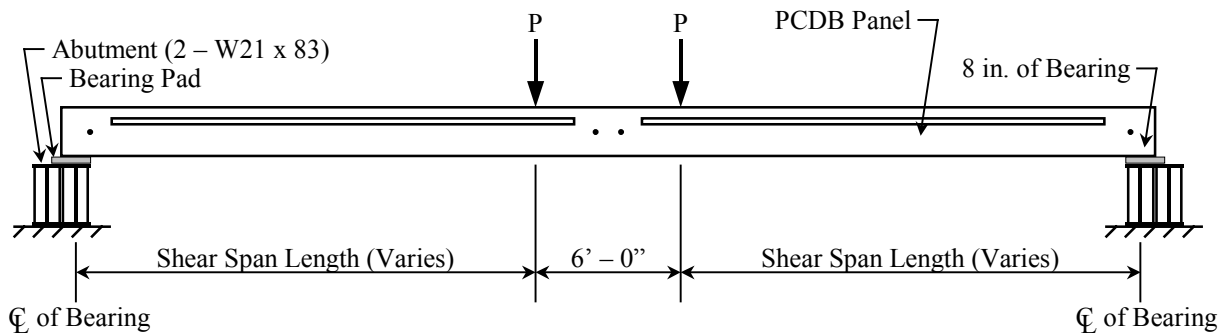


Figure 4.2. Side view of loading setup for individual panel tests.

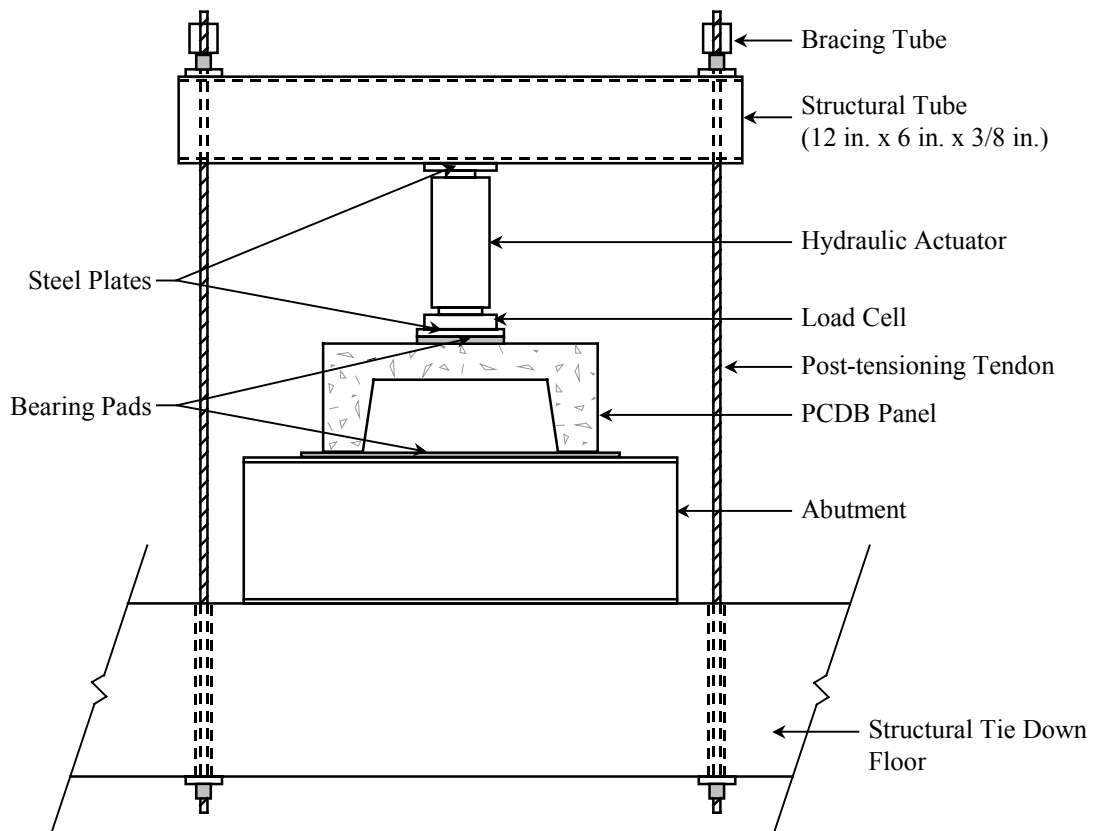


Figure 4.3. Cross-section view of loading setup for individual panel load tests.

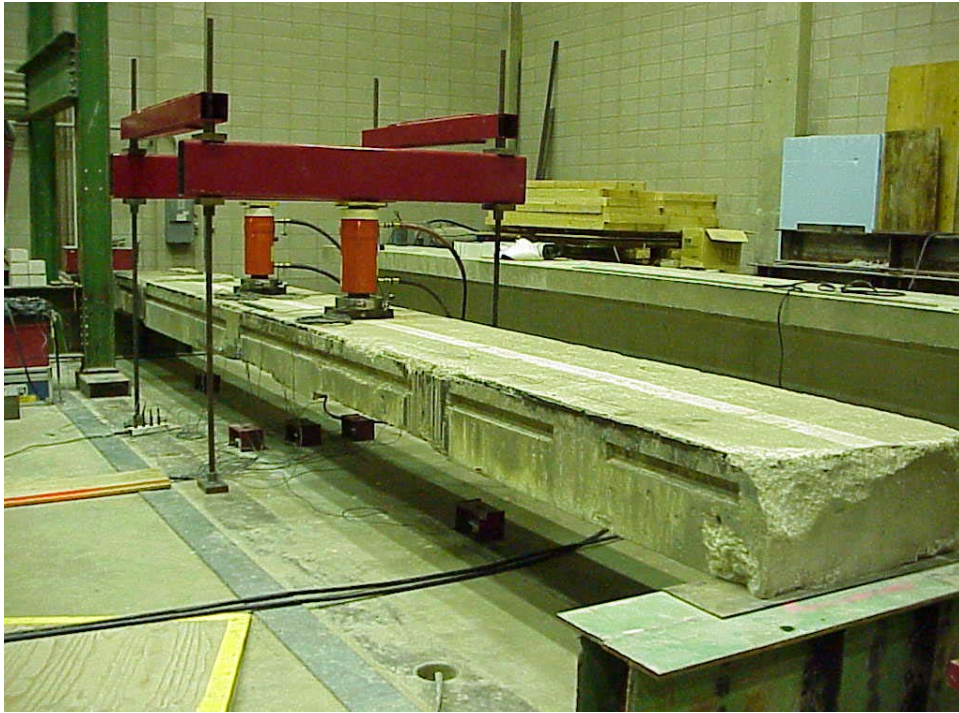


Figure 4.4. Photograph of loading setup for individual panel load tests.

#### **4.1.3. Test Procedure**

Prior to loading, the strain gages and deflection transducers were initialized by the DAS. Load was then slowly applied to the panels. During the elastic portion of the loading, the DAS was programmed to record load, strain, and deflection data at specified load intervals. The interval was typically every 2 or 4 kips of load per actuator. Once the primary reinforcing steel yielded, data were recorded at approximately every 0.1 in. of center deflection. Periodically during the test, the progression of flexural and shear cracks were observed and photographs were taken. The load test was terminated when the panel failed.

#### **4.1.4. Material Properties**

To determine the actual strength of the concrete and reinforcing steel in the panels, samples of these materials were obtained from each group of panels following the load testing. Concrete compression strength was found in accordance to ASTM C 39 (9) and C 42 (10). Full depth 2 in. diameter concrete cores were cut from the deck of the panels using a power core saw. A trial-and-error method was necessary to obtain cores that did not contain reinforcing steel. Following the coring, both ends of each core were trimmed with a

water-cooled cut-off saw. The saw cut was perpendicular to the axis of the cores and was quite smooth; thus the cores did not require capping. A minimum of five cores was tested for each group of panels. The concrete compression strength ( $f_c'$ ) for each group of panels was taken as the average compression strength for the respective group of cores.

Samples of the primary reinforcing steel were removed from each group of panels and tested to determine the yield strength. Samples approximately 3 ft in length were removed from the panel ends using an electric jackhammer and acetylene cutting torch. Prior to testing, a small area near the center of each bar was ground smooth and a strain gage was bonded to the prepared surface. During the tension test, axial load and strain data were continuously recorded using a DAS. The data were used for drawing stress-strain curves, and the yield stress was taken at a 0.02% offset. Cross-sectional area of the bar was taken as the nominal area for the respective bar. A minimum of three bars was tested from each group of panels. The reinforcing steel yield strength ( $f_y$ ) for each group of panels was taken as the average yield strength for the respective set of tension tests.

## **4.2. Test Results**

### **4.2.1. Overview**

In each PCDB panel load test, both elastic and inelastic behaviors were observed. For elastic behavior, steel strains, concrete strains, and deflections were nearly proportional to the midspan bending moment. At all locations, stress in the primary reinforcing steel was below the yield stress of the steel. Elastic behavior ended and inelastic behavior began when the stress in the primary reinforcing steel at midspan exceeded the yield stress of the steel. During inelastic behavior, midspan strains and deflections increased substantially while the midspan moment either remained constant or increased only slightly. The load test concluded when a failure occurred. For all PCDB panels tested, the failure mode was a compressive failure of the concrete deck. The largest bending moment sustained by the panel during the load test was considered to be the ultimate strength of the panel.

For each panel, a moment/deflection curve was constructed by plotting midspan bending moment against midspan vertical deflection. The moment/deflection curves were useful for comparing the behavior of the individual panel in a particular group of panels and for detecting the point where elastic behavior ceased and inelastic behavior began for each

individual panel. This point, hereafter referred to as the yield point, was the last data point on the linear portion of the moment/deflection curve.

The yield point midspan bending moment and the corresponding midspan deflection were used to calculate the stiffness of each panel. These values were substituted into a theoretical load/deflection equation for a simply supported beam subjected to two symmetrically placed concentrated loads. For each group of panels, appropriate span lengths and shear span lengths were also incorporated into the equation. The equation was then solved for the remaining unknown variable, flexural rigidity ( $EI$ ). This value was then used to calculate stiffness ( $4EI/L$  where  $L$ =span length).

Design and theoretical ultimate strengths were calculated and compared to the experimental ultimate panel strengths. Design ultimate strength calculations took the reinforcement yield strength ( $f_y$ ) as 40,000 psi and the concrete compressive strength ( $f'_c$ ) as 5,000 psi. These values were specified by the J-10 Standard. The purpose of this calculation was to replicate calculations performed during the rating of PCDB panels.

Actual reinforcing steel and concrete strengths were found to exceed the values given in the J-10 Standard. Consequently, the experimental strengths were typically greater than the design ultimate strengths. In an attempt to increase accuracy of the calculated ultimate strengths, theoretical ultimate strength calculations using the measured material properties were completed. The stress on the steel stress-strain curve that corresponded to the average measured steel strain at failure was substituted for the reinforcement yield strength ( $f_y$ ). The concrete compressive strength ( $f'_c$ ) was taken as the average compressive strength for a group of panels as previously described. Theoretical ultimate panel strengths were typically in good agreement with the experimental ultimate panel strengths.

Theoretical steel strains, concrete strains, and vertical midspan deflections were calculated at several midspan moment intervals within the elastic portion of the load test. A “cracked” section was assumed and actual material properties were used in the calculations. Effective moment of inertia, as defined by ACI (7), was used in the theoretical deflection calculation. Theoretical strains and deflections compared well with the experimentally measured values.

Maximum moment produced by single lane AASHTO HS20 loading was calculated and plotted on the moment/deflection curve for each group of panels. A load fraction of 0.6, which is representative of the theoretical load fraction calculated for the four field load tests, was used in this calculation.

#### **4.2.2. Cedar County Panels**

Eight Type II (H20) PCDB panels were obtained from a PCDB replacement project in Cedar County, Iowa. The three-span bridge was on a paved county road and had an asphalt cement concrete (ACC) wearing surface. This surface was removed prior to the load testing. Deterioration damage consisted of longitudinal cracks in the panel stems and some exposed reinforcement. Extent of the deterioration damage varied from panel to panel.

Seven of the eight Cedar County panels were standard interior panels (henceforth referred to as Cedar 1-7). The eighth panel (henceforth referred to as Cedar 8) had a monolithically cast concrete curb. Cedar 1, 2, 3, and 8 were tested in their existing condition. The remaining four interior panels were used to construct a laboratory bridge and were later fitted with a strengthening system. Results from ultimate load testing on one strengthened panel are presented in Section 6.3.1.

Standard instrumentation, as described in Section 4.1.1, was applied to the Cedar County panels. Additional instrumentation was applied to Cedar 1 to measure steel strain and displacement at the quarterpoints. At each quarterpoint, steel strain gages were bonded to all four primary reinforcing bars in one panel stem and a displacement transducer was positioned directly below the panel's transverse center.

##### **4.2.2.1. Cedar 1**

Flexural cracks appeared in the panel stems during the elastic stage of the Cedar 1 load test. These cracks originated at the bottom of the stem and the crack tips progressed upward as the load increased. Flexural crack width increased greatly during the inelastic stage of the test, as did the width of pre-existing longitudinal cracks near the primary reinforcing bars. New longitudinal cracks also formed and several pieces of concrete covering the primary reinforcing steel fell from the panel just prior to failure. Experimental ultimate strength of Cedar 1 was 466 ft-kip.

A photograph of the failure is presented in Figure 4.5. Imminent failure was indicated by popping noises from the deck surface. Failure began when one edge of the deck ruptured between the load points. A series of small ruptures then quickly progressed across the deck to the opposite edge. A few seconds later, a large sheet of concrete approximately 30 in. by 24 in. by 1.5 in. thick sheared loose from the panel deck. After the load was removed, it was determined that the ruptured concrete extended down to the level of the upper layer of the longitudinal deck reinforcement.

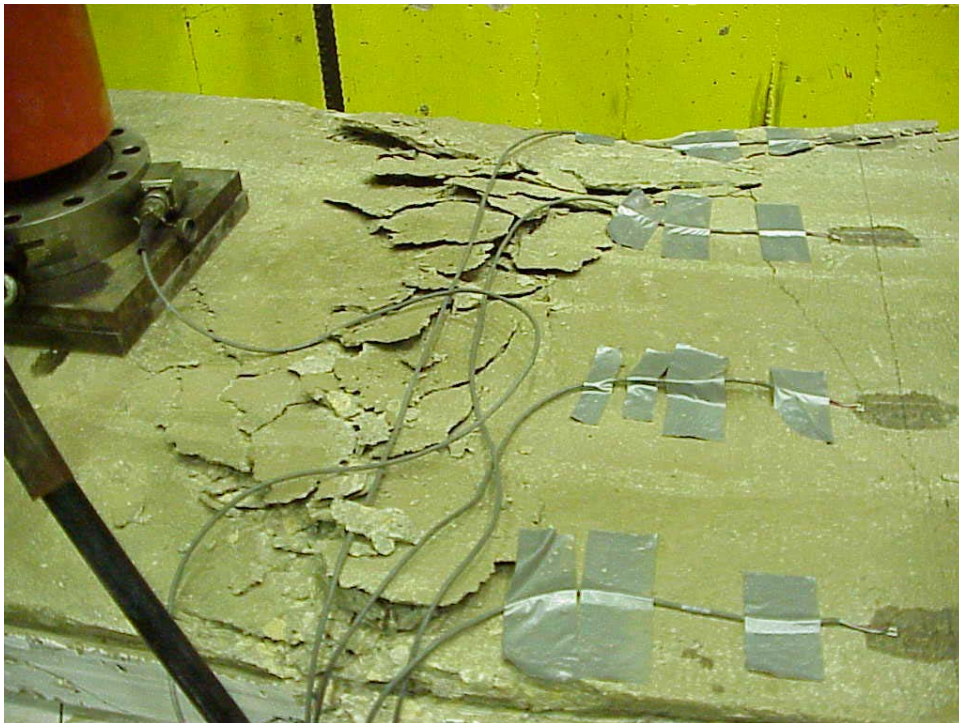


Figure 4.5. Line of ruptured concrete across the deck of Cedar 1.

Quarterpoint and midspan vertical deflections for four values of midspan moment are presented in Figure 4.6. The first two moment values were in the elastic range while the last two moment values were in the inelastic range (the failure strength being the last value). As can be seen, quarterpoint deflections remained symmetric throughout the load test. Midspan vertical deflection at failure was 7.15 in.

Similarly, average steel strain at each quarterpoint and midspan location for the same four midspan moments are presented in Figure 4.7. When panel behavior was elastic, theoretical steel strains compared favorably with the measured steel strains. For example, at

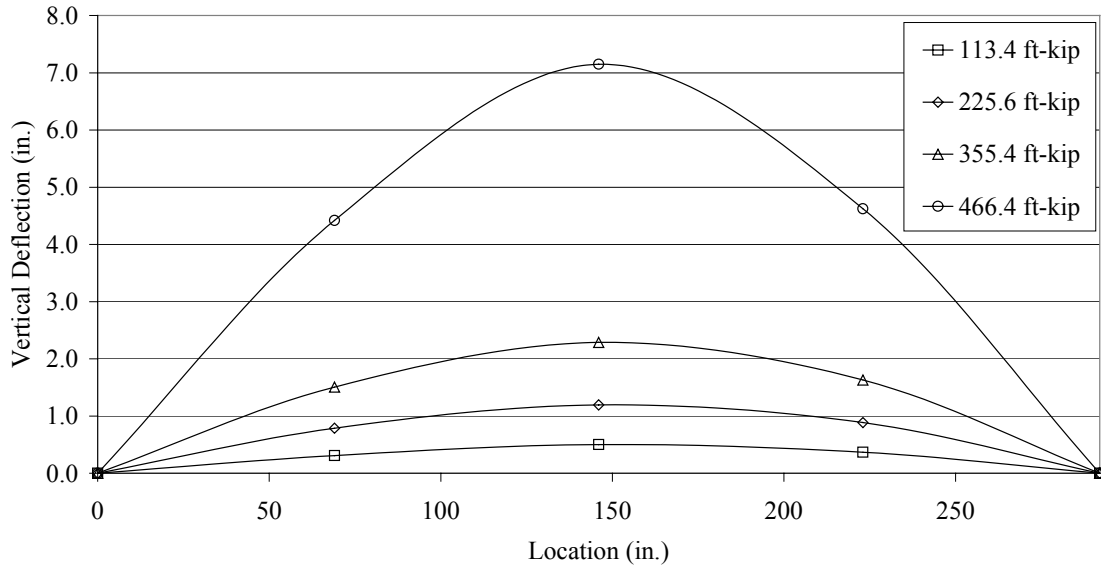


Figure 4.6. Vertical deflection along the length of Cedar 1.

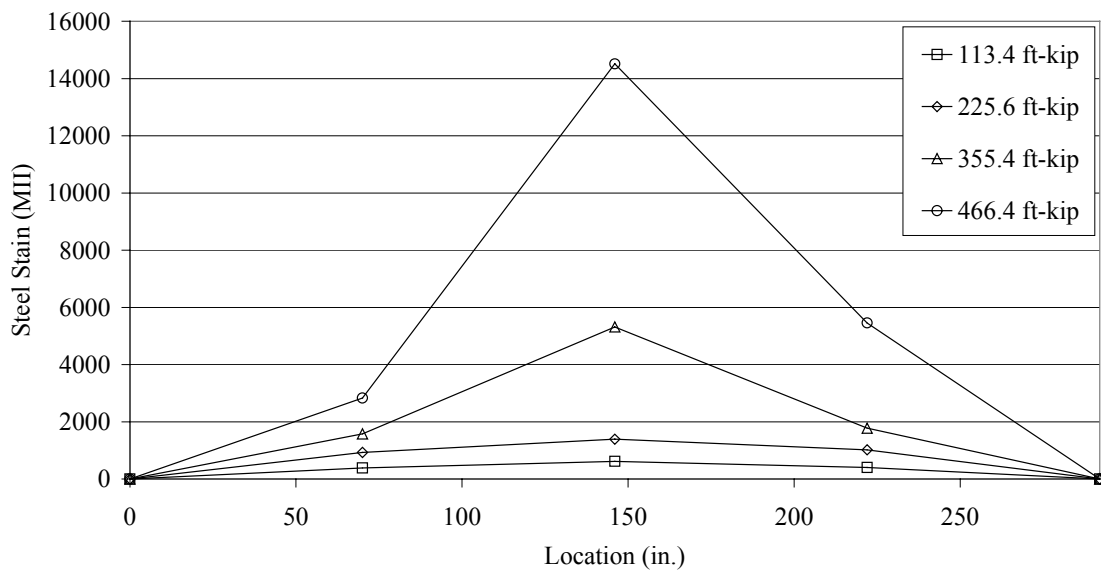


Figure 4.7. Steel strains along the length of Cedar 1.

a midspan moment of 225.4 ft-kip, the calculated quarterpoint and midspan steel strains were 1,002 MII and 1,378 MII, respectively. Corresponding average measured quarterpoint and midspan steel strains were 974 MII (26,100 psi, assuming  $E_s = 29,000,000$  psi) and 1,390 MII (37,000 psi). The good correlation between the calculated and measured strains indicates adequate bond development. The largest measured steel strain prior to failure was 14,515 MII (yield strain = 2300 MII). Quarterpoint steel strains were symmetric for the first three midspan moment values but deviated from each other for the largest midspan moment. The strain increase at the right quarterpoint was likely due to the development of a crack in the concrete at the strain gage location.

A moment/deflection curve and theoretical midspan deflections for Cedar 1 are presented in Figure 4.8. Similarly, a moment/steel strain curve and moment/concrete strain curve for Cedar 1 are presented in Figure 4.9 and 4.10, respectively. All theoretical values correlated well the corresponding experimental values. Due to the similarity between these three curves, only moment/deflection curves are presented for the other panels discussed in subsequent sections.

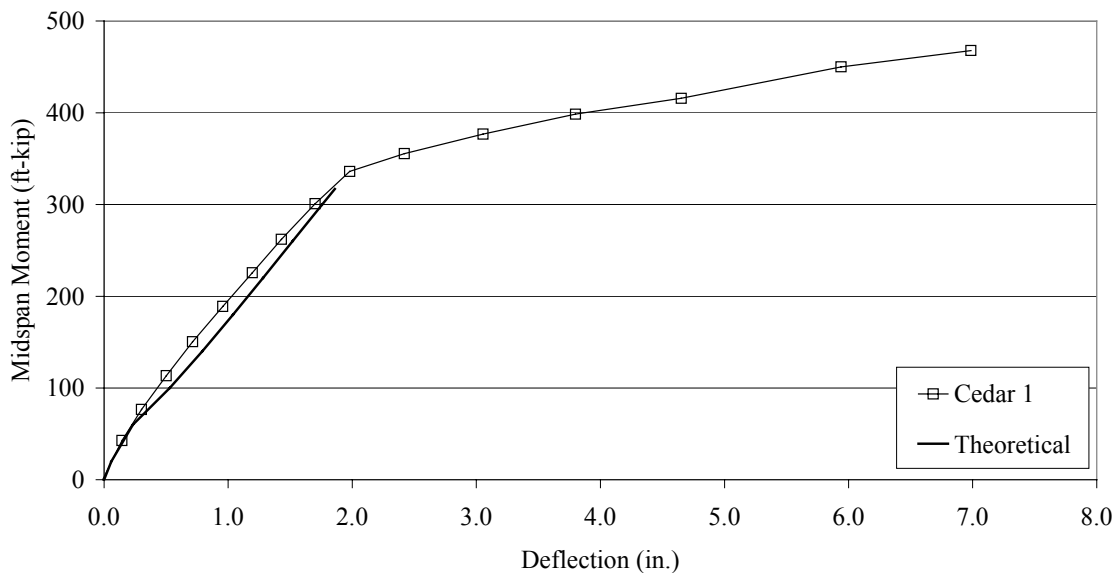


Figure 4.8. Midspan moment vs. midspan deflection for Cedar 1 ultimate strength test.

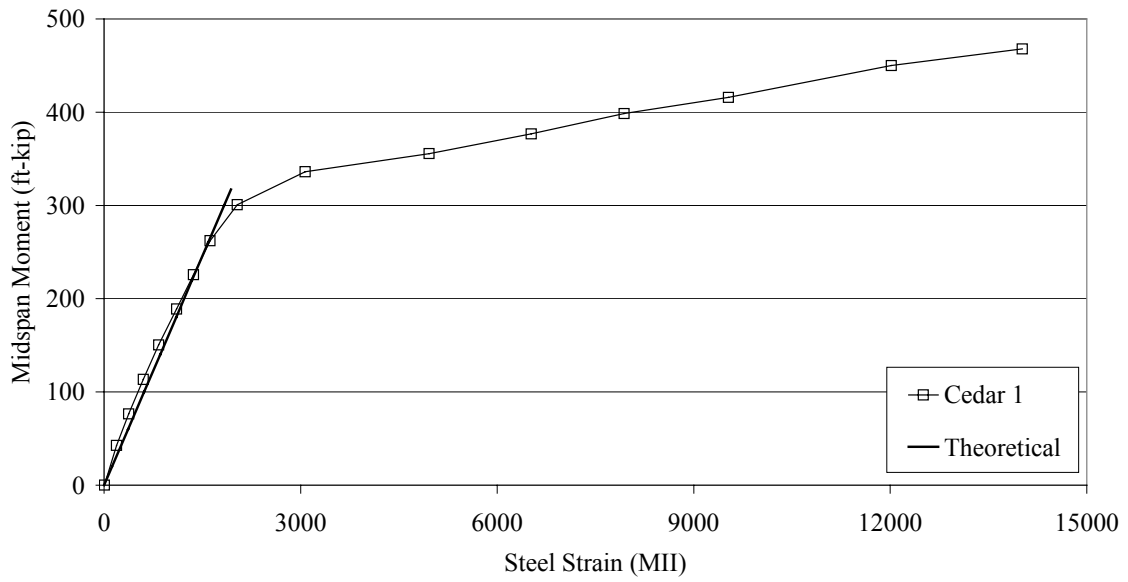


Figure 4.9. Midspan moment vs. midspan steel strain for Cedar 1 ultimate strength test.

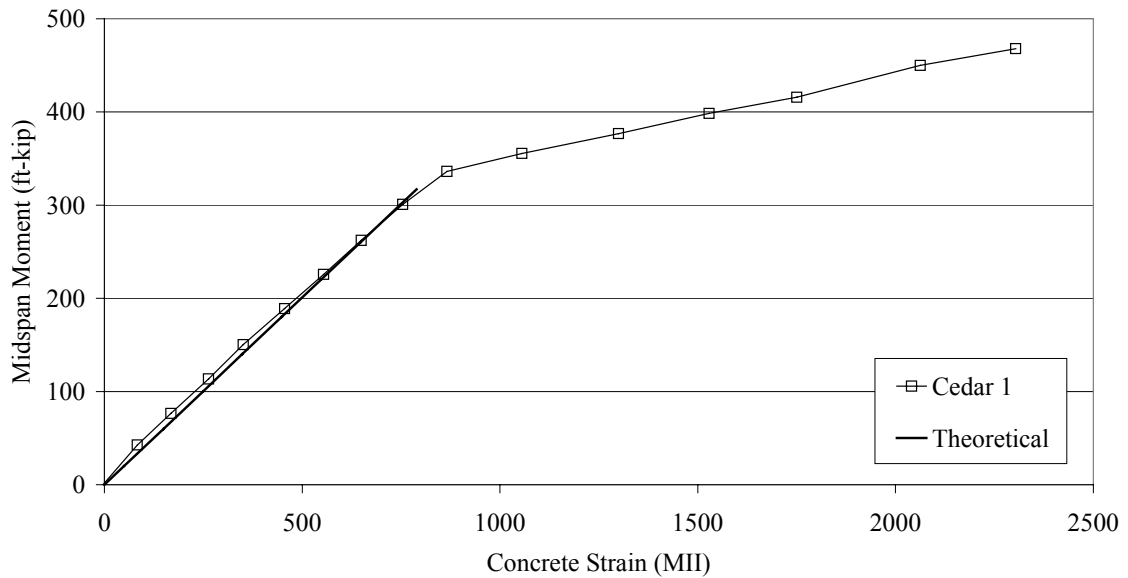


Figure 4.10. Midspan moment vs. midspan concrete strain for Cedar 1 ultimate strength test.

#### 4.2.2.2. Discussion of Results for Cedar 1-3 and Cedar 8 Load Tests

Moment/deflection curves for Cedar 1-3 and Cedar 8 are presented in Figure 4.11. Cedar 1-3, the three interior panels, displayed nearly identical behavior throughout the entire elastic range. In the inelastic range, behavior of these three panels deviated only slightly. Although the amount of deterioration varied between these three panels, the close correlation of the test data indicates that the deterioration had essentially no effect on the strength of the panels.

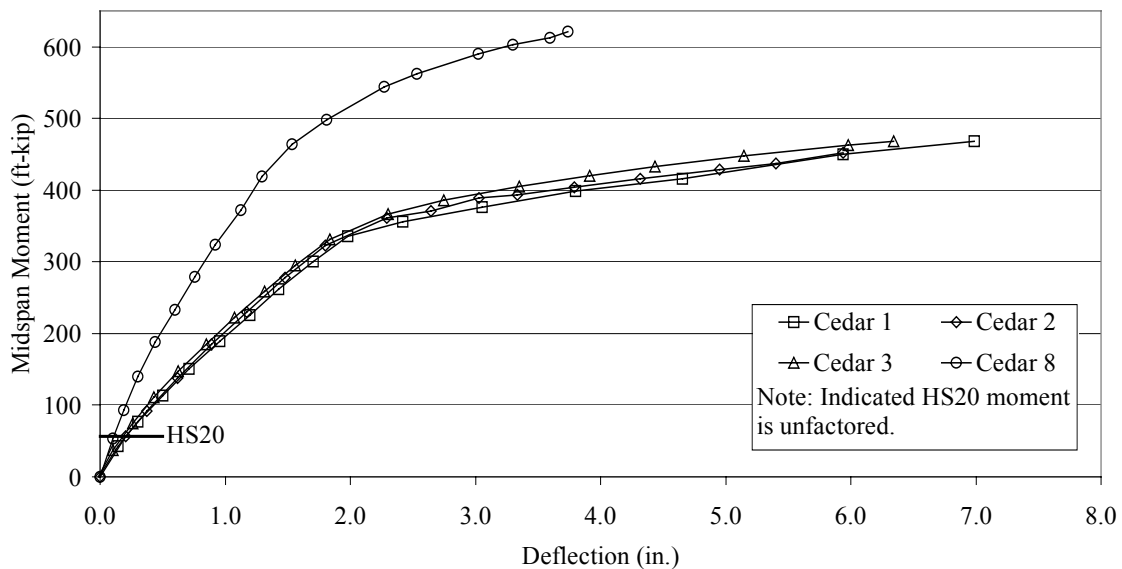


Figure 4.11. Midspan moment vs. midspan deflection for Cedar 1, 2, 3 and 8 ultimate strength tests.

Experimental ultimate strengths, shown in Table 4.1, ranged from 466 ft-kip for Cedar 1 to 488 ft-kip for Cedar 2. Experimental ultimate strengths more than doubled the design ultimate strengths. This large discrepancy is due to the significant increase in actual material strengths over the J-10 Standard material strengths. Actual reinforcement yield strength was 59,200 psi, or 48% higher than the J-10 Standard reinforcement yield strength and actual concrete compressive strength was 10,000 psi, or 100% higher than the J-10 Standard concrete compressive strength. Theoretical ultimate strengths had good correlation with the experimental ultimate strengths.

Table 4.1. Ultimate strengths and stiffnesses for Cedar 1, 2, 3 and 8.

Panel	Ultimate Strength (ft-kip)			Flexural Rigidity (kip-ft)	Stiffness (kip-ft)
	Experimental	Design	Theoretical		
Cedar 1	466	210	452	122,200	20,100
Cedar 2	488	210	467	128,800	21,200
Cedar 3	469	210	466	129,600	21,300
Cedar 8	621	351	541	233,300	38,400

Live load moment for a single lane HS20 loading, as shown in Figure 4.11, was 56.5 ft-kip. This value is well below the yield moment and is only 12% of the average experimental ultimate strength.

The curb on Cedar 8 increased both panel stiffness and ultimate strength. Panel stiffness for Cedar 8 was 38,400 kip-ft; an 84% increase over the average interior panel stiffness (20,900 kip-ft). Ultimate strength increased 31% to 621 ft-kip.

Although Cedar 8 was stiffer and stronger, this panel was also less ductile than the interior panels. Midspan vertical deflection at failure for Cedar 8 was 3.74 in.; 2.68 in. less than the average interior panel deflection at failure. Distance from the neutral axis to the extreme compression fiber was greater for Cedar 8 and therefore concrete in the curb reached failure sooner. As shown in Figure 4.12, failure mode was a compression failure of the concrete curb.

#### **4.2.3. Butler County Panels**

Four 31 ft long Type II (H20) PCDB panels were obtained from Bridge 1 (Butler County Bridge – see Section 3.2). Shortly after the service load test, this bridge was replaced due to the deterioration of the PCDB panels. The research team selected four panels from this bridge (henceforth referred to as Butler 1-4) and had them transported to the Town Engineering Structures Laboratory.

Butler 1, 2 and 4 had significant deterioration. Several 2 ft to 4 ft lengths of primary reinforcing steel were exposed in each stem of these panels. This exposed reinforcement was extensively corroded. Longitudinal cracks in areas of intact concrete cover indicated corrosion of the underlying reinforcement.



Figure 4.12. Failed curb on Cedar 8.

Butler 3 had significantly more deterioration than the other three panels. In addition to exposure of most of the primary reinforcement, there was delamination of the deck at the upper layer of longitudinal deck reinforcement. Missing concrete had been replaced with an ACC patch. Concrete under this patch was found to be in a fractured, ‘rubble-like’ condition. This deck deterioration is shown in Figure 4.13. During transport to the laboratory, one end diaphragm weakened by deterioration became detached from the panel.

#### *4.2.3.1. Discussion of Results for Butler 1-4 Load Tests*

Moment/deflection curves for Butler 1-4 are presented in Figure 4.14. Data were nearly identical for Butler 1 and 2 throughout the entire load test. Experimental ultimate strengths for Butler 1 and 2 were 349 ft-kip and 364 ft-kip, respectively. Behavior of these two panels differed only in ductility. Midspan vertical deflection for Butler 1 was 7.85 in. and midspan vertical deflection for Butler 2 was 9.34 in.

One end of Butler 4 was damaged during an attempt to investigate development. Therefore, the shear span for the ultimate strength load test of this panel was shortened by 19 in. This change resulted in a slight increase in the stiffness of Butler 4. Flexural rigidities and stiffnesses for Butler 1-4 are presented in Table 4.2.



Figure 4.13. Deck deterioration in Butler 3.

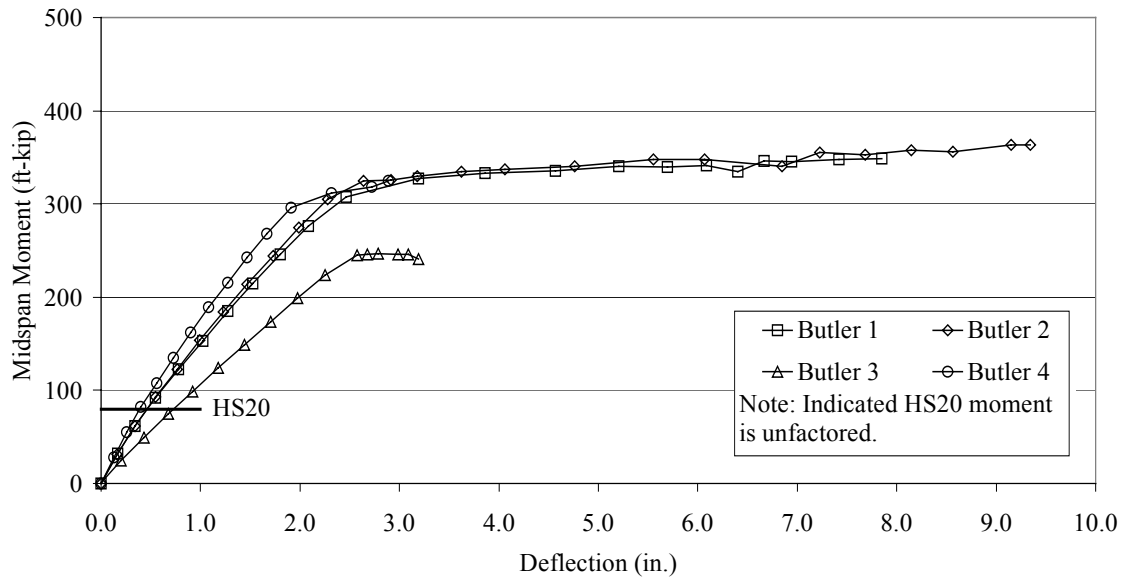


Figure 4.14. Ultimate strength tests of Butler 1-4: midspan moment vs. midspan deflection.

Table 4.2. Ultimate strengths and stiffnesses of Butler 1-4.

Panel	Ultimate Strength (ft-kip)			Flexural Rigidity (kip-ft)	Stiffness (kip-ft)
	Experimental	Design	Theoretical		
Butler 1	349	267	330	143,600	18,900
Butler 2	364	267	332	145,100	19,100
Butler 3	246	267	333	107,600	14,200
Butler 4	325	267	333	136,900	20,200

Butler 4 was less ductile than Butler 1 and 2. Midspan vertical deflection at failure was 2.89 in., or 5.71 in. less than the average for Butler 1 and 2. Although this difference can partially be attributed to the shorter shear span, the primary reason for this difference was a small (approximately 18 in. diameter) ACC deck concrete patch near one load point. Delaminated and missing concrete in this area initiated the failure.

The deterioration of Butler 3 resulted in its poor test performance. Stiffness of Butler 3 was 14,200 kip-ft, or 25% less than the average stiffness of Butler 1 and 2 (19,000 kip-ft). Experimental ultimate strength was 246 ft-kip, 31% less than the average experimental ultimate strength for Butler 1 and 2. Vertical midspan deflection at failure was 3.19 in.

Experimental, design and theoretical ultimate strengths are also presented in Table 4.2. Experimental ultimate strengths for Butler 1, 2 and 4 exceed the design ultimate strengths. Experimental ultimate strength of Butler 3 was 8% below the design ultimate strength. This is cause for concern and strength reductions should be made when PCDB panels are in a state of extreme deterioration similar to Butler 3.

Average compressive strength of cores taken from the Butler County panels was 6,200 psi, 1,200 psi stronger than the corresponding strength given in the J-10 Standard. Average yield strength of the reinforcing steel was 47,300 psi, or 7,300 psi over the J-10 Standard reinforcement yield strength. Theoretical ultimate strengths calculated from the actual material strengths are close to the experimental ultimate strengths of Butler 1, 2 and 4 and greatly exceed the experimental ultimate strength of Butler 3. Once again, this indicates that Butler 3 was structurally deficient.

In comparison with the shorter Cedar County panels, the Butler County panels had less flexural capacity. The longer Butler County panels contained more primary reinforcing

steel and are theoretically stronger, provided concrete and reinforcing steel strengths are equal. In fact, the yield strength of the reinforcing steel in the Cedar County panels was 25% greater and the concrete compressive strength was 61% greater than the corresponding Butler County panel values. Also, the reinforcing steel in the Cedar County panels gained appreciable strength after yielding. Strain hardening of the Butler County reinforcing steel was almost nonexistent. These increases in the material strengths outweighed the differences in areas of reinforcement and resulted in greater ultimate strengths for the Cedar County panels.

#### ***4.2.4. Black Hawk County Panels***

The longest panels tested were four 36 ft long Type II (H15) PCDB panels from Black Hawk County. These panels (henceforth referred to as Black Hawk 1-4) were part of a single span PCDB on a paved road. An ACC wearing surface once covered the panels and was removed before the panels were transported to the structures laboratory. All four panels were interior panels.

Black Hawk 1-4 exhibited less deterioration than Butler 1-4 and slightly less deterioration than Cedar 1-8. Deterioration consisted of longitudinal cracks in the stems and was concentrated mainly in the middle third of each panel. Reinforcing steel was exposed in a few discrete locations.

##### ***4.2.4.1. Discussion of Results for Black Hawk 1-4 Load Tests***

The longer length of the Black Hawk panels resulted in larger midspan deflections. During the load test of Black Hawk 1, the maximum deflection of the loading setup (as described in Section 4.1.2) was reached prior to failure of the panel. This forced a premature termination of the test. Maximum midspan vertical deflection was 10.29 in. Subsequent modifications added approximately 6 in. of deflection capability to the load setup. During the Black Hawk 2 load test, the modified loading setup became unstable and safety concerns ended the load test prior to failure of the panel. The maximum midspan vertical deflection for Black Hawk 2 was 6.47 in.

For the remaining two load tests, the loading setup was extensively modified to increase both safety and deflection capability. This modified loading setup is shown in Figure 4.15. Once the hydraulic actuators were fully extended, the 'B' nuts inside the

jacking chairs were tightened down. With these nuts holding the structural tube in position, hydraulic pressure to the actuators was released allowing the actuators to retract. The 'A' nuts were then tightened down and hydraulic pressure was restored to the actuators. This cycle continued until panel failure occurred. The modified load setup, as well as the large ductility of the Black Hawk panels, is shown in Figure 4.16.

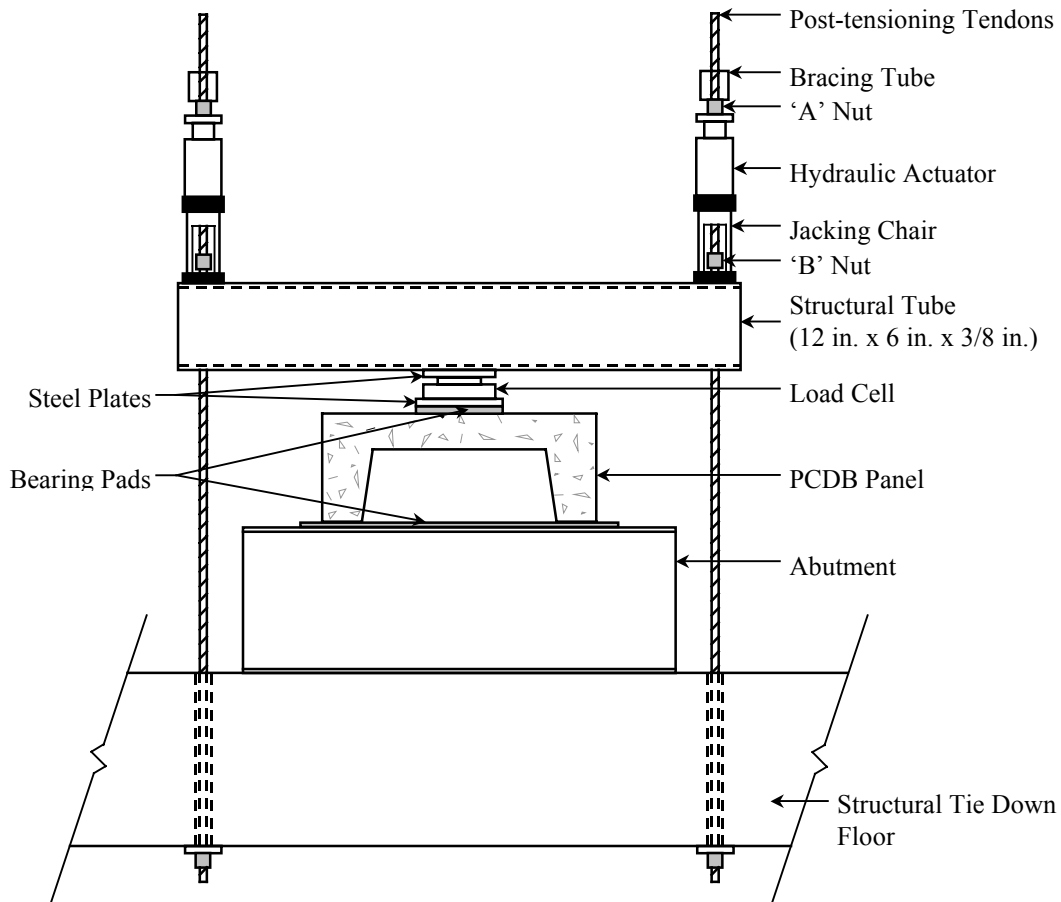


Figure 4.15. Modified loading setup.



Figure 4.16. Black Hawk 3 at imminent failure.

Moment/deflection curves for Black Hawk 1-4 are presented in Figure 4.17. Elastic behavior for all four panels was nearly identical. Stiffness, as shown in Table 4.3, ranged from 19,500 kip-ft to 22,200 kip-ft, and the reinforcing steel yielded at approximately 330 ft-kip. Inelastic behavior of Black Hawk 1-4 varied only slightly. Maximum midspan vertical deflection for Black Hawk 3 and 4 was 13.63 in. and 12.91 in., respectively. Ultimate strength for Black Hawk 3 and 4 was 430 and 405 ft-kip, respectively.

As was the case for the first two groups of panels, experimental ultimate strengths exceeded design ultimate strengths. Design ultimate strength was 352 ft-kip, or 16% less than the average experimental ultimate strength for Black Hawk 3 and 4. Increased actual material strengths were, again, responsible for this discrepancy. Actual concrete strength was 7,300 psi and actual yield strength of the reinforcing steel was 44,850 psi. Theoretical ultimate strengths were closer to the experimental ultimate strengths, however, the correlation was not as good as in the other two groups of panels.

Black Hawk 1-4 were the longest PCDB panels tested. Due to their length, these panels contained more primary reinforcing steel than the other panels. Consequently, the Black Hawk panels were theoretically stronger than the others; this was not the case

experimentally. Cedar 1-3 were the shortest panels tested and theoretically the weakest, but experimental ultimate strengths for these panels exceeded all others. This anomaly was due to the fact that the Cedar County panels had the highest material strengths. Reinforcing steel in the Cedar County panels had the highest yield strength and exhibited a significant amount of strain hardening. Strain hardening was far less prevalent in the other two groups of panels. This is apparent through a comparison of the moment/deflection curves of all three groups of panels.

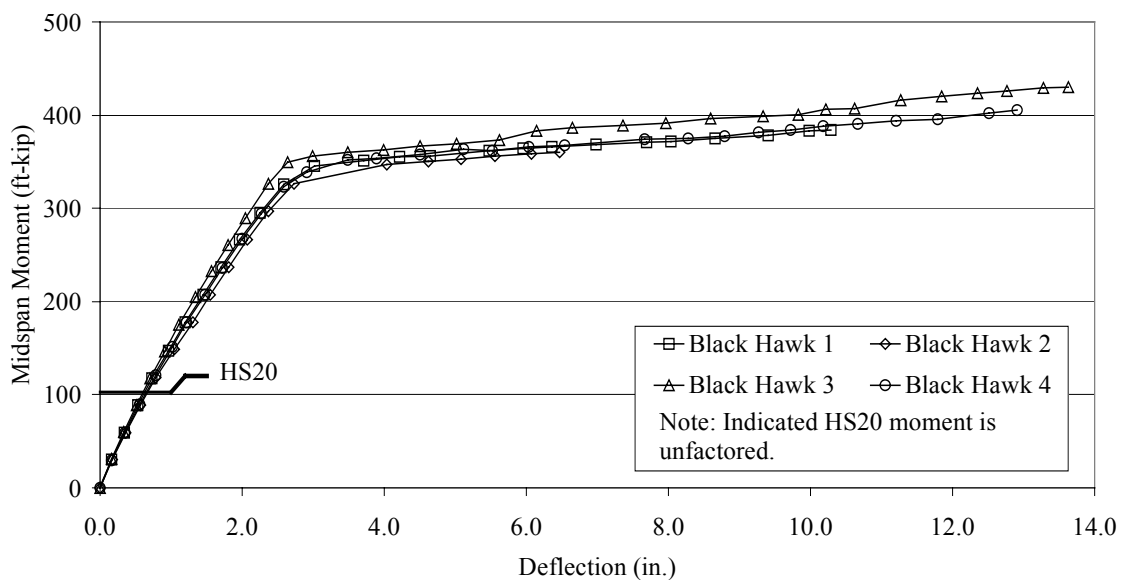


Figure 4.17. Midspan moment vs. midspan deflection for Black Hawk 1-4 ultimate strength tests.

Table 4.3. Ultimate strengths and stiffnesses for Black Hawk 1-4.

Panel	Ultimate Strength (ft-kip)			Flexural Rigidity (kip-ft)	Stiffness (kip-ft)
	Experimental	Design	Theoretical		
Black Hawk 1	384*	299	345	181,400	20,500
Black Hawk 2	360*	299	334	172,600	19,500
Black Hawk 3	430	299	364	193,600	22,200
Black Hawk 4	405	299	341	180,200	20,400

\* Failure not achieved; value is maximum midspan moment.

## 5. TESTING OF FOUR PANEL LABORATORY PCDB

From the field test data, the presence of shear connectors was shown to have a significant influence on transverse load distribution. To further investigate the performance of various joint configurations, a portion of a PCDB was assembled and tested in the Town Engineering Structures Laboratory. Limitations on laboratory space and available panels restricted the laboratory PCDB to four 25 ft long Type II (H20) PCDB panels (Cedar 4,5,6 and 7 - see Section 4.2.2).

The laboratory PCDB was subjected to three separate testing programs. The first consisted of placing a series of service level point loads at predetermined locations. Three different joint configurations were tested with this type of loading. The second testing program was quite similar to the first except it was conducted after the laboratory PCDB was strengthened (see Chapter 6). In the third testing program, the strengthening retrofit was removed and the laboratory PCDB was loaded to failure. In this chapter, the first and third testing programs are presented. Load testing of the retrofitted laboratory PCDB is presented in Chapter 6.

### 5.1. Laboratory PCDB Setup

#### 5.1.1. Configuration

A plan view and photograph of the laboratory PCDB are presented in Figure 5.1 and Figure 5.2, respectively. The individual panels were joined together by three different joint configurations. For the first joint configuration, hereafter referred to as ‘loose bolts only’, the long, galvanized bolts (hereafter simply referred to as bolts) were installed in the six locations (see Figure 5.1). The bolts connecting P1 and P2 were loosely installed while all other bolts were tightened with a torque wrench to 40 ft-lbs. This torque value was assumed to represent typical field conditions for bolt tightness. For the second joint configuration, hereafter referred to as ‘tight bolts only’, all panels were again connected only with bolts, all which were tightened to 40 ft-lbs. In the third joint configuration, hereafter referred to as ‘tight bolts plus shear connectors’, the shear connectors (concrete-filled galvanized pipes) were installed in all panel joints and all of the bolts were installed and tightened to 40 ft-lbs.

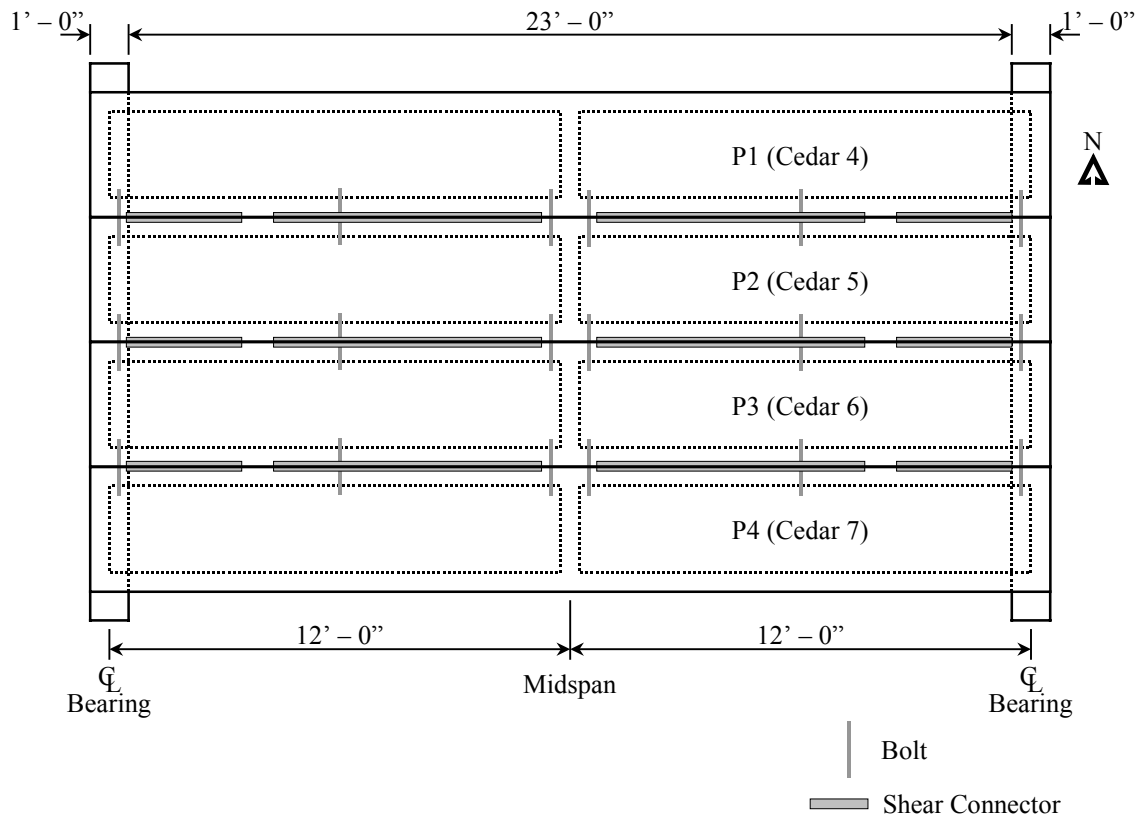


Figure 5.1. Plan view of laboratory PCDB.



Figure 5.2. Photograph of the laboratory PCDB.

Precast concrete abutments were used to support the panels. Bearing at each panel end was 1 ft with one-inch thick elastomeric pads placed between the abutments and panels.

### 5.1.2. Instrumentation

Instrumentation for the laboratory PCDB was essentially the same as the instrumentation used during the field service load tests. All instrumentation was placed at midspan, as shown in Figure 5.3. A steel strain gage was bonded to one of the bottom primary reinforcing bars in each panel stem. Two concrete strain gages were bonded to the deck surface (3 in. from the panel edge) of each panel. Vertical deflection of each stem as well as the center of each panel was measured with deflection transducers at these points. To measure compression of the elastomeric bearing pads, an additional deflection transducer was connected to the transverse center of the loaded panel at a point approximately 18 in. from the west abutment. Compression of the bearing pads for the other panels was assumed to be proportional to the load fractions for each respective panel. Strain and deflection measurements were recorded using a Hewlett-Packard 3852A computer controlled DAS.

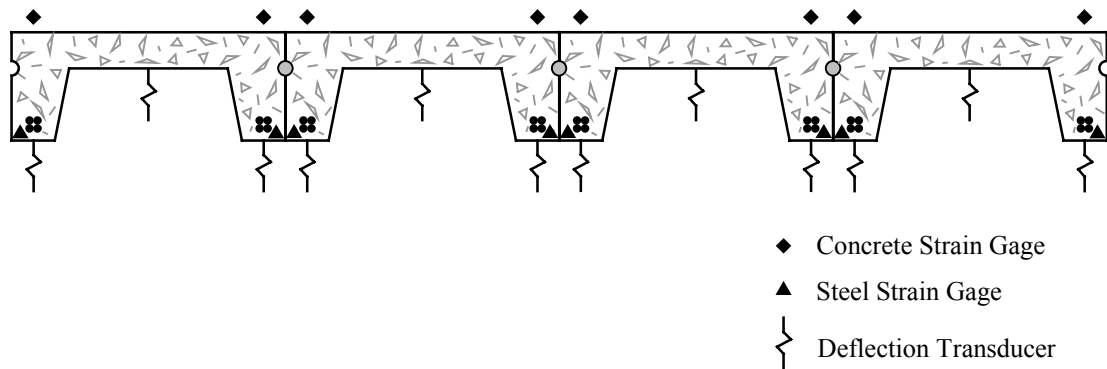


Figure 5.3. Laboratory PCDB instrumentation at midspan.

## 5.2. Joint Configuration Testing Program

### 5.2.1. Load Setup

The main components of the load setup for joint configuration tests were a reaction frame and a single hydraulic actuator. The reaction frame, shown in Figure 5.4, consisted of a 17 ft long wide flange beam (W21 x 82), two structural tubes (12 in. x 4 in. x 3/8 in.), two channels (MC12 x 40), and four post-tensioning tendons (1 in. diameter Dywidag

Threadbars). The beam (transverse to the laboratory PCDB) was positioned at midspan of the panels. By moving the hydraulic actuator, load could be applied at essentially any midspan transverse location. As can be seen in Figure 5.4, through the system of the load beam, structural tubes and post-tensioning tendons, the applied loads were resisted by the structural tie-down floor.

The hydraulic actuator was a 60 ton hollow core single acting actuator that was pressured by a hand operated hydraulic pump. An elastomeric pad (12 in. x 12 in. x 1 in.) and steel plate (12 in. x 12 in. x 1 in.) distributed load evenly over a 1 sq. ft contact area. An electronic load cell positioned between the steel plate and the hydraulic actuator was used to measure the magnitude of applied load.

Load was applied at four discrete positions, which were centered, both transversely and longitudinally, on a particular panel. Load position 1 (LP1) was on P1, load position 2 (LP2) was on P2, and so forth; these four load positions are shown in Figure 5.5.

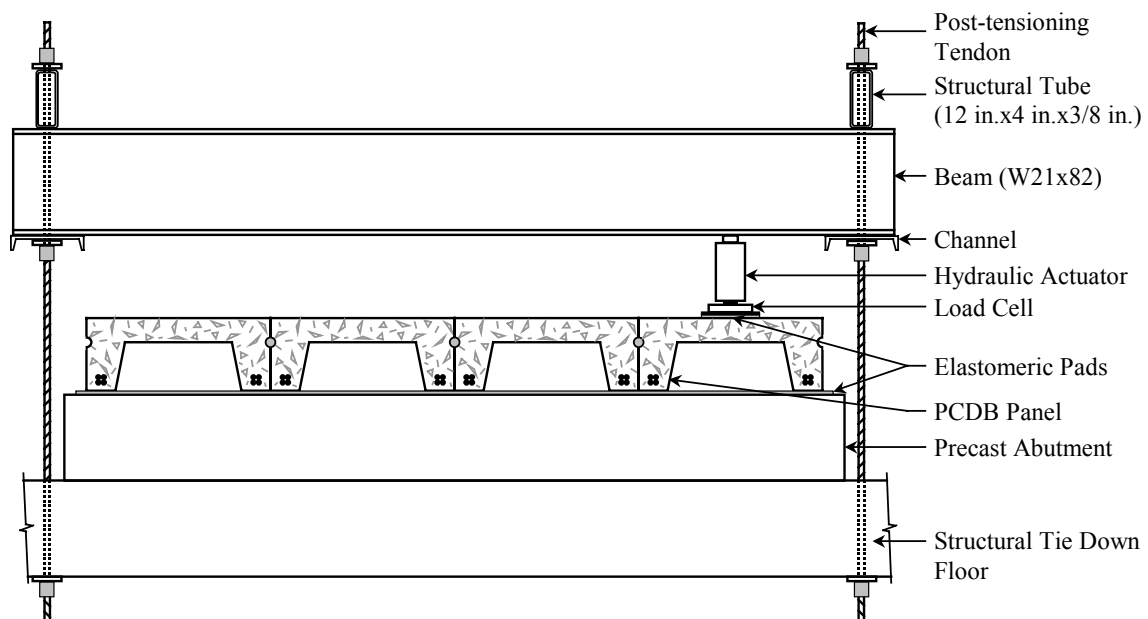


Figure 5.4. Load setup for joint configuration tests.

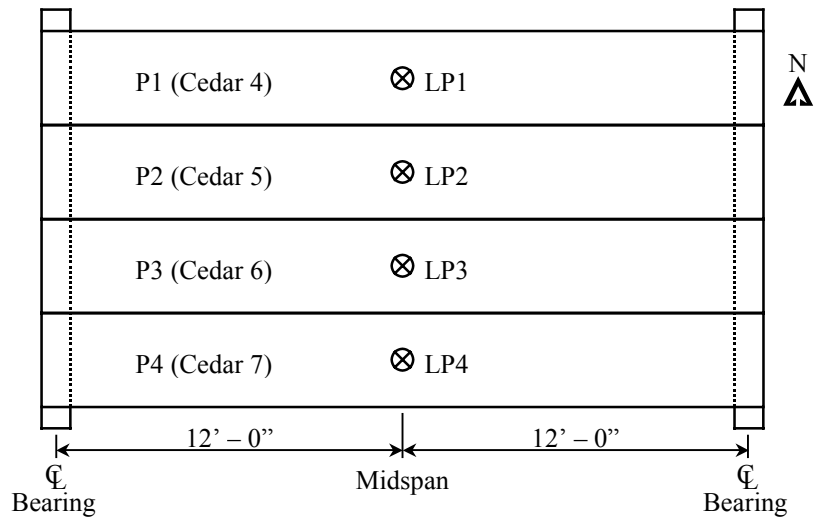


Figure 5.5. Load positions used in the joint configuration tests.

### 5.2.2. Test Procedure

For the two primary joint configurations ('tight bolts only' and 'tight bolts plus shear connectors'), load was applied twice to each of the four load points (see Figure 5.4). For the 'loose bolts only' joint configuration, load was twice applied to only LP1. Since only the bolts between P1 and P2 were loose, the response from loading at the other load points for the loose bolts only configuration would be very similar to the response of the tight bolts only configuration. Loading each load point twice verified the repeatability of the test results. For each load application, load was increased in 4 kip intervals up to a maximum load of 28 kip. A load of 16 kip corresponds to the load induced by an HS20-44 design wheel line. Loads higher than this were useful for determining if the magnitude of load affected transverse load distribution. Strains, deflections, and the magnitude of applied loads were recorded by the DAS at each increment of load.

### 5.2.3. Discussion of Results

To numerically compare the results of the joint configuration tests, load fractions were calculated from the deflection data using Equation 2.

$$LF_i = \frac{\Delta_i}{\sum_{j=1}^4 \Delta_j} \quad (2)$$

where:

$LF_i$  = Load Fraction for  $i^{th}$  panel

$\Delta_i$  = Deflection of  $i^{th}$  panel

$\Delta_j$  = Deflection of  $j^{th}$  panel

For each panel, the two stem deflections were averaged with the transverse center deflection to give the panel deflection value used in Equation 2. Load fractions were primarily calculated at the maximum load (28 kips). It will be later shown that the load fraction remained essentially constant for the various magnitudes of load.

#### 5.2.3.1. Comparison of Strain and Deflection Data

Deflection data from each field load test were used to calculate load fractions for use in the rating of each bridge. In relation to concrete and steel strains, deflections are the simplest type of response to accurately measure during a load test. Conventional strain gages require a great deal of surface preparation before they can be applied to either steel or concrete. The use of only deflection transducers during a PCDB load test would significantly reduce the setup time. To verify that deflection measurements give an accurate representation of the bridge response, load fractions were calculated from concrete and steel strain data for the laboratory PCDB and compared to load fractions based on deflection data. Maximum load fractions for each load position (tight bolts plus shear connector joint configuration) are presented in Table 5.1.

Table 5.1. Load fractions based on deflection, steel strain, and concrete strain data.

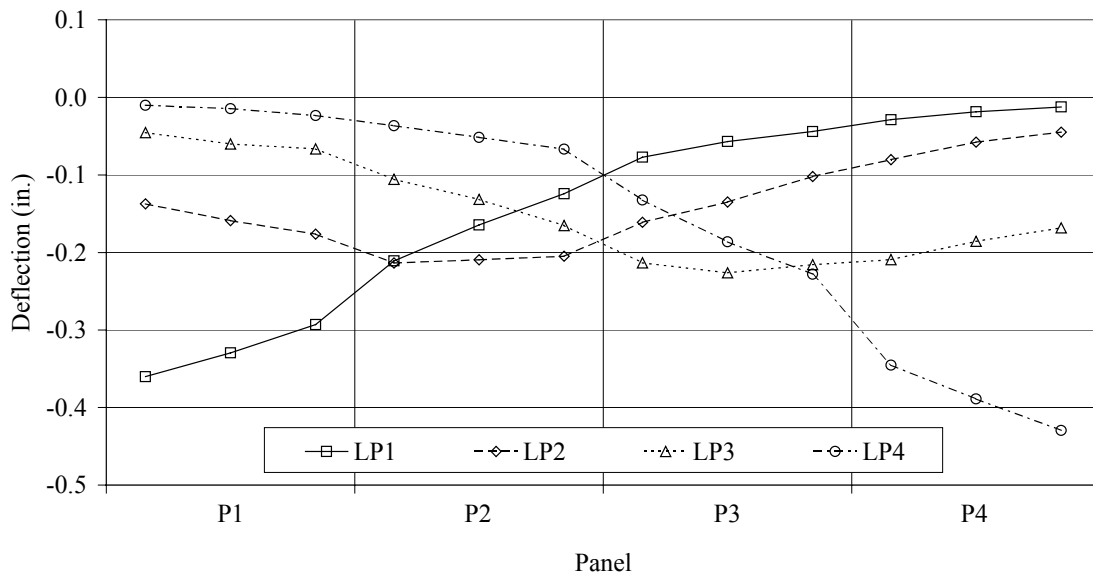
Data Type	Maximum Load Fraction			
	LP1	LP2	LP3	LP4
Deflection	0.57	0.37	0.37	0.61
Steel Strain	0.58	0.41	0.45	0.59
Concrete Strain	0.62	0.49	0.32	0.60

All load fractions for LP1 and LP4 correlated extremely well while load fractions for LP2 and LP3 did not correlate as well. For LP2 and LP3, load fractions based on concrete strain were erratic. This is likely due to the influence of the load point on the concrete strain gages that were only 9 in. from the edge of the load point footprint. Load fractions based on steel strains were essentially the same as those based on deflections. Thus, PCDB ratings

based on the deflection load fractions and steel strain load fractions will be essentially the same.

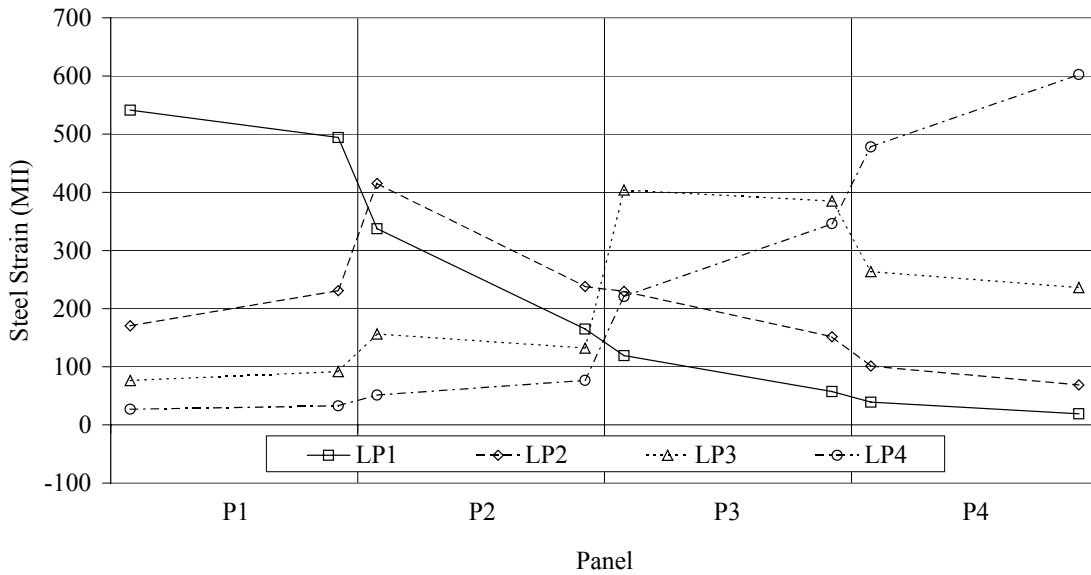
Data used to calculate the above load fractions are presented in Figure 5.6. In terms of symmetry, the deflection curves showed slightly better symmetry than the steel strain curves and considerably more symmetry than the concrete strain curves. Concrete strains were close to being symmetric on the unloaded panels but varied greatly for the loaded panels. As previously noted, this variation most likely is due to the close proximity of the concrete strain gages in relation to the load points.

All three plots in Figure 5.6 indicated similar trends in behavior of the laboratory PCDB. The loaded panel, as expected, experienced the highest strains and deflections. The magnitude of the strains and deflections then decreased with increasing distance away from the loaded panel. This behavior correlated with the behavior of the four field tested PCDBs. Since the deflection and strain data indicated the same behavior, only the deflection data is presented in the rest of this chapter.

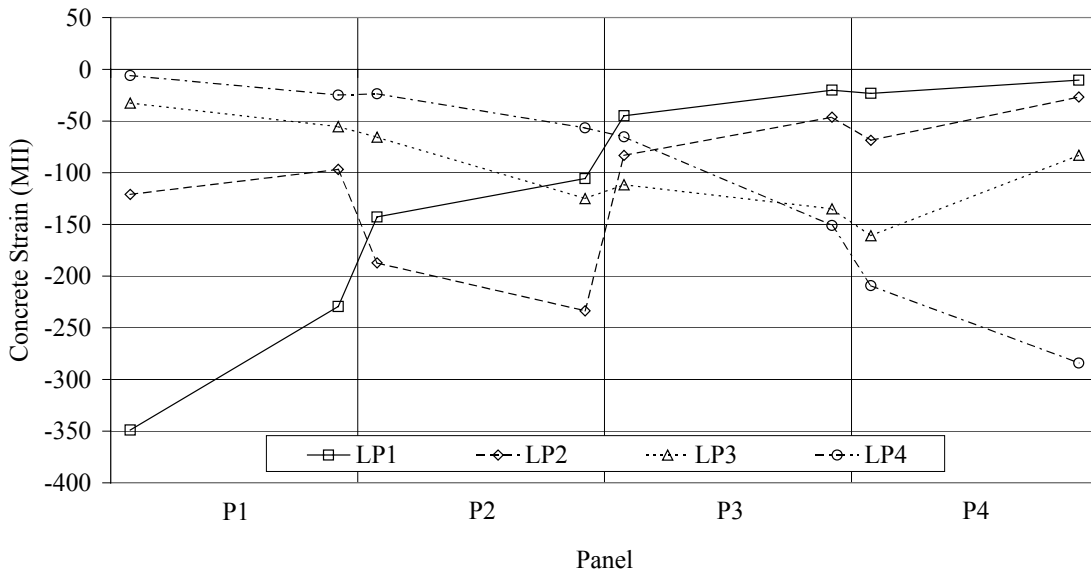


a. Midspan vertical deflection

Figure 5.6. Laboratory PCDB response curves at 28 kip for ‘tight bolts plus shear connectors’ joint configuration.



b. Midspan steel strain



c. Midspan concrete strain

Figure 5.6. Continued.

### 5.2.3.2. Magnitude of load

To determine if the load fractions varied with the magnitude of load, load fractions were calculated at four different load increments for both the ‘tight bolts only’ and the ‘tight bolts plus shear connectors’ joint configurations. These load fractions are presented in Table 5.2. For both joint configurations, the load fractions remained essentially constant as the load was increased. Therefore, load fractions at 28 kip represent the lateral distribution of load for all loads less than 28 kip.

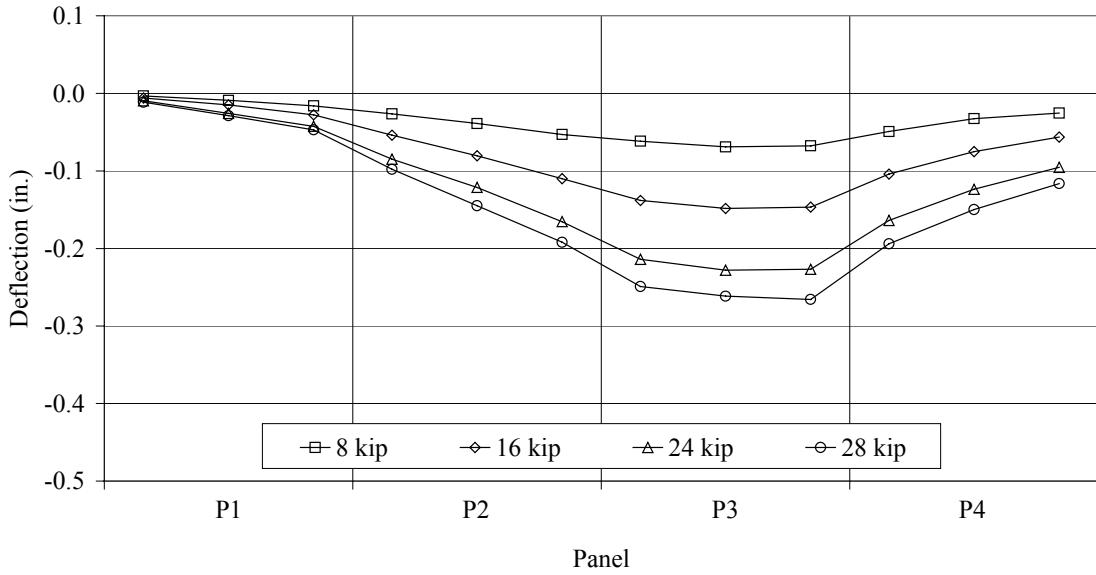
Table 5.2. Load fractions at various loads for LP3.

Joint Configuration	Load (kip)	Panel			
		P1	P2	P3	P4
Tight Bolts Only	8	0.06	0.26	0.44	0.24
	16	0.05	0.25	0.45	0.24
	24	0.05	0.25	0.45	0.25
	28	0.05	0.25	0.44	0.26
Tight Bolts Plus Shear Connectors	8	0.09	0.23	0.37	0.31
	16	0.09	0.22	0.37	0.31
	24	0.09	0.23	0.37	0.31
	28	0.10	0.22	0.37	0.31

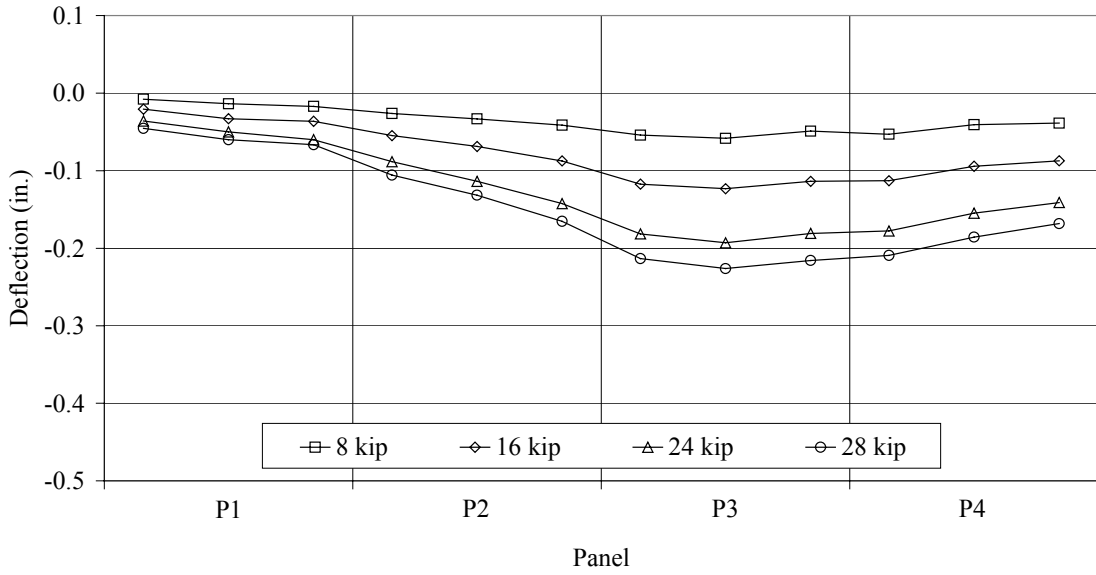
### 5.2.3.3. Joint Configuration

Deflection data for LP3 were used to calculate the load fractions in Table 5.2 and are presented in Figure 5.7. By comparing the two plots, one can easily see improved transverse load distribution for the ‘tight bolts plus shear connectors’ joint configuration. P1 and P4 deflected more and therefore carried more load when the shear connectors were in place. The northern stem of P1 deflected 0.01 in. at 28 kip for the ‘tight bolts only’ joint configuration. For the ‘tight bolts plus shear connectors’ joint configuration, the same stem deflected 0.05 in.

For both joint configurations, relative displacement between adjacent stems increased with increasing load. By tightening the bolts, the outer surfaces of adjacent stems are forced together. The normal force between the panels creates a friction force that reduces relative movement between the stems. At low loads, as shown in Figure 5.7, the panels moved very little in relation to each other. As the load was increased, the friction force was



a. Tight bolts only



b. Tight bolts plus shear connectors

Figure 5.7. Midspan deflection curves at various load increments with load applied at LP3.

overcome and the relative deflection between adjacent panels increased. At high loads, the presence of shear connectors limited the amount of relative movement between panels. This can more easily be seen in Figure 5.8. For the ‘tight bolts only’ and ‘tight bolts plus shear connectors’ joint configurations, relative displacement between adjacent stems of P1 and P2 was 0.16 in. and 0.08 in., respectively. Presence of the shear connectors reduced the relative displacement between the loaded panel, P1, and the adjacent panel, P2, by 50%.

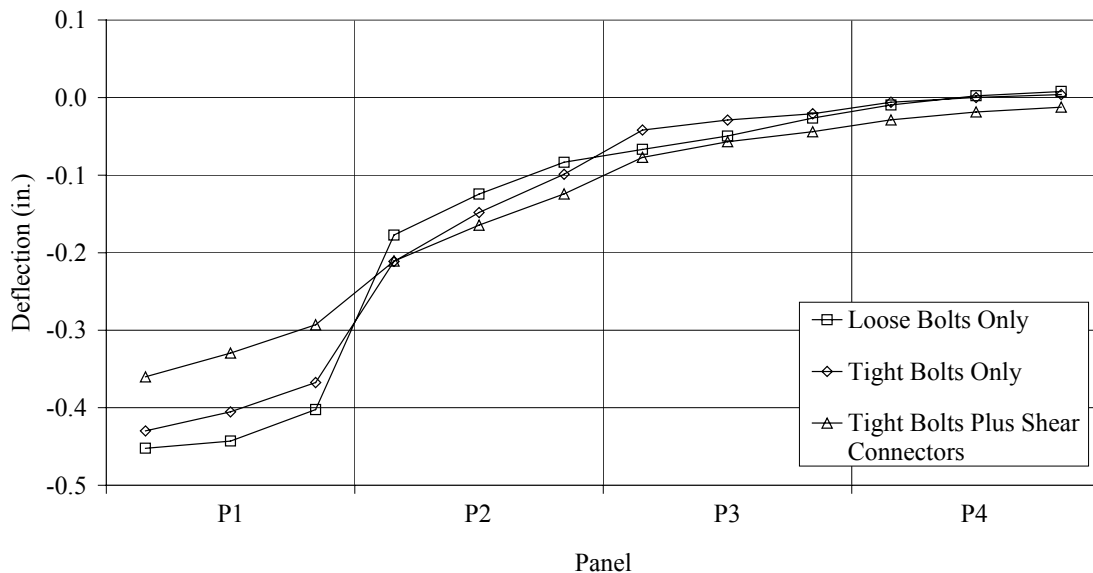


Figure 5.8. LP1 midspan deflection at 28 kip for all three joint configurations.

Load fractions for all joint configurations and load positions are presented in Table 5.3. For LP1, load fractions varied only slightly between the ‘loose bolts only’ and ‘tight bolts only’ joint configurations. A more substantial difference exists between the ‘tight bolts only’ and ‘tight bolts plus shear connectors’ joint configurations. This indicates that the shear connectors play more of a role in the transverse distribution of load than the tightness of the bolts.

### 5.3. Ultimate Strength Testing Program

#### 5.3.1. Load Setup

The load setup used in the ultimate strength test of the laboratory PCDB applied load to a single panel (P3) in a four point bending arrangement. This loading arrangement

corresponded to that of the individual panel ultimate strength tests (see Chapter 4). The joints between adjacent panels were in the tight bolts plus shear connectors configuration as described in Section 5.1.1. A photograph of this loading setup is shown in Figure 5.9.

Table 5.3. Load fractions at 28 kip for all load positions and joint configurations.

Joint Configuration	Load Position	Panel			
		P1	P2	P3	P4
Loose Bolts Only	LP1	0.71	0.21	0.08	0.00
Tight Bolts Only	LP1	0.69	0.26	0.05	0.00
	LP2	0.27	0.39	0.25	0.08
	LP3	0.05	0.25	0.44	0.26
	LP4	0.00	0.07	0.22	0.72
Tight Bolts Plus Shear Connectors	LP1	0.57	0.30	0.10	0.03
	LP2	0.28	0.37	0.24	0.11
	LP3	0.10	0.22	0.37	0.31
	LP4	0.03	0.08	0.29	0.61

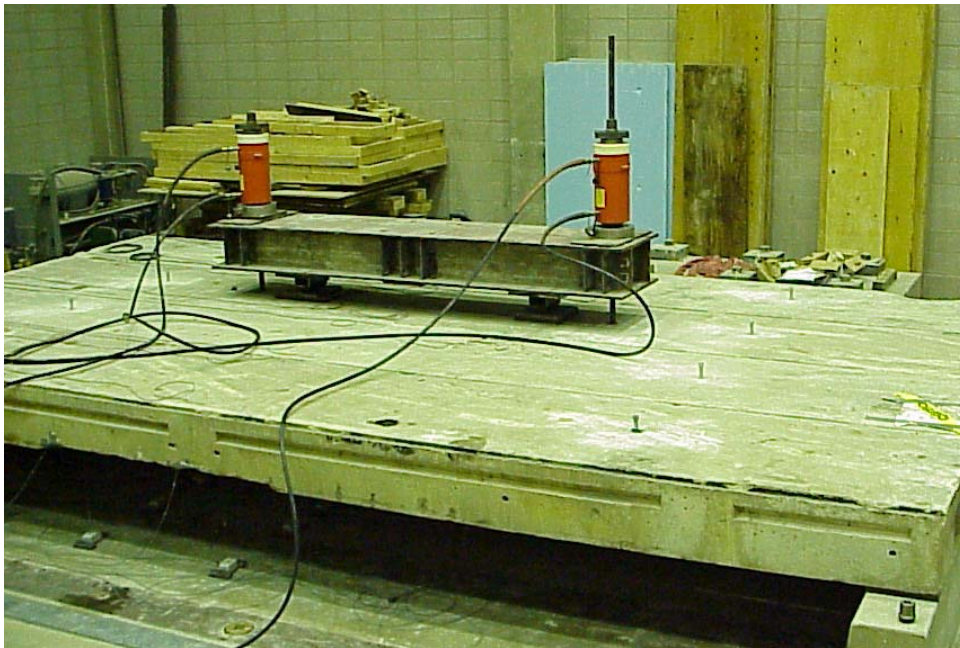


Figure 5.9. Photograph of load setup used in the ultimate strength test of the laboratory PCDB.

The reaction frame, shown in Figure 5.10, consisted of a fabricated beam and two post-tensioning tendons (1 in. diameter Dywidag Threadbars). The beam consisted of two W12 x 87's welded continuously together at the mating flange tips. Web stiffeners and 1/4 in. plate strengthened the beam at the load points. Post-tensioning tendons passed through 3 in. diameter holes in the deck of P3 and were secured in the structural tie-down floor. Load points on P3 were spaced 6 ft apart and consisted of elastomeric bearing pads (12 in. x 12 in. x 1 in.), steel plates (12 in. x 12 in. x 1 in.), and fabricated rockers. Load was applied to the ends of the fabricated beam by two 100 ton hollow core hydraulic actuators which were pressured by a single hand operated hydraulic pump. The actuators were connected in parallel to equalize the load applied by each actuator.

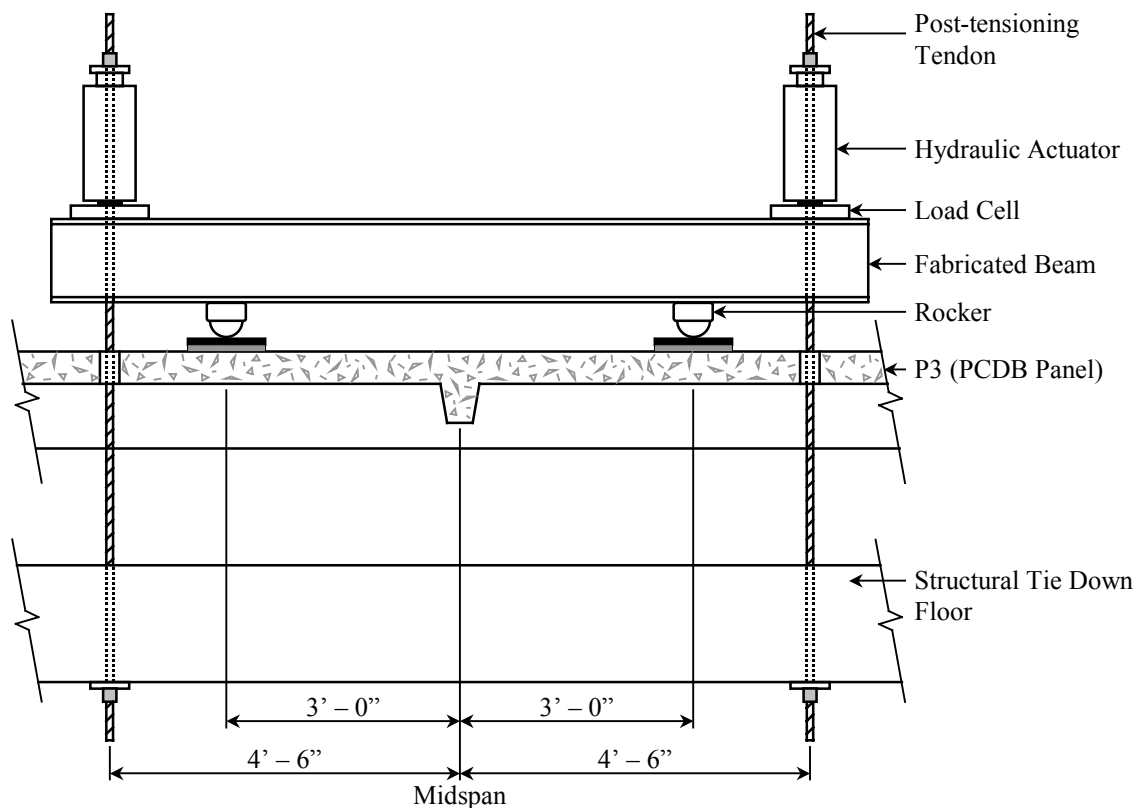


Figure 5.10. Details of load setup for ultimate strength test of the laboratory PCDB.

### **5.3.2. Test Procedure**

The ultimate strength test of the laboratory PCDB was similar to the ultimate strength tests on the individual PCDB panels. Load was increased slowly in 4 kip (per actuator) increments while the DAS recorded strain, deflection, and load data. Near failure, data were taken more frequently. Once failure occurred, load was removed and the failure was observed.

### **5.3.3. Discussion of Results**

Total load on the laboratory PCDB at failure was 212 kip (106 kip per actuator). (Note: Loads in all graphs are load per actuator; the total load applied is thus twice this value.) When loaded individually to failure, the average total load supported by the Cedar County panels (the same panels used in the laboratory PCDB) was 103 kip. The additional capacity of the laboratory PCDB was obviously due to the transverse distribution of load to the adjacent panels. To put the strength of the laboratory PCDB into perspective, the total failure load was equivalent to applying 2.94 HS20-44 design trucks to a single panel in a four panel PCDB. This is an excellent testament to the strength of the PCDB.

The mode of failure was a shear failure of the concrete directly above the shear connector between P2 and P3. At imminent failure, a crack in the deck of P3 began near midspan and propagated towards both ends. Failure progressed rather quickly as the crack continued to grow. Loud, popping sounds indicated failing concrete. Only a small amount of additional load was applied during the progression of the failure. The crack in the deck of P3 is shown in Figure 5.11.

Following failure, the laboratory PCDB was disassembled and the extent of the failure was investigated. The crack in the deck of P3 was found to extend downward towards the shear connector. As shown in Figure 5.12, the concrete in this area was not confined by the stirrup and thus sheared free from the corner. This was due to the upward force exerted by the shear connector on this concrete. A photograph of P3 with the loose concrete removed is presented in Figure 5.13.

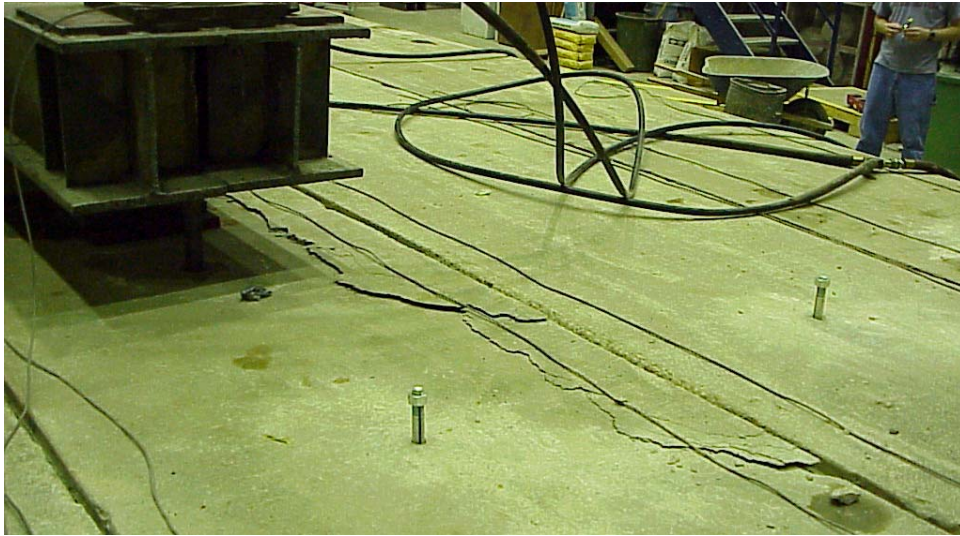
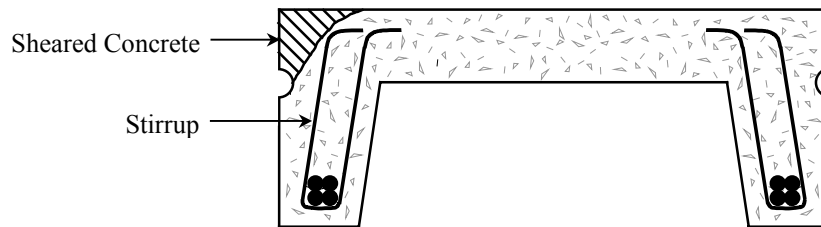


Figure 5.11. Crack in deck of P3 at failure.



Note: Deck reinforcement not shown

Figure 5.12. Detail of shear failure on P3 (looking east).

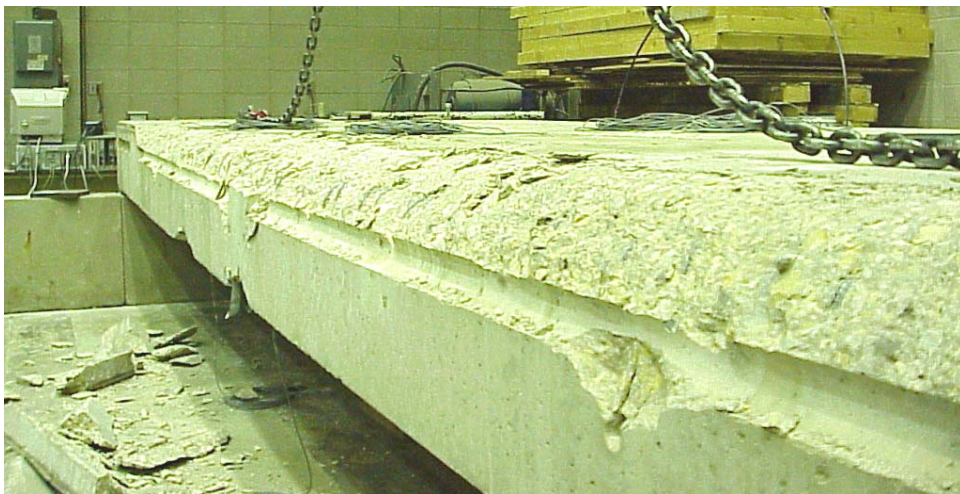


Figure 5.13. Failed concrete above shear connector in P3 (looking east).

Primary reinforcing steel in both stems of P3 and in the northern stem of P4 yielded while the steel in P1, P2 and the southern stem of P4 remained elastic. For each panel, the steel strains of each stem were averaged and plotted against load as shown in Figure 5.14. As may be seen, the average steel strains were highest in P3 and lowest in P1.

Midspan deflections at four discrete loads, including failure, are shown in Figure 5.15. As load increased, the amount of relative deflection between adjacent panels also increased. At 28 kip, all four panels deflected approximately the same amount. At the failure load (106 kip), P3, the loaded panel deflected approximately 1.25 in. more than the two adjacent panels. The large difference in displacements across the joints between P2, P3, and P4 clearly indicate a failure of the shear connection at these joints.

At failure, the average deflection of P3 was 2.93 in. or, in terms of a deflection to span ratio,  $L/100$ . This amount of deflection is quite noticeable and provides an indication of impending failure.

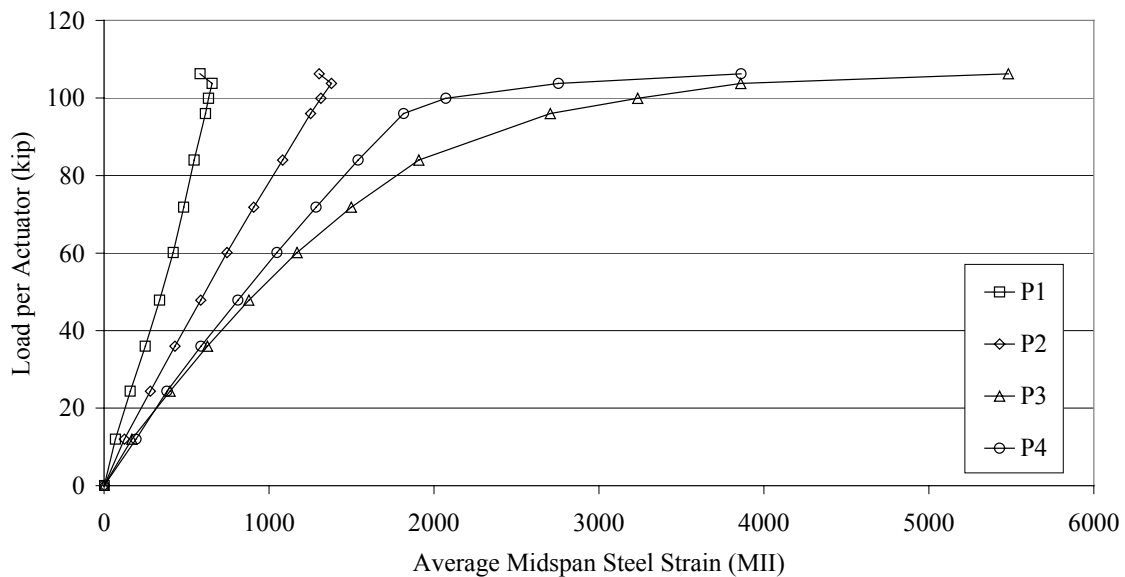


Figure 5.14. Load/steel strain plot for laboratory PCDB ultimate strength test.

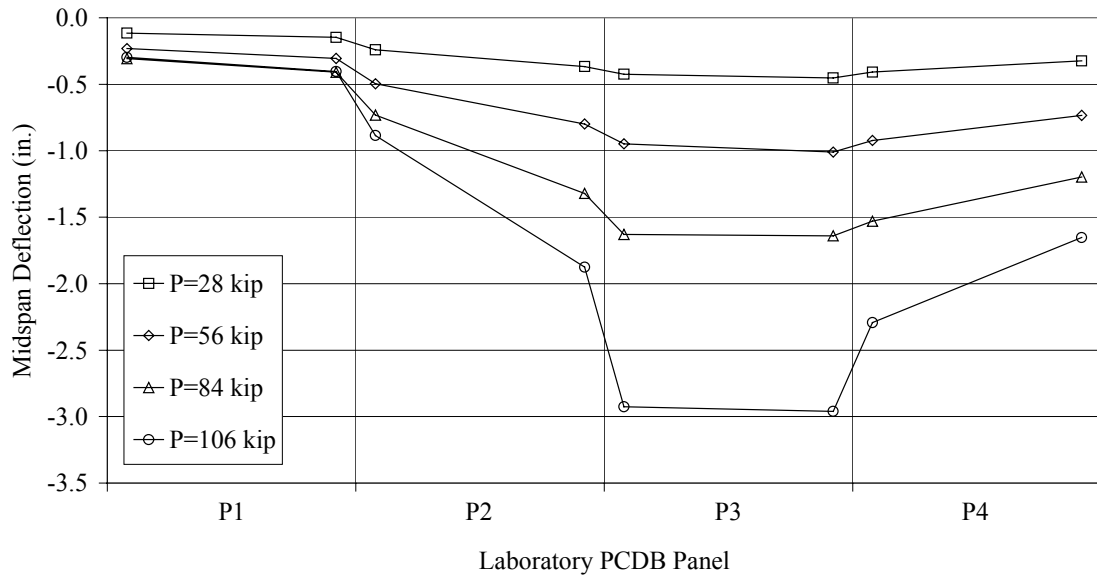


Figure 5.15. Midspan deflections at various loads for laboratory PCDB ultimate strength test.



## 6. STRENGTHENING OF PANELS

During the conceptual stages of this project, the research team predicted that some PCDBs would be found deficient due to deterioration. As an alternative to posting or replacing the deficient bridges, the research team investigated a retrofit for the PCDBs that could restore a portion or all of the lost structural capacity. Thorough experimental testing revealed that in all but one extreme case, deterioration did not reduce the strength of these bridges. The research team did, however, find two situations where these bridges were deficient.

In the first case, the shear connectors, either concrete-filled pipes or grouted keyways, were not in place. This reduced the transverse distribution of load and caused an overstress of individual panels. Properly installing the shear connectors would correct this problem.

The other case where PCDBs were found deficient was due to the original design of these bridges. Type I PCDB panels and some Type II panels were designed for H15 loading while other Type II panels were designed for H20 loading. Today, heavier design loads such as HS20 are commonly used in bridge designs. When PCDBs, particularly those designed for H15 loading, are rated for HS20 loading, they are frequently found deficient. Instead of posting or replacing the deficient bridge, its capacity could be increased by a strengthening retrofit.

To be of use, a strengthening retrofit should be practical and economical. A practical retrofit is one that is relatively simple and can be implemented by county maintenance crews with minimal complications. Economy plays a major role in most engineering decisions and is quite important in the design of this retrofit. Due to the age and condition of these bridges, a county engineer would most likely replace one of these bridges if the strengthening alternative were costly. Lastly, a retrofit must sufficiently increase the capacity of the bridge so that it can carry legal loads.

### 6.1. Strengthening System Design and Installation

Several retrofit systems were investigated and the most practical and economical system was selected and experimentally tested on the Cedar County panels. This strengthening system involved a post-tensioning king-post arrangement (a 1/2 in. seven-wire

prestressing strand and a fabricated metal strut at midspan). The strand was cut slightly longer than the panels and passed through a hole drilled in the center of each end diaphragm. A prestressing chuck was used on each end of the strand to transmit the post-tensioning force to the end diaphragms. The strut was approximately 6.5 in. tall and was connected to the underside of the midspan diaphragm with anchor bolts and epoxy.

Harping the strand downward over the strut and tensioning the strand induced an upward reaction on the midspan diaphragm. The magnitude of the upward force depended upon the amount of tension in the strand, the height of the strut, and length of the panel. For the Cedar County panels, the upward force (4.13 kip) produced by the combination of a 6.5 in. tall strut and 27.1 kip strand tension created a midspan moment of 24.75 ft-kip. This moment was equal and opposite to the midspan moment due to the weight of the panel. Effectively eliminating the dead load moment resulted in an adequate increase in the live load carrying capacity of the panels.

Struts were fabricated by welding together sections of wide flange beam (W4 x 13) and various plates. Details of the strut are shown in Figure 6.1. A curved saddle on one end of the strut allowed the strand to slide smoothly during the strand tensioning. Additionally, grease was applied to the saddle to reduce friction between the strand and the saddle. A wide plate (6 in. x 4 in. x 3/8 in.) on the other end of the strut anchored the strut to the midspan diaphragm. As previously noted, concrete anchor bolts, which passed through holes in the plate, anchored the struts to the midspan diaphragms. This connection was strengthened by the application of high strength epoxy to the mating surfaces. An installed strut is shown in Figure 6.2.

The primary drawback of this retrofit is the need to access the end face of the panels for drilling and tensioning. About 3 ft of clearance beyond the end of the panels is needed. This can be accomplished with relative ease on a gravel road, however, on a paved road, the pavement would need to be removed. A hammer drill and 3/4 in. masonry drill bit were used to drill the holes in the end diaphragms. To ensure the hole was pitched downward at the correct angle ( $\approx 4^\circ$ ), a plywood template was used to guide the drill.

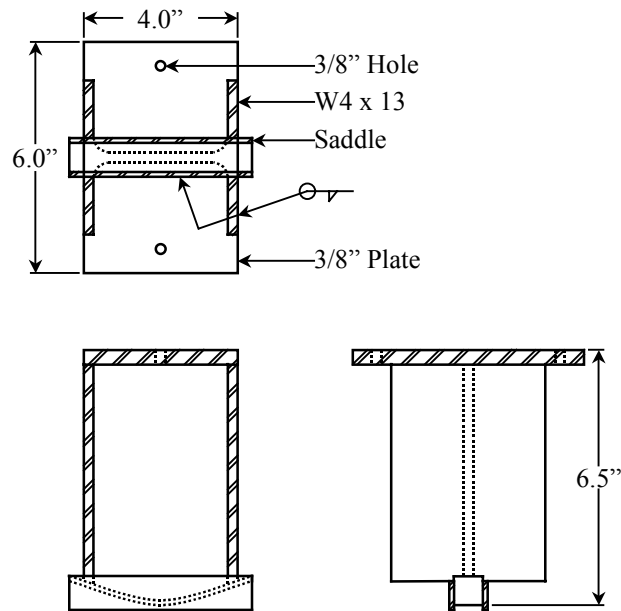


Figure 6.1. Strut developed for strengthening retrofit.

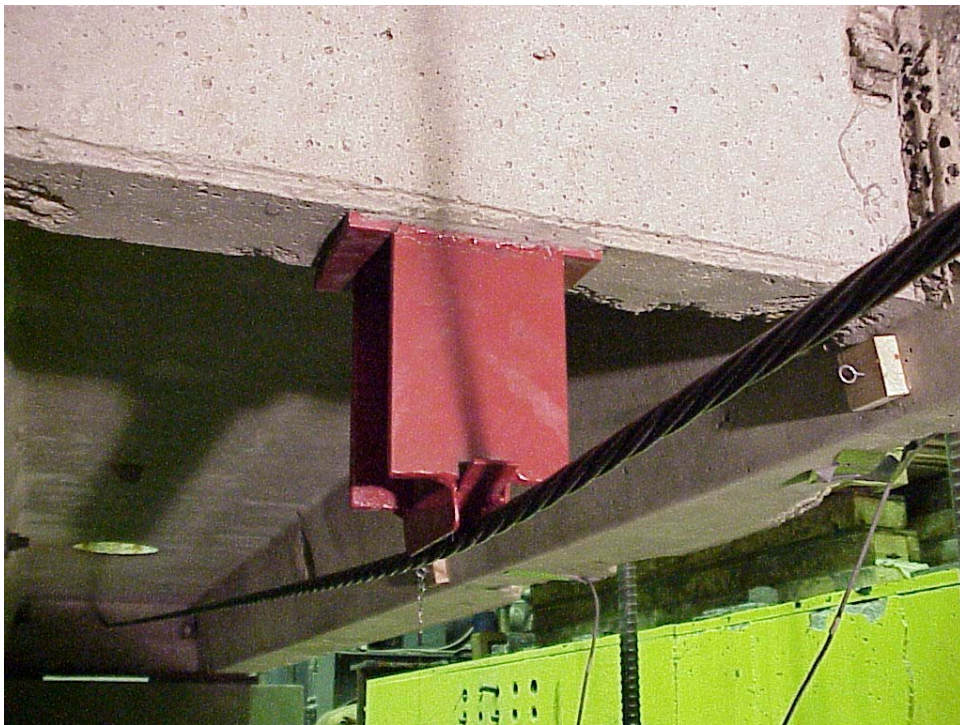


Figure 6.2. Photograph of strut installed on midspan diaphragm.

After the strand was properly installed (through the holes and over the saddle) the tensioning system was positioned on one end of the strand and a prestressing chuck was installed on the other end. A steel plate (6 in. x 4 in. x 1 in.) and a tapered washer evenly distributed force from the chuck to the end diaphragm. As shown in Figure 6.3, the tensioning system consisted of a jacking chair, a load cell, a 20 ton hollow core hydraulic actuator, and two chucks. A photograph of the tensioning system installed on all four panels of the laboratory PCDB is shown in Figure 6.4.

The jacking procedure was similar to the procedure used for post-tensioned concrete members. Force from the actuator reacted against the outer chuck thus tensioning the strand. Tension in the strand was measured by the load cell and was slowly increased until the desired tension force was slightly exceeded (by approximately 1 kip). Overstressing the strand was done to compensate for seating losses. The inner prestressing chuck and tapered washer were then positioned tight against the steel plate. Actuator pressure was then slowly released and the inner prestressing chuck was checked to ensure it was seating properly.

## **6.2. Strengthening System Testing Program**

The strengthening system was subjected to three different testing programs. Prior to ultimate strength testing of the laboratory PCDB, the laboratory PCDB was retrofitted and utilized for two of these testing programs: post-tensioning force distribution and service load testing. Once this testing was completed, the strengthening retrofit was removed and the laboratory PCDB was tested for ultimate strength. Following failure of the laboratory PCDB, the bridge was disassembled and the strengthening retrofit was reinstalled on Cedar 4 (P1). This individual panel was tested for ultimate strength in the same manner as the other PCDB panels (see Section 4.1). Cedar 4 was chosen for this testing because it was the only panel not damaged during the laboratory PCDB ultimate strength testing.

In some PCDBs, only a few panels may require strengthening. In these situations, due to the transverse continuity, a portion of the post-tensioning force on a strengthened panel will be transferred to the adjacent, non-strengthened panels. To determine this post-tensioning force distribution, each panel in the laboratory PCDB was individually post-tensioned while the other three panels remained in their original condition (i.e. not post-tensioned). Throughout this testing, the ‘tight bolts plus shear connectors’ joint configuration

was utilized. At the maximum post-tensioning force (27.1 kip), the response of the entire PCDB was recorded by the DAS. Instrumentation from the joint configuration testing was utilized during this testing with additional strain gages on the post-tensioning tendons.

The maximum post-tensioning force was then simultaneously applied and locked on all four panels in the laboratory PCDB. In this configuration, another service load test was performed similar to the joint configuration testing (see Section 5.2.2). The joint configuration and instrumentation used in the post-tensioning force distribution tests was also used in the service load testing of the strengthened laboratory PCDB.

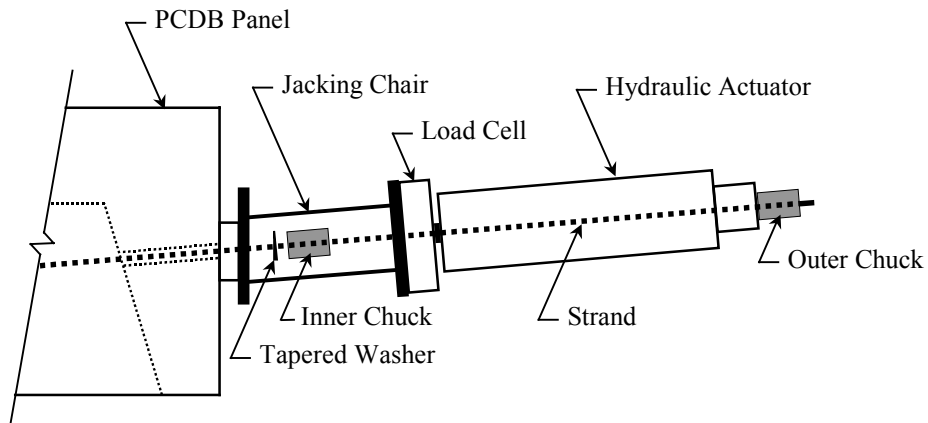


Figure 6.3. Details of tensioning system.



Figure 6.4. Tensioning system during tensioning of the strand.

### 6.3. Discussion of Results

Results from the post-tensioning force distribution tests will be presented first, followed by the service load testing results. Results from the ultimate strength testing of the individual retrofitted panel will conclude this chapter.

#### 6.3.1. Post-Tensioning Force Distribution

From the deflection data, load fractions were calculated for the post-tensioning of each panel. These values are presented in Table 6.1. Also presented in Table 6.1 are load fractions from the ‘tight bolts plus shear connectors’ joint configuration testing as presented in Section 5.2.3.3.

Table 6.1. Post-tensioning force distribution load fractions.

Test	Tensioned or Loaded Panel	Panel			
		P1	P2	P3	P4
Post-Tensioning Force Distribution	P1	0.58	0.30	0.09	0.02
	P2	0.33	0.37	0.21	0.09
	P3	0.06	0.14	0.45	0.35
	P4	0.03	0.09	0.32	0.56
'Tight Bolts Plus Shear Connectors' Joint Configuration	P1	0.57	0.30	0.10	0.03
	P2	0.28	0.37	0.24	0.11
	P3	0.10	0.22	0.37	0.31
	P4	0.03	0.08	0.29	0.61

As can be seen, the load fractions from the post-tensioning force distribution tests are essentially the same as the load fractions from the joint configuration tests. This indicates that the load fraction values used in the rating of a particular bridge can also be used in the design of the strengthening retrofit if it is required.

The slight variation in load fractions between the tensioning of P2 and P3 is most likely due to the difference in friction between adjacent panels. Deflection data from the post-tensioning force distribution tests are presented in Figure 6.5. The key for this figure – P1, P2, etc. – indicates the panel that is being post-tensioned. The deflections shown in this figure are approximately an order of magnitude less than the corresponding deflections from the joint configuration tests. At this relatively small level of response, friction, which varies with the smoothness of the panel sides and the tightness of the joint between two panels, has

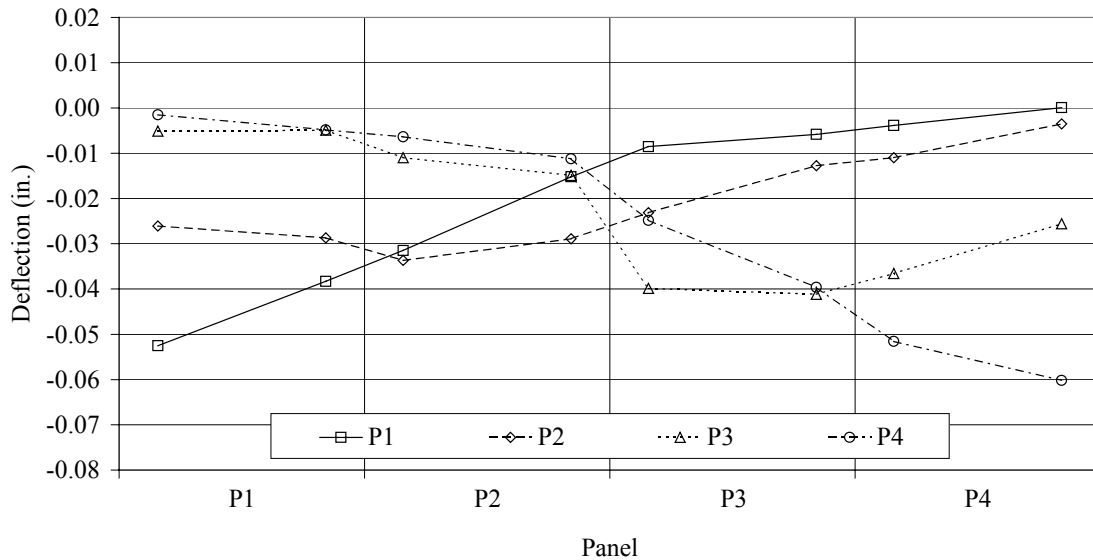


Figure 6.5. Deflection curves for post-tensioning force distribution testing.

a greater influence on the joint behavior. This variation in friction consequently affects the load fractions.

### 6.3.2. Service Load Testing on Strengthened Laboratory PCDB

Results from service load tests on the retrofitted laboratory PCDB were compared to results from similar testing on the laboratory PCDB prior to strengthening. Midspan steel strains induced by a 28 kip point load at LP3 are presented in Figure 6.6. As can be seen, steel strains were greatly reduced by the strengthening. For the loaded panel, P3, the steel strain was reduced by 51%. On the average, steel strains for the retrofitted laboratory PCDB were approximately 150 MII less than the corresponding strains before the strengthening. Concrete strains and vertical deflections were similarly reduced. Lowering the magnitude of the strains due to dead load obviously increases the live load carrying capacity of the PCDB.

The strengthening system was not designed to increase transverse load distribution since the joint configuration between adjacent panels remained unchanged. Maximum load fractions from before and after the retrofit are presented in Table 6.2. Variation between corresponding maximum load fractions was less than 0.01. This indicates that the strengthening system did not affect transverse load distribution as previously noted.

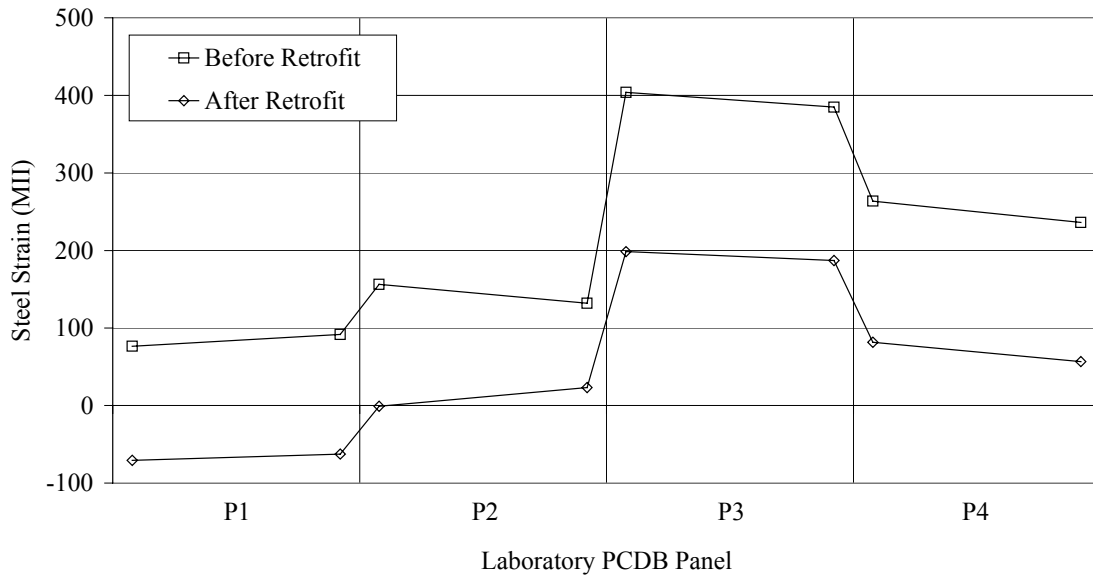


Figure 6.6. Midspan steel strains for LP3 at 28 kip.

Table 6.2. Maximum load fractions before and after strengthening.

Strengthening	Load Fraction			
	LP1	LP2	LP3	LP4
Before	0.57	0.37	0.37	0.61
After	0.58	0.37	0.36	0.62

### 6.3.3. Ultimate Strength Testing of a Strengthened PCDB Panel

During the post-tensioning of a single panel, the seating losses were found to be greater than expected. The desired strand force was 27.1 kip, or 12.4% greater than the actual measured strand force of 24.1 kip. Strand force after release of the actuator was calculated from the measured strand strains. Although not tried experimentally, additional overstressing of the strand prior to release should compensate for the greater seating losses.

Steel and concrete strains due to the dead load were theoretically calculated and compared to the actual steel and concrete strains induced by the strengthening system; these values are presented in Table 6.3. Both the steel and concrete strains were in good agreement. This indicates that although the actual strand force was less than the design

strand force, the strengthening retrofit was still effective in counteracting the dead load midspan moment. (Note: The sign differences in this table indicate the effectiveness of the strengthening system in reducing the effects of the dead load).

Table 6.3. Comparison of steel and concrete strains due to dead load and the strengthening system.

Source	Strain (MII) *	
	Steel	Concrete
Dead Load	155	-63
Strengthening System	-165	56

\* (+) indicates tensile strain

Moment/deflection curves for Cedar 1 and 4 are presented in Figure 6.7. Elastic behavior of Cedar 4, the retrofitted panel, was almost identical to the elastic behavior of Cedar 1. The slight offset between the two curves was due to the initial upward deflection induced by the strengthening system. Identical slopes indicate that the strengthening did not affect stiffness.

Once the primary reinforcing steel began to yield, behavior of the two panels deviated. Cedar 4 supported significantly more load than Cedar 1 for a given deflection. Strand strains indicated that the amount of force in the strand increased at a higher rate once the primary reinforcement had yielded; an indication that the strand was responsible for the added capacity.

Testing was temporarily halted for safety concerns when the strand reached 75% of its ultimate strength. At this point, the tensioning system was used to release the force in the strand and testing continued on the now unstrengthened panel until failure occurred.

As can be seen in Figure 6.7, the behavior of Cedar 4 after the strand was released was identical to Cedar 1. Ultimate strength of Cedar 4 was 460 ft-kip. The failure mode of both panels was a crushing failure of the deck concrete between the two load points.

#### 6.4. Strengthening Variations

Another advantage of this strengthening system is that it can be easily adapted to different types and lengths of PCDB panels. With a few simple modifications, this strengthening retrofit should function equally well on all PCDBs.

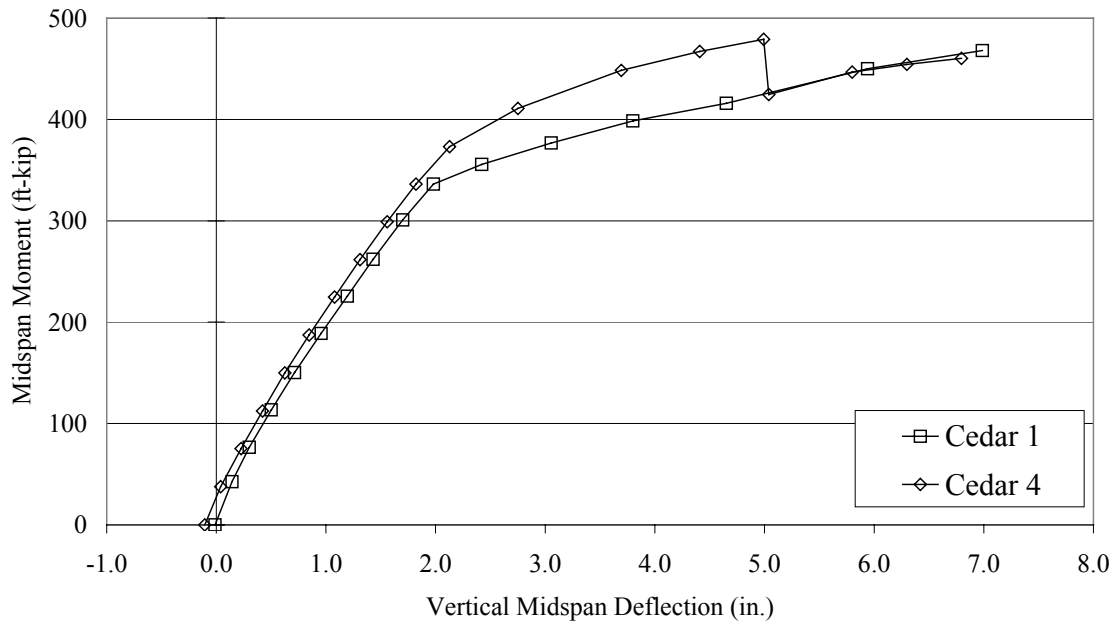


Figure 6.7. Midspan moment vs. midspan deflection for Cedar 1 and 4 during the ultimate strength tests.

PCDB lengths range from 19 ft to 36 ft. The longer bridges obviously have larger dead load midspan moments. To counteract this moment, a larger upward reaction from the strengthening system is required. There are three methods to accomplish this. First, the strand tension can be increased. Strand diameter may also need to be increased if the required strand force exceeds an allowable value for 1/2 in. diameter strand. Secondly, the height of the strut can be increased; the maximum height of the strut is only limited by clearance requirements under the bridge. Struts that protrude excessively below the PCDB may be damaged by debris during flood events. Lastly, the number of strands and struts per panel can be increased. Instead of running a single strand along the centerline of the panel, a strand may be placed next to the inner side of each stem so that there are two strands per panel. If additional force is required, a third strand could be added between the other two strands.

Diaphragm locations vary for Type I PCDB panels. Instead of a single diaphragm at midspan, 25 ft and 31 ft Type I PCDB panels have multiple diaphragms. The 25 ft panels have diaphragms approximately located at each third point and the 31 ft panels have diaphragms at the approximate quarter points. For the 25 ft panels, struts would be needed

on each diaphragm. This would change the retrofit from a king-post configuration to a queen-post configuration and would also cause some flexural stresses in the struts. Further investigations into this arrangement would need to be made before the retrofit is implemented on 25 ft Type I panels. For the 31 ft panels, a strut at least 5 in. in height placed on the midspan diaphragm will lower the strand enough to clear the other two diaphragms.



## 7. STRUCTURAL MODELING AND ANALYSIS

Experimentally tested PCDBs and individual PCDB panels were modeled and analyzed by Qin [11] using ANSYS [12], a general finite element software program. Analytical deflections and strains were compared with the experimental results. The analytical models were for predicting the behavior of the bridges and panels under service load, rather than for determining their ultimate strengths. Thus, only a linear elastic analysis was performed. Details on the theory of the element types used in these analyses can be found in the ANSYS User's Manual [12].

### 7.1. Modeling of Individual PCDB Panels

The laboratory tested PCDB panels, presented in Chapter 4, were modeled using ANSYS since they are the basic units of the PCDBs. In the library of the ANSYS program, there are 189 different elements for modeling different structural elements; it is important to determine which of these elements are most applicable. After some initial trials, theoretical results obtained using the Solid45 - Link8 and Solid73 - Pipe16 models were determined to be the most accurate when compared to the experimental data and the theoretical results based on ACI 318-99 [7].

In the analytical models, simple support conditions (hinge at one end and a roller at the other end) were assumed. The span length was taken as the center-to-center distance between supports.

#### 7.1.1. Solid45 - Link8 model

A three-dimensional element that connects four or more non-planar nodes forms a volume which are modeled using the family of Solid elements in the ANSYS. Solid45 element, illustrated in Figure 7.1, is defined by eight nodes, each with three degrees of freedom (DOFs): translations in the nodal x, y, and z directions [12].

Link8 element is a uniaxial tension-compression element with three DOFs at each node: translations in the nodal x, y, and z directions. It is defined by two nodes, the cross-sectional area, and an initial strain, as shown in Figure 7.2.

This Solid-Link model is a combination of Solid45 and Link8 elements. In modeling the PCDB panels, the Solid45 element was used to model the concrete portion of the beam,



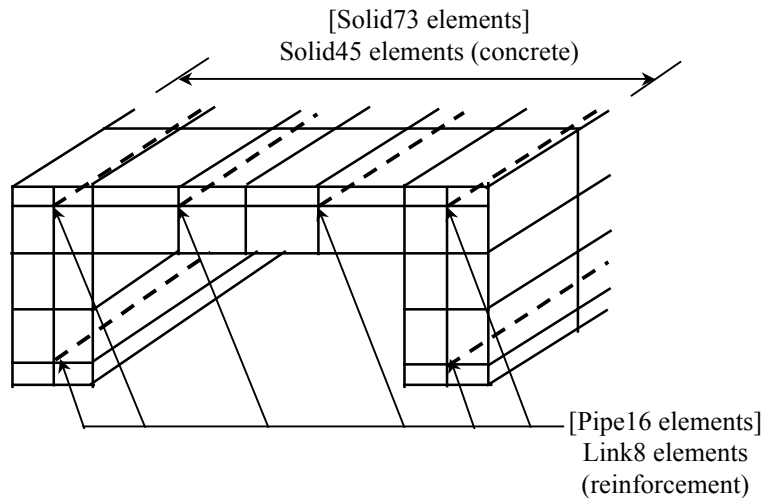


Figure 7.3. Finite element models.

This model represents the actual shape of the panel; various elements are connected to each other at the nodes, thus forming a monolithic channel beam model. Reinforcement is also included in the appropriate positions with the desired area and material properties. In this configuration, the model was assumed uncracked and thus had an uncracked moment of inertia,  $I_{\text{uncr}}$ . Results obtained using this model were compared with theoretical results from beam theory. Under the same loading, this model predicted a maximum deflection of 0.0387 in., while beam theory using  $I_{\text{uncr}}$  resulted in a 0.0390 in. displacement. Strain profiles along the depth of the cross-section from the model and beam theory are illustrated in Figure 7.4. By comparing the two strain profiles, it can be concluded that this model is very accurate in representing the PCDB panel in the uncracked condition.

### 7.1.2. *Solid73 - Pipe16 model*

The difference between a Solid73 and the Solid45 element is that Solid73 has six DOFs instead of three at each node: translations in the nodal x, y, and z directions and rotations about the nodal x, y, and z axes [12]. A Pipe16 element is a one-dimensional element with tension-compression, torsion, and bending capabilities. It has six DOFs at each of the two nodes it connects: translations in the nodal x, y, and z directions and rotations about the nodal x, y, and z axes. The basic input data include the pipe outer diameter (OD) and wall thickness (Tkwall) [12]. Details of this element type are shown in Figure 7.5. The

geometry of the Solid73 - Pipe16 model, as illustrated in Figure 7.3, is the same as that of the Solid45 - Link8 model.

This elastic Solid73 - Pipe16 model is more refined than the Solid45 - Link8 model in that it has six DOFs, which include the rotational behavior of the nodes. The deflection and strain profiles derived from this model were determined to be essentially the same as those obtained using the Solid45 - Link8 model. The main reason for constructing this model was for investigating the connection between the PCDBs, which will be presented in Section 7.2.

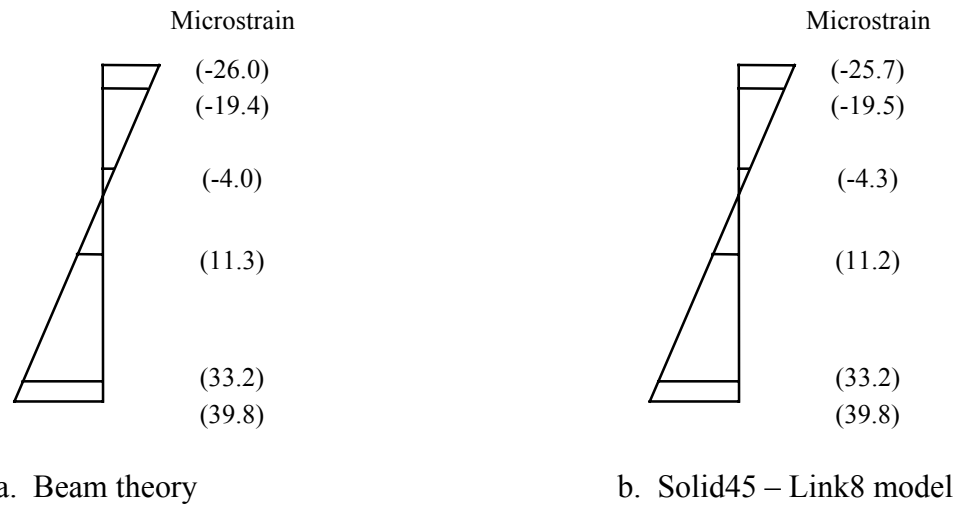


Figure 7.4. Comparison between the beam theory and Solid45 – Link8 model.

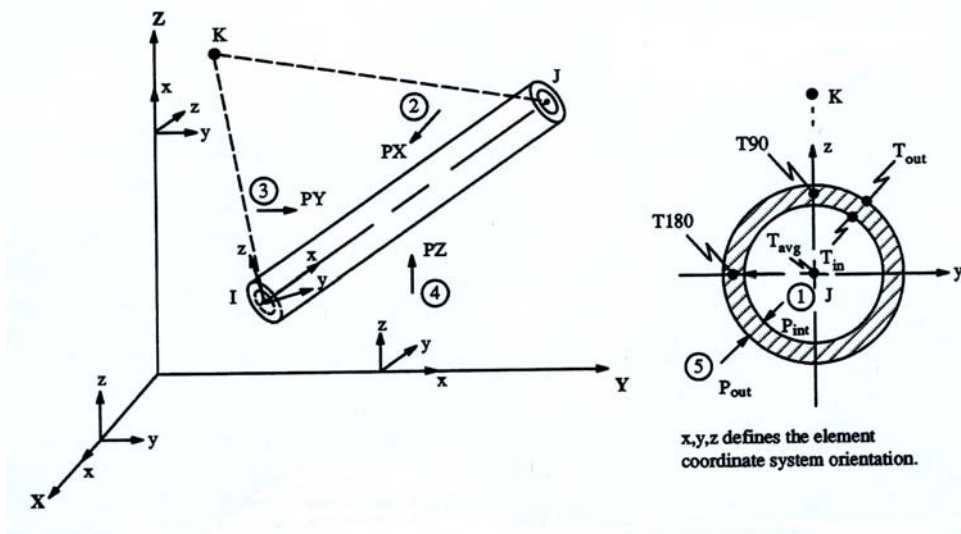
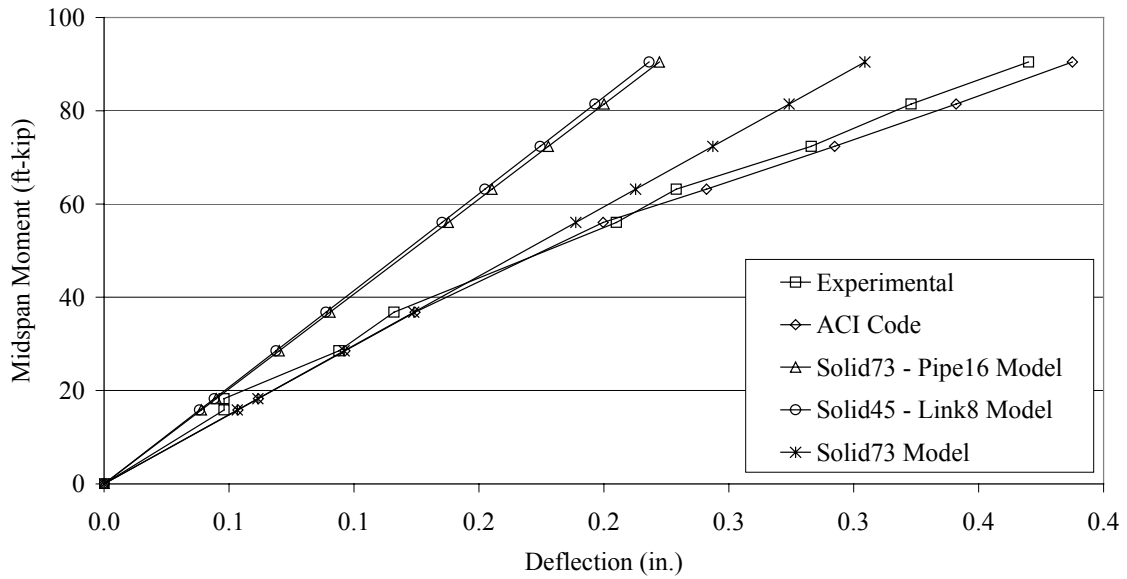


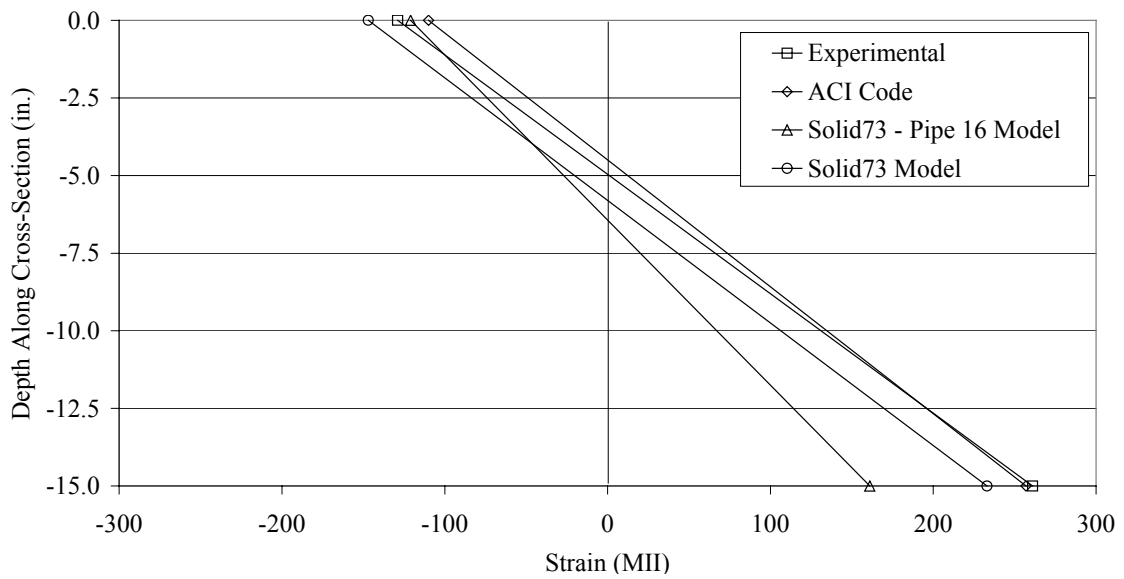
Figure 7.5. Pipe16 element [12].

**7.1.3. Discussion of Results**

Results from the elastic analytical models, the experimental results, and the theoretical calculations based on ACI 318-99 for the maximum moment produced by single lane AASHTO HS20 loading (determined in Section 4.2.1) are presented in this section. Figure 7.6 presents the comparison of the midspan deflections and strain profiles along the depth of cross-section for Cedar 1, while Figure 7.7 presents data on Butler 1.

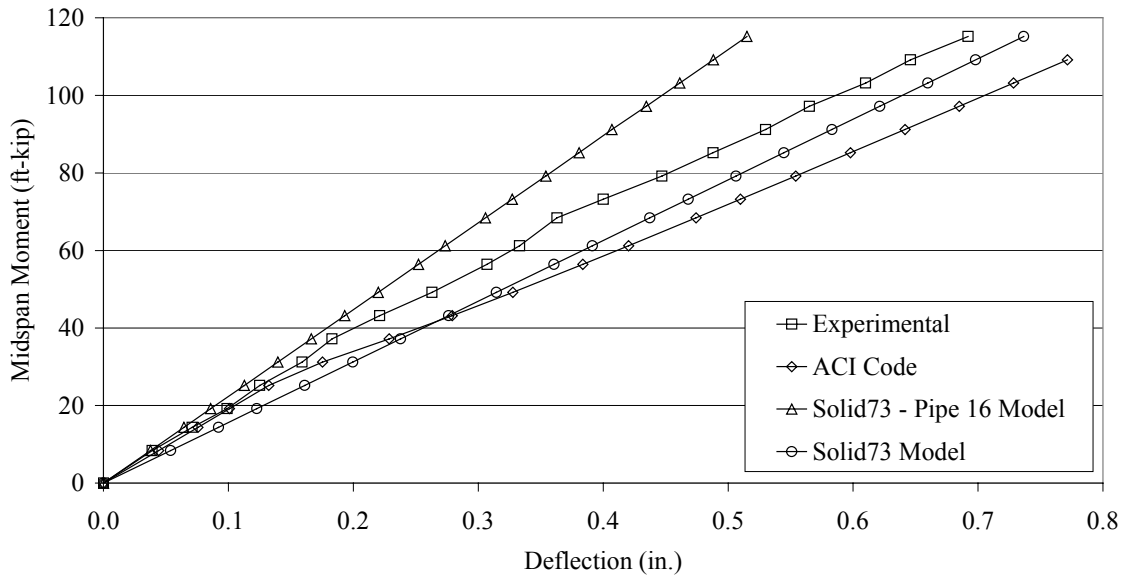


a. Midspan deflection

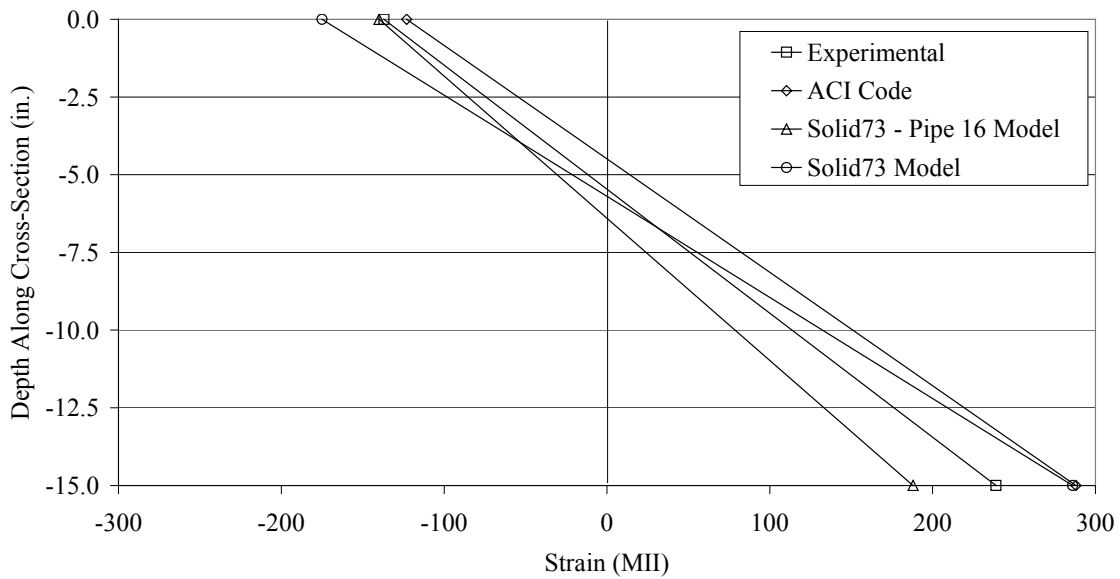


b. Strain profiles along the depth of the cross-section

Figure 7.6. Comparison of results for Cedar 1.



a. Midspan deflection



b. Strain profiles along the depth of cross-section

Figure 7.7. Comparisons of results for Butler 1.

From Figures 7.6a and 7.7a, it can be seen that the results from the Solid45 - Link8 model are very close to the results from the Solid73 - Pipe16 model. These two models, however, always underestimate the structural behavior of the tested panels, which may be attributed to their stiffness. As previously noted, a “perfect bond” between the concrete and

reinforcement was assumed in these models. Thus, slip between the reinforcement and the concrete, or deterioration of the concrete in the actual beams was not included. As shown in Figure 7.4, the Solid45 - Link8 and Solid73 - Pipe16 models results match the calculations based on  $I_{uncr}$  closer than the results based on  $I_e$ . The relative difference in the results from the models and the laboratory test results is less than 30% in the linear elastic stage. This difference increases gradually after the crack occurred, due to both the nonlinear behavior of the actual beams and the stiffness of the elastic models which do not consider the effect of cracking.

Based on the preceding observations, a model neglecting reinforcement was constructed to represent a beam with an  $I_g$  rather than  $I_{uncr}$ . In this model, there was only the Solid73 element to represent the concrete; the Pipe16 element (used to represent the reinforcement) was removed. The results from this Solid73 model are also shown in Figures 7.6a and 7.7a. As can be seen, within the linear elastic stage, the Solid73 model is very close to the results based on the ACI code, thus it is more consistent with the experimental result than the models that included the reinforcement for Cedar 1. For Butler 1, the experimental results are between those from the models that include and neglect the reinforcement.

Figure 7.6b presents the strain profiles along the depth of Cedar 1 when the bending moment of 63.18 ft-kip was applied which is greater than the cracking moment for this panel. With the cracked neutral axis, results based on the ACI code are very similar to the experimental result. Since the finite element models are elastic, they always underestimate the strain values. However, the curvature which resulted from the finite element model neglecting reinforcement (Solid73 model), is very close to the experimental result. The finite element model with reinforcement (Solid73 - Pipe16 model) produced the smallest curvature and tensile strain values and the lowest neutral axis (greatest distance from top fibers), since it has the largest stiffness value.

Similar results are illustrated in Figure 7.7b, when a bending moment of 61.2 ft-kip was applied to Butler 1. The finite element model neglecting reinforcement (Solid73 model) predicted a compressive strain at the top of the beam very close to the experimental result. The curvature of the panel, based on the experimental data, is between those obtained using the finite element models with and without reinforcement. Once again, the elastic finite

element model with reinforcement (Solid73 - Pipe16 model) underestimated tensile strain and curvature in the panel.

#### 7.1.4. Summary of models

The Solid45 - Link8 and Solid73 - Pipe16 models are appropriate for modeling the individual PCDB panels and were selected for the following reasons:

1. They represent the actual physical shape of the panels and their components.
2. Within the elastic range, results from the finite element analyses are in good agreement with results based on the ACI code.
3. They provide compatibility in modeling the critical connection components.

The differences between the analytical and experimental results within the elastic range are mainly due to the stiffer analytical models.

## 7.2. Modeling of the Laboratory PCDB

The laboratory PCDB, presented in Chapter 5, was modeled based on the models presented in the previous section. The influence of the connections used with PCDBs: (1) bolt connections, (2) pipe connections, and (3) bolt plus pipe connections was investigated.

### 7.2.1. Modeling of Bolt Connections

#### 7.2.1.1. Mechanism of Load Transfer Through Bolts

An analytical model of two PCDB panels (Panel A and Panel B) with a bolt connection, and an external vertical load,  $P$ , applied to Panel A is presented in Figure 7.8a. Due to  $P$ , Panel A will deflect downward, creating contact stresses between the bolt and Panel A, from point 1 to point 2, and the bolt and Panel B, from point 2 to point 3.

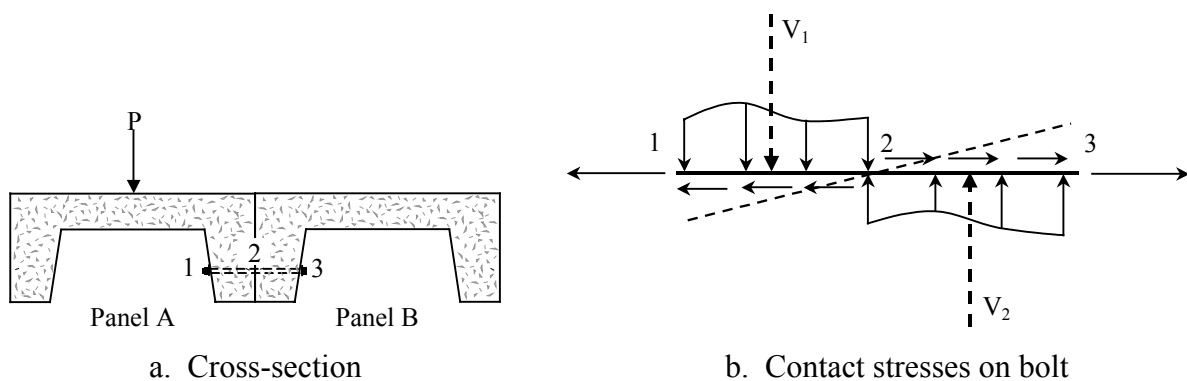


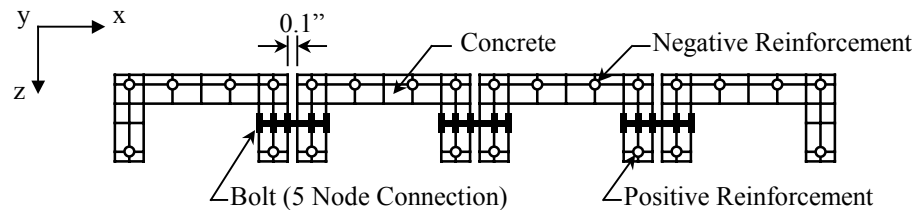
Figure 7.8. Mechanism of load transfer through bolts.

Figure 7.8b shows the contact stresses on the bolt. To achieve equilibrium, the force  $V_1$  from point 1 to point 2 must equal the force  $V_2$  from point 2 to point 3. Therefore, Panel B is subjected to a downward force  $V_2$ , while the load on Panel A is  $P-V_1$ . In other words, a portion of the load  $P$  is transferred from Panel A to Panel B.

It can be seen that the bolt is also subject to a bending moment, resulting from the contact stresses shown in Figure 7.8b. Thus, the bolt has an additional rotational degree of freedom.

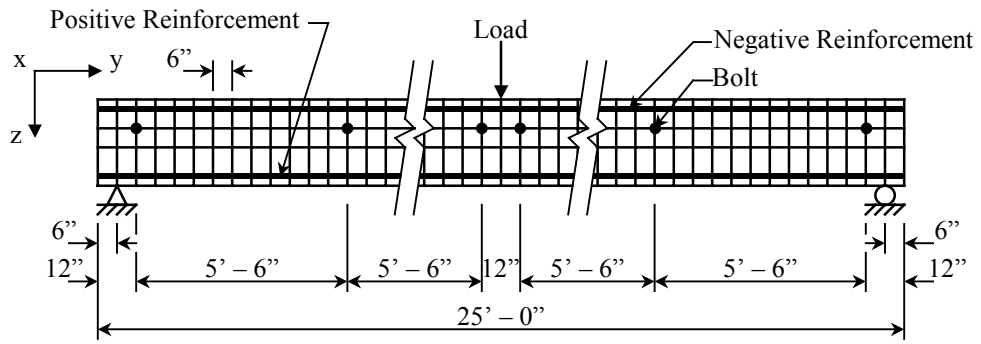
#### 7.2.1.2. Selection of Bolt Model Element

Based on the study performed to model the individual PCDB panels, the Solid45 - Link8 model with 3 DOFs and the Solid73 - Pipe16 model with 6 DOFs were adopted to analyze the laboratory PCDB with only the bolt connections. In the Solid45 - Link8 model, the Link8 element is used to model both the reinforcement and the bolt connections, whereas in the Solid73 - Pipe16 model, the Pipe16 element is used for both. Based on laboratory tests, the modulus of elasticity of the concrete and the modulus of elasticity of the reinforcement was determined to be 5,700 ksi and 26,500 ksi, respectively. The modulus of elasticity of the bolts was assumed to be 29,000 ksi. Details of the two models are presented in Figure 7.9 and Table 7.1. For comparison, identical mesh sizes, support conditions, load position (LP2, see Section 5.2.1) and load magnitude were applied to the two models. Deflection profiles from the two models are shown in Figure 7.10.



a. Cross-section of models

Figure 7.9. Details of the Solid45 - Link8 and Solid73 - Pipe16 laboratory PCDB models.



b. Side view of models

Figure 7.9. Continued.

Table 7.1. Element types and properties used in the analytical models.

Model Type	Concrete	Negative Reinforcement (1 - #4)	Positive Reinforcement (3 - #8s and 1 - #7)	Bolt (Dia.=5/8 in.)
Solid45 - Link8	Solid45	Link8 - Areas (in <sup>2</sup> )		
		0.2	2.97	0.31
Solid73 - Pipe16	Solid73	Pipe16 - Dia (in)		
		0.50	1.95	0.63

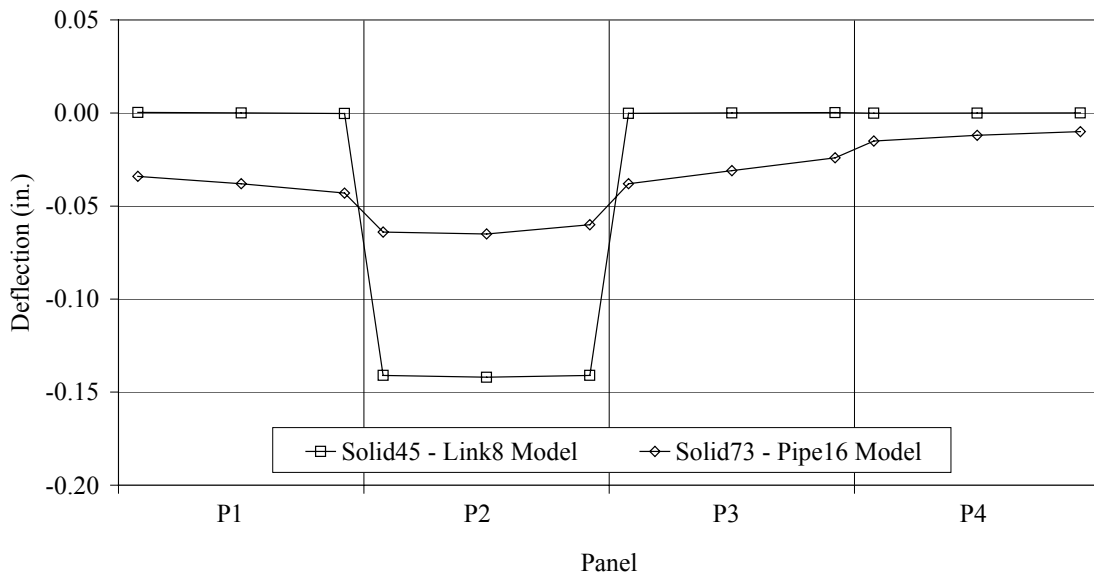


Figure 7.10. Comparison of the Solid45 – Link8 and Solid73 – Pipe16 models for LP2.

From Figure 7.10, it can be seen that the Link8 element cannot represent the bending behavior of the bolt because it has no rotational nodal DOFs. From the Solid45 - Link8 model, P2 deflects under load while the other panels do not. Thus, no load is transferred to the adjoining panels. There is load transfer when the Pipe16 element is used to model the bolt connections. Therefore, the Solid45 - Link8 model cannot be used to analyze PCDBs with bolt connections. Before using the Solid73 - Pipe16 model for modeling other PCDBs with bolt connections, a node connection sensitivity study was performed.

#### *7.2.1.3. Node Connection Sensitivity Study*

The Solid73 - Pipe16 model is sensitive to the number of nodes connected by the Pipe16 element; the more nodes connected by the Pipe16 element, the more load is transferred through the element. However, currently no information on how many nodes are required to best represent the behavior of the bolts is available. Moreover, an unavoidable practical problem - the amount of bolt slip - makes an accurate analysis extremely difficult. Thus, a sensitivity study was conducted using three bolt connection scenarios: 4-nodes, 5-nodes, and 7-nodes as described in Figure 7.11. Deflection profiles for these three bolt connection scenarios are compared to the laboratory deflection data in Figure 7.12. For this laboratory PCDB, the 5-node connection model (Model B) is more consistent with the laboratory results than the other two bolt connection models. However, the 4-node and 7-node connection models may be applicable to other PCDBs that have looser or tighter bolt connections.

#### *7.2.1.4. Discussion of Results*

From Figure 7.12, it can be seen that the elastic models slightly underestimate the behavior of the laboratory PCDB. This may be attributed to the nonlinear behavior of the actual structures or the stiffness of the analytical model. The panel analyses described in Section 7.1 can be used to address this issue, since this laboratory PCDB is composed of the panels taken from the Cedar County Bridge.

Based on the assumption that the deflection is proportional to the load resisted, P2 resisted 38.9% of the total load on the bridge. This percentage was obtained by dividing the deflection of P2 by the sum of all panels' deflections measured in the laboratory test. Since the total applied load is 12 kips, P2 is calculated to resist a load of  $38.9\% \times 12 = 4.67$  kips.

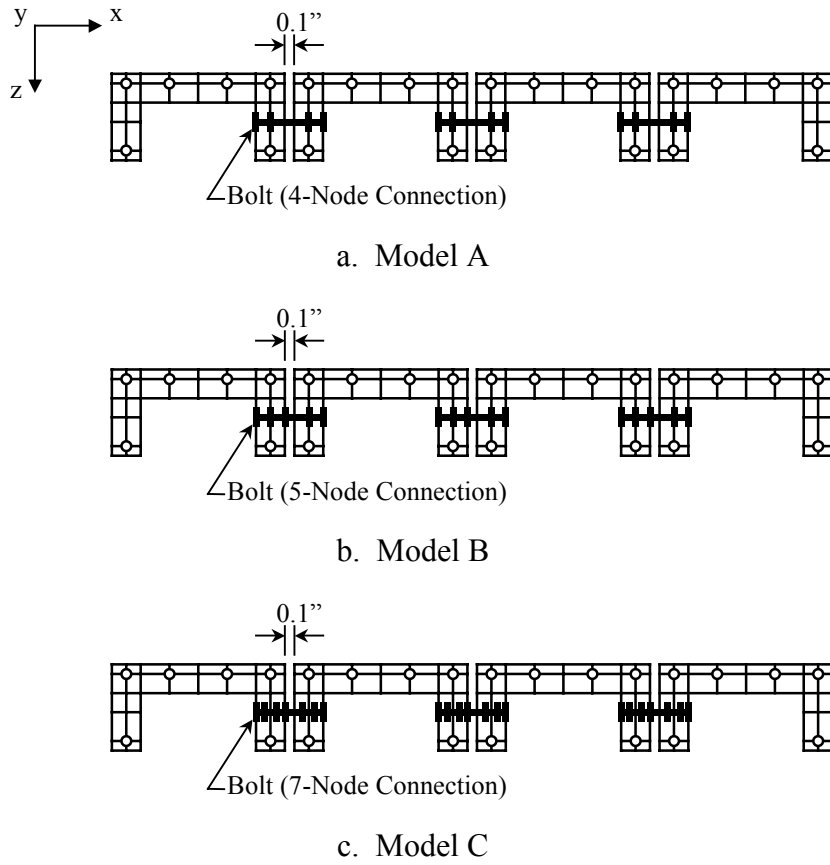


Figure 7.11. Models of bolt connections.

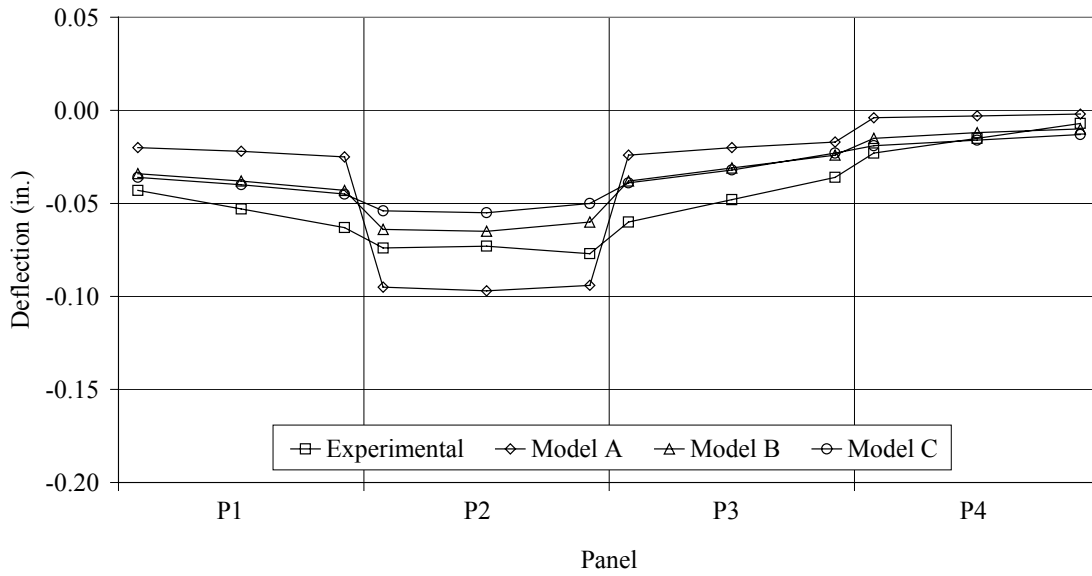


Figure 7.12. Comparison of node connections scenarios of bolt model for LP2.

Under this load, a maximum midspan bending moment,  $4.67 \times 24.33 / 4 = 28.4$  ft-kip, occurs in P2, which is less than its cracking moment of 36.02 ft-kip. From Figure 7.6a, for this loading it can be seen that the experimental deflection of P2 is approximately 0.09 in., while the ANSYS elastic Solid73 - Pipe16 model predicts a deflection of 0.07 in. From Figure 7.12, it can be seen that similar experimental and theoretical results using Model B are obtained for P2. Thus, the 5-node connection Pipe16 element (Model B) was adopted for modeling the bolt connections.

From the preceding discussion, it can be seen that under this load, theoretically the beam has not cracked. The difference between the experimental and analytical results is mainly induced by the stiffness of the analytical model. As previously noted in Section 7.1, a model neglecting reinforcement was constructed to represent panels with gross moment of inertia,  $I_g$ . In this Solid73 - Pipe16 model, the Pipe16 elements modeling the reinforcement were removed, whereas those modeling the bolt connections were kept. This model is henceforth described as the “model w/o reinforcement”. Figure 7.13 illustrates the effect of the reinforcement on the deflections of one of the laboratory PCDB. It can be seen that the results from the model neglecting reinforcement are very close to the experimental data. The maximum deflection predicted by the model neglecting reinforcement is 0.08 in., only 7% more than the experimental results. For P2, which received the load directly, the experimental data are between the two models. Both of the analytical models underestimated the deflection of P3 by 33% and 17%, respectively. The differences in the results obtained using the models and the experimental data for P1 and P4 are small.

## **7.2.2. Modeling of Pipe Connections**

### *7.2.2.1. Mechanism of Load Transfer through Pipes*

An analytical model of two channel beams (Panel A and Panel B) with a steel pipe connection is shown in Figure 7.14. Under a vertical load,  $P$ , contact stresses and shear stresses (or friction stresses) develop perpendicular to and along the surface of the pipe. Thus, a certain amount of  $P$  will be transferred from Panel A to Panel B. To simplify the analysis, the pipe is usually idealized as a hinge connection, thus only shear is transferred between the adjacent panels.

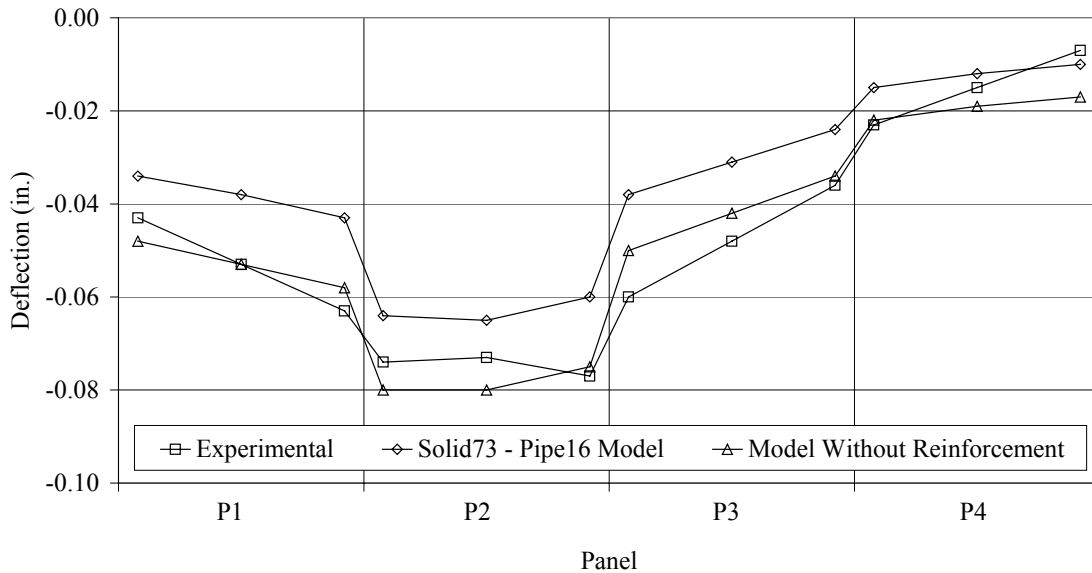


Figure 7.13. Effect of reinforcement and model on deflection.

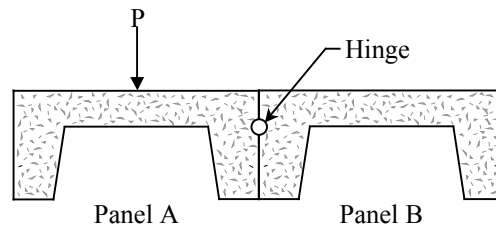


Figure 7.14. Mechanism of load transfer through pipe.

#### 7.2.2.2. Selection of Pipe Model Elements

Based on the hinge assumption, the Combin7 element of the ANSYS program was selected to model the steel pipe connections. The Combin7 element is a three-dimensional pin joint which may be used to connect two or more parts of a model at a common point. Capabilities of this element include joint stiffness, friction, and other certain control features.

It was determined that the model is sensitive to the translational stiffness,  $K1$ , of the Combin7 element. Due to the complexity of the contact behavior of the panels and pipes, it is difficult to assign a value to  $K1$ . Thus, a sensitivity study was performed where  $K1$  was assumed to be 5, 10, 15, 20, 100 kip/in, respectively. The deflection profiles from these models are shown in Figure 7.15. When  $K1$  is set to 5 kip/in, load transfer between panels is negligible, whereas, when  $K1$  is 100 kip/in, the panels are very rigidly connected. Although

no experimental verification is available, results from the laboratory bridge testing with only bolt connections presented in Section 7.2.1 can be used as a reference if it is assumed that the pipes are at least as effective as the bolts. Based on this assumption,  $K1 = 20$  kip/in was assumed since it closely models the rotation of the adjoining panels.

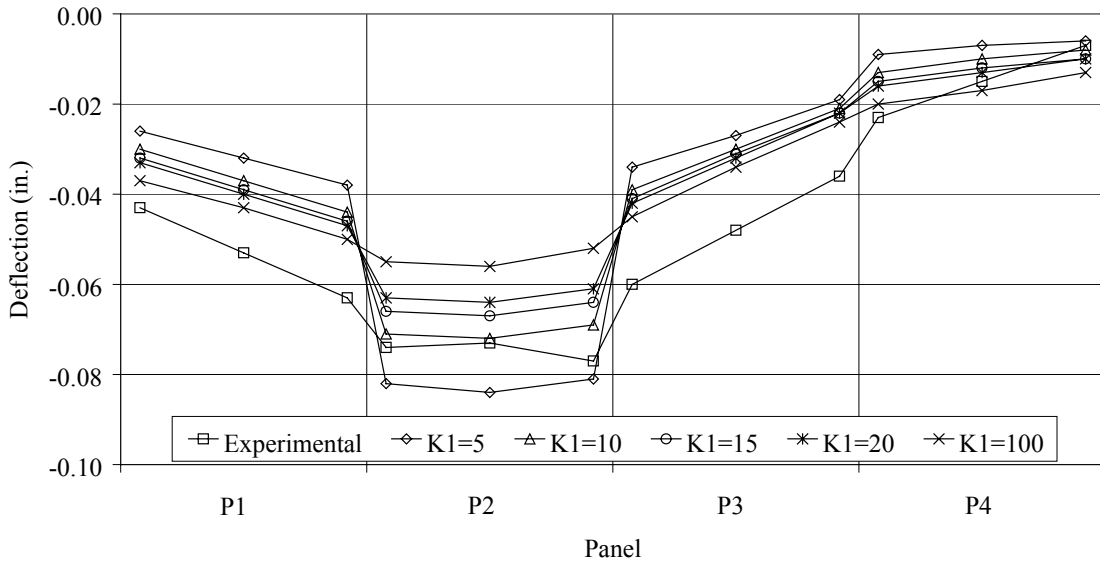


Figure 7.15. Effect of translational stiffness of Combin7 element on deflection for LP2.

### 7.2.3. Modeling of PCDBs with Bolt and Pipe Connections

Based on the investigation of bolt and pipe connections, the Solid73 - Pipe16 - Combin7 model was selected to model PCDBs with bolt and pipe connections. A cross-section of the model is illustrated in Figure 7.16. Experimental results were used to verify the appropriateness of this model.

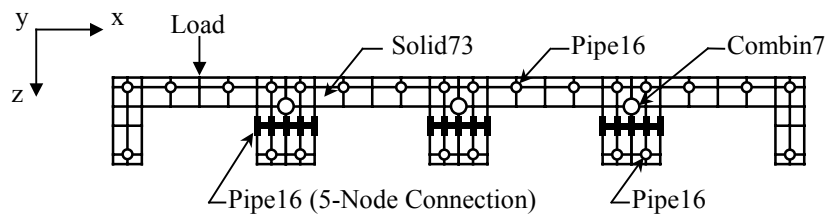


Figure 7.16. Cross-section of the Solid73 - Pipe16 - Combin7 model.

#### **7.2.4. Summary of Models**

After a careful comparison with the laboratory test results, the Pipe16 element and the Combin7 element were determined to model the bolt and the pipe connections, respectively. A 5-node-connection element was selected to model the bolts and a translational stiffness of  $K1 = 20$  kip/in was assigned to the pipe model, since they provide an appropriate rotation between the adjoining panels of the laboratory PCDB.

With a smaller stiffness, the analytical model neglecting reinforcement is more consistent with the laboratory PCDB than the model including reinforcement. Due to the deterioration, the field PCDBs should also have a smaller stiffness than the analytical models including reinforcement. However, since it is difficult to determine the decrease in stiffness due to the deterioration, the models including reinforcement were used to analyze the field PCDBs. Thus, the theoretical results are unconservative.

### **7.3. Modeling of Field PCDBs**

The four field PCDBs, presented in Chapter 3, were modeled using the ANSYS program. Deflections and strains between the analytical models and the field tests were compared and discussed. Results from two of them are presented in the following sections.

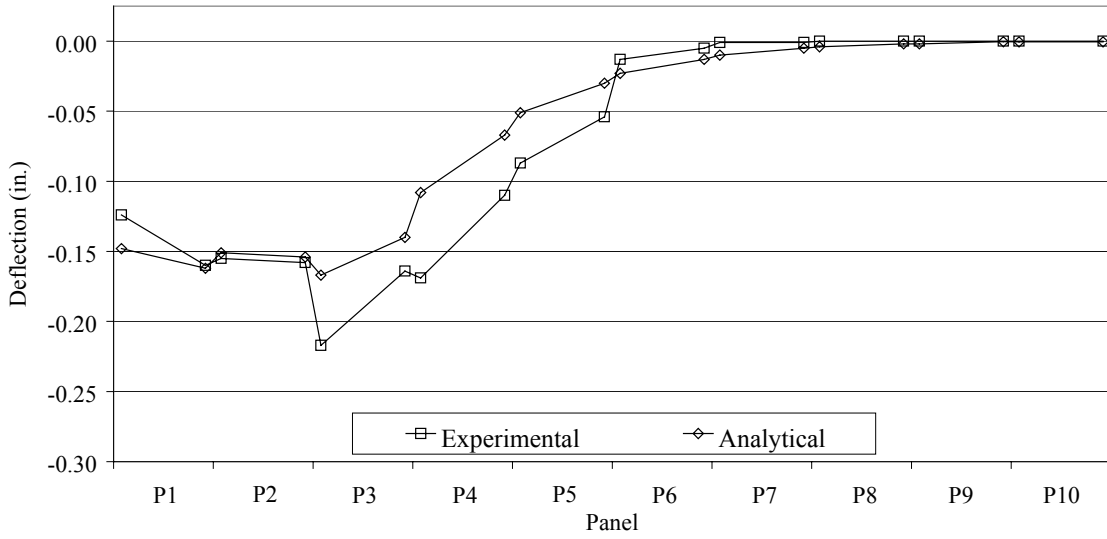
#### **7.3.1. Bridge 1: Butler County Bridge**

##### *7.3.1.1. Model Description*

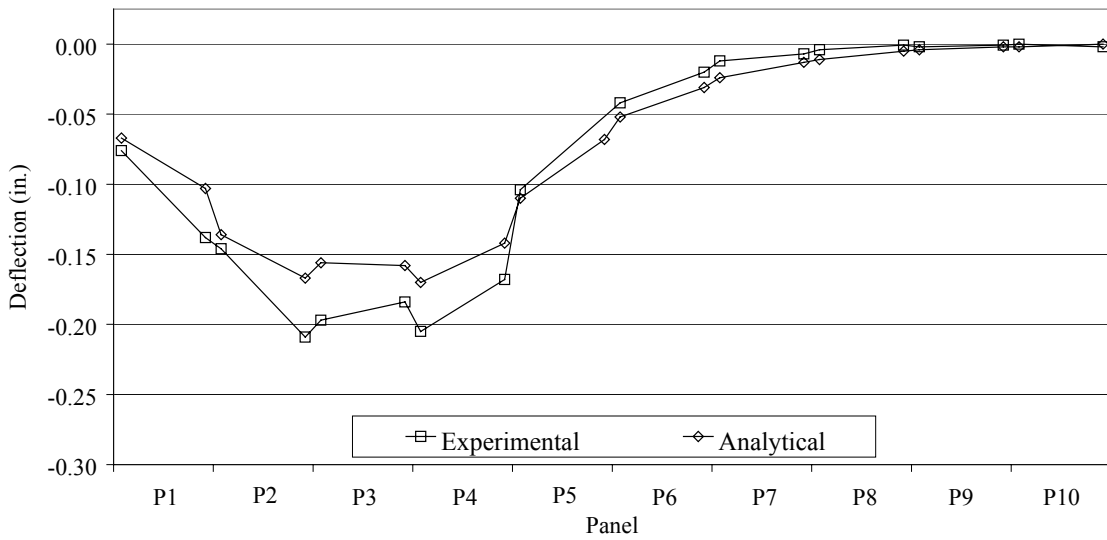
Based on the study performed in Section 7.2, the Solid73 - Pipe16 - Combin7 model was adopted to analyze the Butler County Bridge which has bolt and pipe connections. Concrete and reinforcement were modeled using the Solid73 and Pipe16 elements, respectively. Support conditions were assumed to be a pin at one end and a roller at the other end; span length was taken as the distance from the center to center of the supports. The test vehicle was positioned to produce a maximum longitudinal bending moment at the midspan of the panels.

##### *7.3.1.2. Discussion of Results*

Midspan deflection and primary reinforcement strains from the analytical model and field test results were compared for various transverse wheel load positions as shown in Figures 7.17 and 7.18. (See Section 3.2.3 for descriptions of load positions).

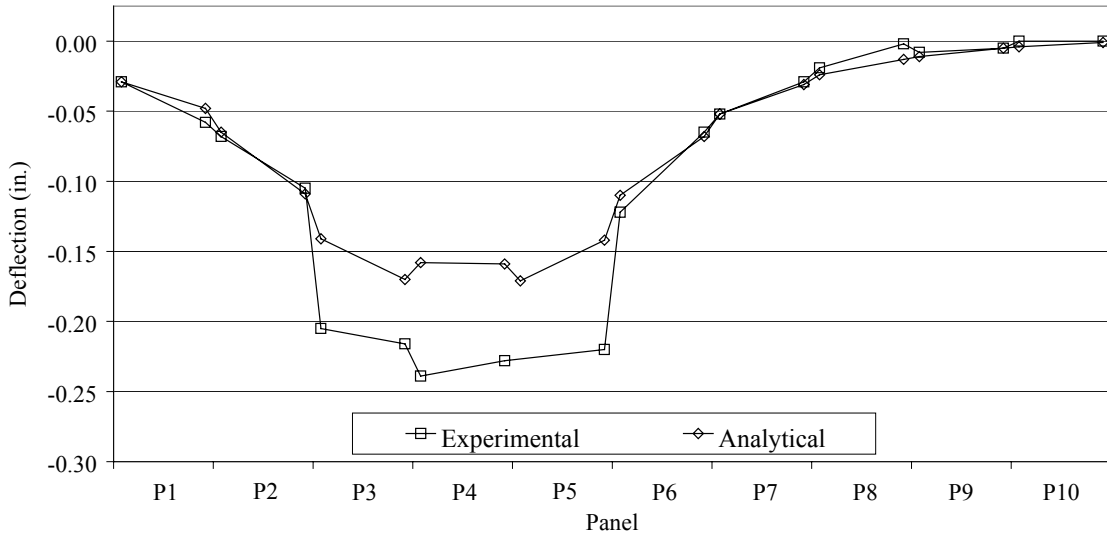


a. Midspan deflection for 1-LP13.B

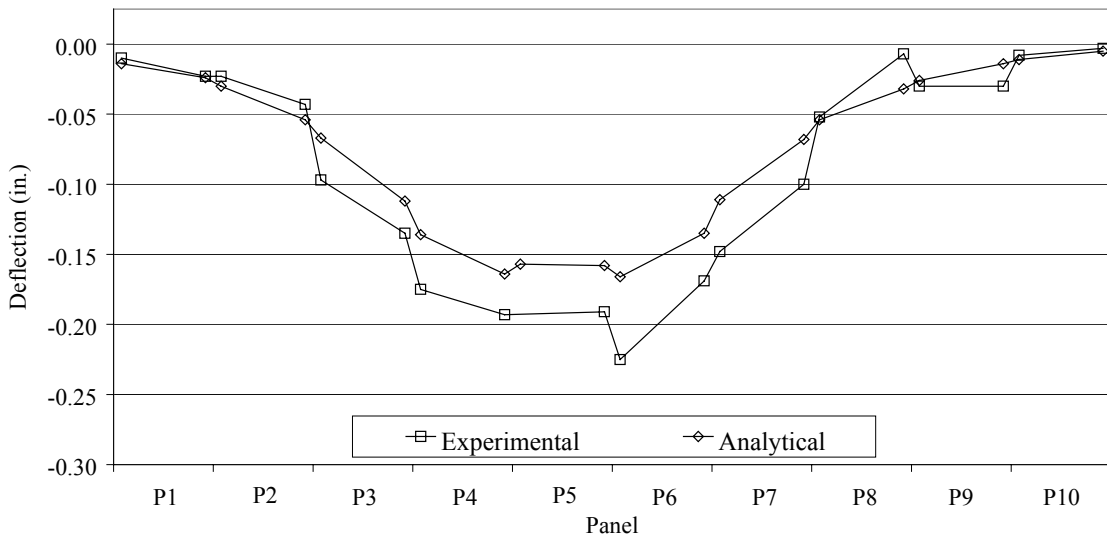


b. Midspan deflection for 1-LP24.B

Figure 7.17. Comparison of deflection profiles for Bridge 1.

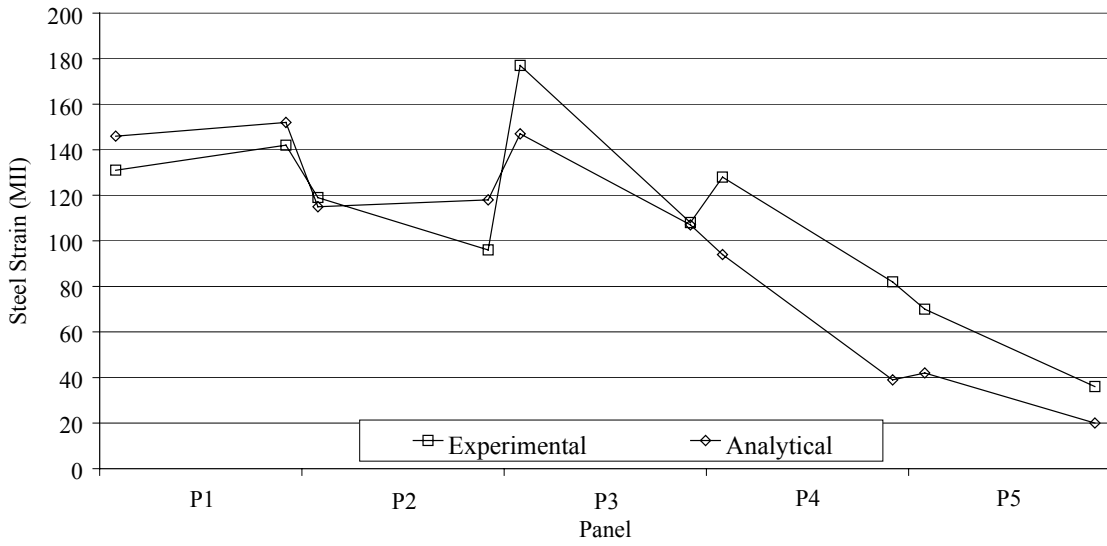


c. Midspan deflection for 1-LP35.B

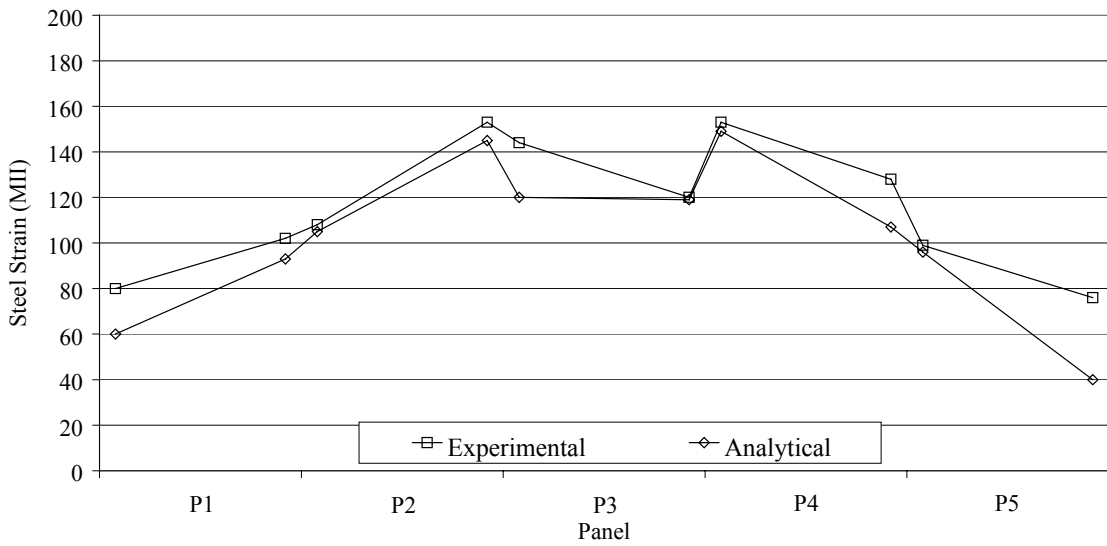


d. Midspan deflection for 1-LP46.B

Figure 7.17. Continued.



a. Steel strain for 1-LP13.B



b. Steel strain for 1-LP24.B

Figure 7.18. Comparison of primary reinforcement strain profiles for Bridge 1.

With a larger stiffness, the analytical model produces smaller deflections than the experimental results. As can be seen, there was slip between P2 and P3, P4 and P5, and P5 and P6. The bridge's behavior at the connections was significantly affected by the slip occurrence, but the overall behavior of the bridge is still similar to the analytical model. Theoretical results obtained using the 5-node-connection Pipe16 and Combin7 model with a translational stiffness of 20 kip/in. are close to the experimental results.

When the wheel loads are applied on the edge panel of the bridge, the edge-stiffening effect of the bridge is significant. However, the analytical model doesn't adequately predict this effect, even when the curbs and rails are included. Under load position 1-LP13.B (see Figure 7.17a), the edge panel of the bridge only deflects 0.125 in., while the analytical model predicts a deflection of 0.15 in. – a 20% difference. When the wheel loads are applied away from the edge panel, this edge-stiffening effect is reduced as may be seen in Figure 7.17b, c, and d.

The strain profiles that resulted from the tests and the analytical model are very consistent. The analytical model predicted a maximum bottom strain 20% lower than the experimental strain. Slip occurrence and edge-stiffening effect are also observed.

### **7.3.2. Bridge 2: Delaware County Dairy Bridge**

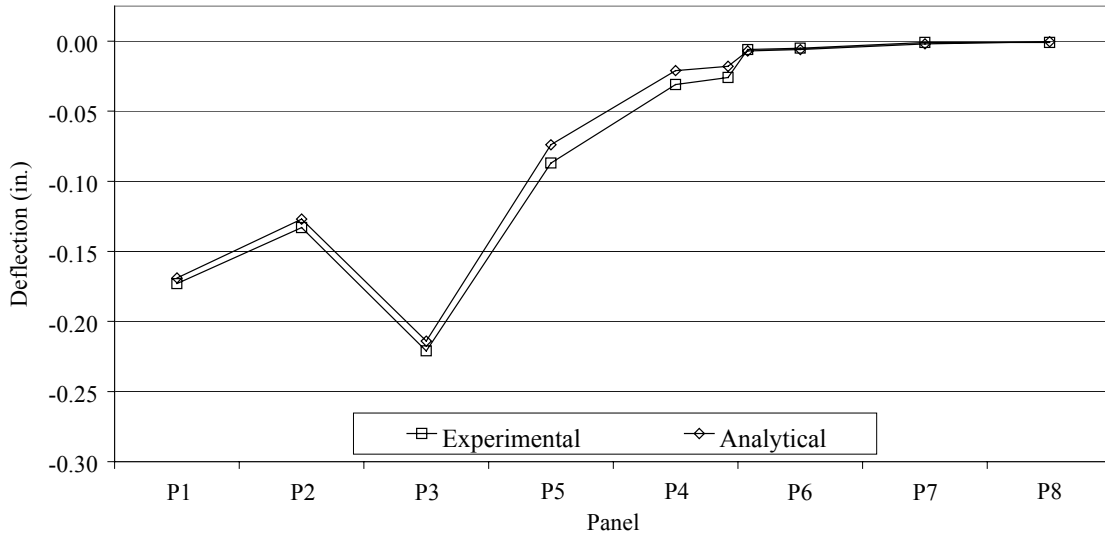
#### *7.3.2.1. Model Description*

The Solid73 - Pipe16 model was adopted to analyze the Delaware County Dairy Bridge that had only bolt connections. Based on the test results that indicate significant slip in this bridge, a 4-node connected Pipe16 element was used to model the bolt connections.

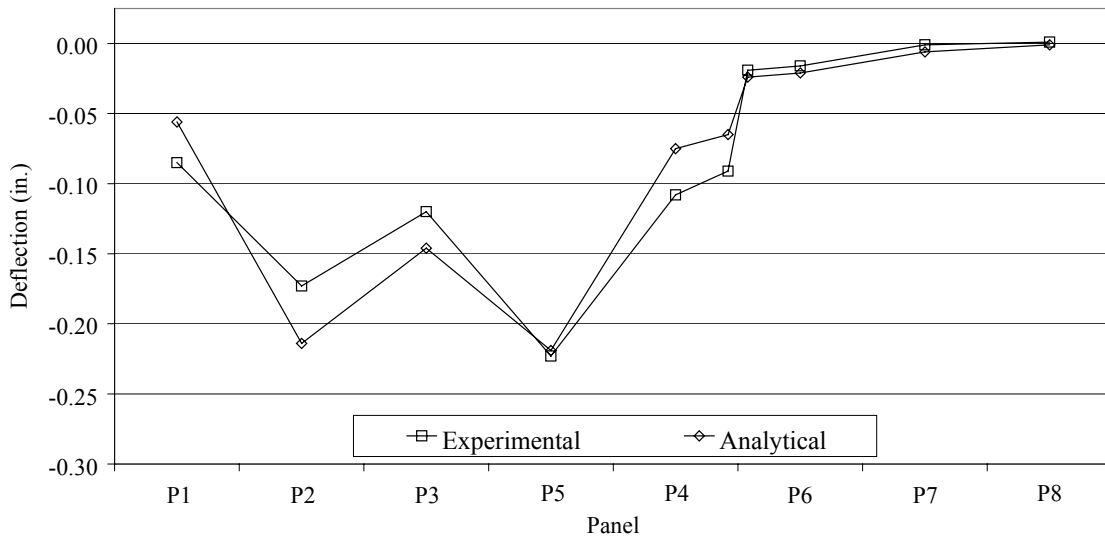
#### *7.3.2.2. Results and Discussion*

Midspan deflection and bottom strain profiles – theoretical and experimental – are presented in Figures 7.19 and 7.20.

The deflection profiles obtained using the analytical model are close to the experimental results. A maximum deflection of 0.22 in. was measured as well as theoretically predicted. For 2-LP24.B, the model underestimates the deflection of P1 by 32% and it overestimates the deflection of P2 by 23%. In both cases, however, the deflections are quite small. Edge stiffening in this bridge is also apparent.

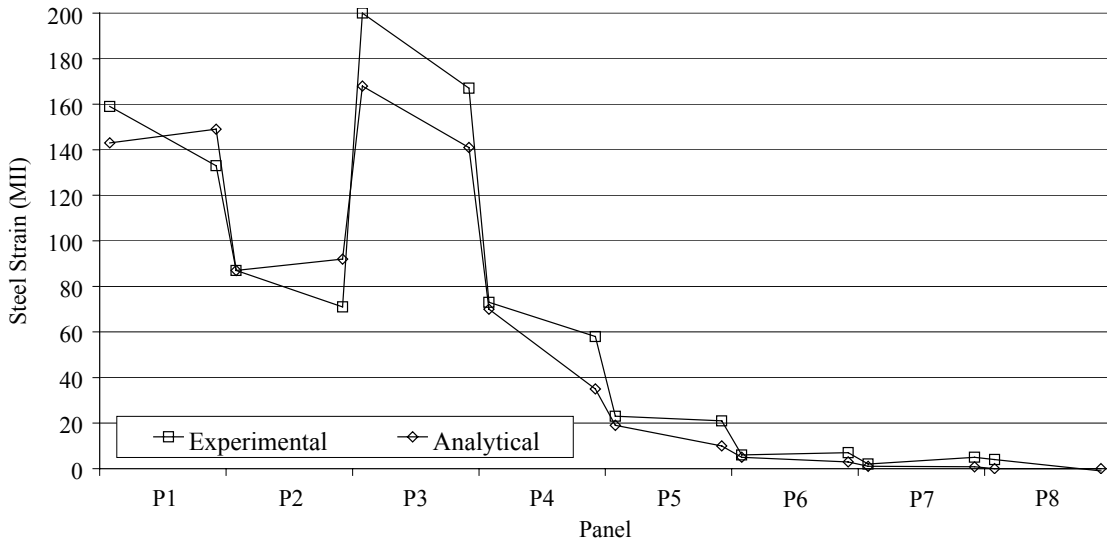


a. Midspan deflection for 2-LP13.B

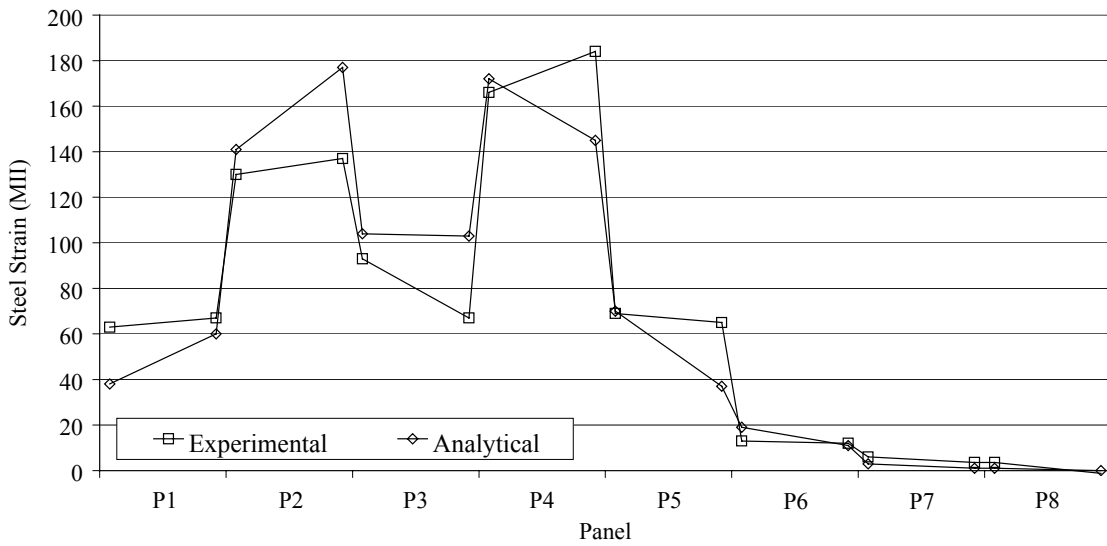


b. Midspan deflection for 2-LP24.B

Figure 7.19. Comparison of deflection profiles for Bridge 2.



a. Steel strain for 2-LP13.B



b. Steel strain for 2-LP24.B

Figure 7.20. Comparison of primary reinforcement strain profiles for Bridge 2.

The steel strain profiles (Figure 7.20) indicate slip occurred in this bridge. A maximum of 200 MII in the bottom reinforcement was measured in the field test, while the model predicted a maximum of 165 MII. It can be seen, however, that the overall strain profiles, resulting from the analytical model with 4-node-connection bolt elements, are very similar to the experimental data.

### **7.3.3. Conclusions**

As presented in Section 7.2, the Solid73 - Pipe16 model with 5-node-connection bolt elements is appropriate for the laboratory PCDB with only bolt connections. However, due to the occurrence of slip in the field PCDBs with only bolt connections, the model with a 4-node connection bolt element is more appropriate.

Slip is less likely to occur in the PCDBs with bolt and pipe connections. The combination of the Pipe16 element with a 5-node-connection and the Combin7 element with an assumed translational stiffness of 20 kip/in. presents an appropriate rotation behavior of the bolt-pipe connections. Due to its greater stiffness, the analytical model usually underestimates the bridge's behavior. Deflection and strain profiles along the transverse cross-section obtained from the analytical model are consistent with the experimental results. The edge-stiffening effect on the bridge is obvious. Unfortunately, even including the curb and rail, the analytical model still does not represent this effect accurately.

Although the model can be used to perform a detailed analysis of a PCDB, its primary value is for calculating live load distribution in the rating of PCDBs.



## 8. SUMMARY AND CONCLUSIONS

### 8.1. Summary

In this investigation the affects of deterioration on the performance of precast concrete deck bridges (PCDBs) were studied. In this study, several tasks were completed. A search for similar research performed prior to this project and other relevant literature was conducted. This included reviewing the Iowa DOT J-10 Standard Specification and subsequent design revisions by Iowa Concrete Products Company. Additionally, a questionnaire was sent to all county engineers in Iowa requesting information on the number and condition of the PCDBs in their counties.

Using the results of the questionnaire, four deteriorated PCDBs were selected for service load field testing. Two bridges in Delaware County and a single bridge in both Butler County and Story County were tested. Loaded trucks were used as the test vehicles. Response of the various bridges was obtained by measuring concrete and steel strains and deflections at critical locations. From the test data, load fractions were calculated and compared to theoretical values calculated from AASHTO Standard Specification equations. Test data were also used to detect deficiencies and to validate an analytical PCDB model.

A total of sixteen PCDB panels were tested in the laboratory. The panels originated from bridge replacement projects in three Iowa counties (Black Hawk, Butler and Cedar). The ultimate strength of twelve panels was found by loading each panel to failure in a four point flexural arrangement. In these tests, instrumentation similar to that used during the field tests was used to measure deflections and steel and concrete strains. Strain and deflection data were compared with theoretical values and were found to be in good agreement. Similarly, theoretical ultimate panel strengths were calculated and compared to the experimental ultimate strengths. Actual material strengths were found by testing concrete cores and reinforcement specimens taken from each group of panels.

A laboratory PCDB was constructed from four panels; this laboratory model was subjected to both service load testing and an ultimate strength test. Three joint configurations were investigated in the service load tests: one with a combination of tight and loose bolts, one with only tight bolts, and one with both shear connectors and tight bolts.

Point loads were applied at four positions on the model bridge and load fractions were calculated using the measured response data. Load fractions from the three different joint configurations were compared and the effectiveness of the shear connectors was evaluated. For the ultimate strength test, an interior panel was loaded in a four point flexural arrangement. In addition to determining the ultimate strength, observation of the failure mode of an overloaded PCDB was also a benefit of this test. Both shear connectors and tight bolts were installed during this test.

A strengthening system was designed to strengthen deficient panels. The goal of the retrofit was to eliminate the self weight stresses in a given panel. The retrofit consisted of a strut and a post-tensioned tendon installed on each panel. All four panels in the laboratory PCDB were strengthened with this system. Service load tests were performed on the strengthened model bridge and the resulting test data were compared to data obtained during the unstrengthened laboratory PCDB service load tests. An investigation was also made into the effects of a retrofitted panel on adjacent non-retrofitted panels. The ultimate strength of a single strengthened panel was determined using a loading system that was similar to that utilized during the testing of the individual non-retrofitted panels.

An analytical model was developed and was validated with data from the field and laboratory tests. This model can serve as a useful tool for analyzing and rating PCDBs. Analytical results can be used to calculate load fractions for used in place of AASHTO values during the rating of a PCDB.

## **8.2. Conclusions**

Deterioration of the type most common to PCDBs did not compromise the strength of these bridges. In fact, the flexural capacities of panels displaying a significant amount of primary reinforcement corrosion consistently exceed design capacities. This additional strength is attributed to concrete compressive strengths and reinforcement yield strengths that were determined to be greater than the values specified by the J-10 Standard. Deterioration in the form of delaminating and spalling deck concrete did however result in reduced ultimate strengths and ductility. This type of deterioration was found on relatively few panels and only in the most extreme case did the experimental ultimate strength fall below the design ultimate strength.

Based on laboratory test results, load ratings of PCDBs having the type of deterioration observed in the panels tested in this investigation need not be adjusted due to the deterioration. Using the design capacity in load rating calculations will result in a conservative load rating. Care must be taken when using this information on other bridges. One needs to make sure that the corrosion of the reinforcement has not caused a significant reduction in area and that the hooked ends of the reinforcement are anchored in sound concrete. If an engineer encounters a situation where either of these two conditions are not the case, the findings of this investigation are not applicable.

PCDB load ratings should, however, be modified when shear connectors are absent from the joints between adjacent panels. Missing shear connectors limit the amount of live load transversely distributed from a loaded panel to adjacent unloaded panels, which in turn requires the loaded panel to support a larger portion of the live load. Load fractions calculated using AASHTO Standard Specification equations are less than the experimental load fractions for PCDBs without shear connectors. In this situation, load fractions could be conservatively taken as 0.7 for one lane loading and 1.0 for two lane loading.

When reconstructing a PCDB from salvaged panels, care should be taken to ensure that the panels are connected as specified by the J-10 Standard. This would include, depending on the panel type, either installing the galvanized concrete-filled pipes between adjacent panels or repacking grout in the shear keys. The bolts which connect adjacent panels must also be reinstalled and appropriately tightened (approximately 40 ft-lbs).

The following are additional conclusions from this study:

- Although corrosion likely reduced the bond between the primary reinforcement and concrete, the hooked ends on the lower pair of reinforcing bars adequately compensated for the weakened bond. Hence, a bond failure was never observed during the testing.
- All panels loaded individually to failure experienced a compressive failure of the concrete deck. This occurred after the primary steel had yielded and a significant amount of deflection always preceded failure of a panel.
- The laboratory PCDB performed exceptionally well during ultimate strength testing. Total load on the bridge at failure was 2.94 times that of an HS20-44

truck. The mode of failure was a rupture of the concrete directly above the shear connector; excessive deflections, however, were observed prior to the failure.

- For PCDBs with shear connectors in place, load fractions from AASHTO Standard Specifications are conservative when compared to the load fractions calculated from the field test data. In these instances, use of actual load fractions in place of AASHTO load fraction in load ratings will result in increased capacities.
- If additional flexural capacity is required, it can be obtained through the use of the strengthening system described in this report. When tested on a single panel, the retrofit counteracted the dead load effects and essentially increased the panel flexural capacity by an amount equal to the dead load moment. Similar effects were observed on the strengthened laboratory PCDB. Transverse load distribution was not effected by the strengthening system. A small increase in ultimate strength of the strengthened panels was also observed.
- Based on data obtained from the strengthening tests on the laboratory PCDB, live load distribution load fractions can be used to determine the amount of post-tensioning effect induced in adjacent non-retrofitted panels.
- The analytical model can accurately predict the transverse distribution of live load. Load fractions calculated from the analytical results can be used in place of the less accurate AASHTO values in the rating of a PCDB.

## 9. ACKNOWLEDGMENTS

The study presented in this report was conducted by the Bridge Engineering Center under the auspices of the Engineering Research Institute of Iowa State University. The research was sponsored by the Project Development Division of the Iowa Department of Transportation and the Iowa Highway Research Board under Research Project TR-440.

The authors wish to thank the following county engineers for their assistance with this project:

- Robert Haylock – Butler County Engineer
- Harold Jensen – Story County Engineer
- Richard King – Black Hawk County Engineer
- Donald Torney – Cedar County Engineer

Critical to the success of the field and laboratory testing was the assistance of Doug Wood, Manager of the Iowa State University Structural Engineering Laboratory. His support was greatly appreciated. The authors would also like to thank John Rhodes and David Tarries, Structural Engineering graduate students, for their assistance during the testing phase of this project. In addition, the authors would like to recognize the following Civil Engineering undergraduate students for the many hours they contributed to this project: Emily Allison, Ben Dreier, Ken Hoevelkamp, Elizabeth Kash, Meredith Nelson, Maegan Page and Brian Williams.



## 10. REFERENCES

1. Federal Highway Administration. National Bridge Inventory Data, 2000. Washington, D.C., Federal Highway Administration, 2000.
2. Standard Design: Precast Concrete Bridges. Ames, Iowa, Iowa State Highway Commission, 1954.
3. Design for Precast Concrete Bridges. Ames, Iowa, Iowa Concrete Products Company, 1956.
4. Pullar-Strecker, Peter. Corrosion Damaged Concrete: Assessment and Repair. Construction Industry Research and Information Association, London, 1987.
5. Prestressed Concrete Quad Tee Bridges. Ames, Iowa, Iowa Concrete Products Company, 1991.
6. American Association of State Highway and Transportation Officials. Standard Specifications for Highway Bridges, Sixteenth Edition. Washington, D.C., American Association of State Highway and Transportation Officials, 1996.
7. American Concrete Institute. Building Code Requirements for Structural Concrete (318-99) and Commentary (318R-99). Farmington Hills, Michigan, American Concrete Institute, 1999.
8. American Association of State Highway and Transportation Officials. Manual for Condition Evaluation of Bridges 1994. Washington, D.C., American Association of State Highway and Transportation Officials, 1994.
9. “Standard Test Method for Compressive Strength of Cylindrical Concrete Specimens.” ASTM C 39, Annual Book of ASTM Standards, American Society for Testing and Materials, Vol. 04.02, Philadelphia, Pennsylvania, 2000.
10. “Standard Test Method for Obtaining and Testing Drilled Cores and Sawed Beams of Concrete.” ASTM C 42, Annual Book of ASTM Standards, American Society for Testing and Materials, Vol. 04.02, Philadelphia, Pennsylvania, 2000.
11. Qin, XiaoPeng. Finite Element Analysis of Multi-Channel-Beam Bridges. M. S. Thesis, Iowa State University, Ames, Iowa. (In preparation).
12. ANSYS User’s Manual for Revision 5.1. Swanson Analysis System, Inc., Houston, PA, 1992.



**APPENDIX A**  
**QUESTIONNAIRE**



**Iowa State University**  
**Research Project TR 440**

**“Field and Laboratory Evaluation of Precast Concrete Bridges”**

---

Questionnaire completed by \_\_\_\_\_

Title \_\_\_\_\_

County \_\_\_\_\_

Please return the completed questionnaire (mail or fax) and return by June 19 to:

Prof. F. W. Klaiber  
 Dept. of Civil and Construction Engineering  
 Iowa State University  
 Ames, IA 50011  
 Phone: (515) 294-8763  
 Fax: (515) 294-8216

---

1) Does your county have any precast concrete deck bridges (PCDBs) in service?

**YES**            **NO**

If **yes**, please state total number: \_\_\_\_\_

If **no**, you may skip the remaining questions.

2) Are all your PCDBs carrying legal loads?            **YES**            **NO**

3) If you answered no to question 2, how many are posted and what is the posted limit?

Number Posted: \_\_\_\_\_

Posted limit: \_\_\_\_\_ (If there are different values, please provide the various values)

4) If the bridges are posted, were they rated?            **YES**            **NO**

5) If they were rated, would you be willing to provide us with the rating calculations?

**YES**            **NO**

- 6) Please briefly describe the deterioration in the posted bridges. If it is easier, please provide sketches and/or photographs.

---

---

---

---

---

- 7) Are you planning to replace any PCDBs during the next two years?

**YES**      **NO**

If yes, please give an estimated date that the bridge will be removed and its location.

Removal Date

Location

<hr/>	<hr/>

- 8) Would you allow us to service load test one or more of the PCDBs you plan on replacing?

**YES**      **NO**

- 9) If you are replacing a PCDB, could we obtain a few of the precast units from it for testing?

**YES**      **NO**

- 10) If you have PCDBs, but do not plan on removing them in the near future, would you be willing to let us service load test one of them?

**YES**      **NO**

**APPENDIX B**  
**RATING CALCULATIONS**



## Bridge 1 Rating Calculations:

### Bridge Properties:

$L := 29\text{ft}$	(Span Length of Bridge Measured Between Bearing Centers)
$N_b := 10$	(Number of PCDB Panels in Bridge)
$S := 38\text{in}$	(Width of Individual PCDB Panel)
$\text{surface} := 0 \frac{\text{lb}}{\text{ft}^2}$	(Weight of Wearing Surface per Square Foot)

### Panel Properties:

$A_s := 8.0\text{in}^2$	(Area of Primary Longitudinal Reinforcement)
$d := 12.50\text{in}$	(Distance To Reinforcement Centroid From Extreme Comp. Fiber)
$w := 344 \frac{\text{lb}}{\text{ft}}$	(PCDB Panel Weight per Foot)

### Material Properties According To J-10 Standards:

$f_c := 5000\text{psi}$	(Concrete Compression Strength)
$f_y := 40000\text{psi}$	(Nominal Reinforcement Yield Strength)
$\mu := 0.18$	(Poisson's Ratio)

### Units:

$\text{kip} := 1000\text{lb}$

### Curb to Curb Bridge Width:

$$W := N_b \cdot S - 2 \cdot 8\text{in} \quad \boxed{W = 30.33\text{ft}}$$

### Dead Load Moment:

$$M_D := \frac{w \cdot L^2}{8} + \frac{\text{surface} \cdot S \cdot L^2}{8} \quad \boxed{M_D = 36.2\text{ft} \cdot \text{kip}}$$

### Geometrical Properties:

$$y_{\text{top}} := \frac{38\text{in} \cdot 5\text{in} \cdot 2.5\text{in} + 2 \cdot 6\text{in} \cdot 10\text{in} \cdot 10\text{in} + 2 \cdot 0.5 \cdot 2\text{in} \cdot 10\text{in} \cdot 8.33\text{in}}{38\text{in} \cdot 5\text{in} + 2 \cdot 6\text{in} \cdot 10\text{in} + 2 \cdot 0.5 \cdot 2\text{in} \cdot 10\text{in}} \quad \text{(Distance To Centroid From Top Of Panel)}$$

$$\boxed{y_{\text{top}} = 5.581\text{in}}$$

$$I_g := \left( \frac{1}{3} \cdot 38\text{in} \cdot y_{\text{top}}^3 \right) - \left[ \frac{1}{3} \cdot 22\text{in} \cdot (y_{\text{top}} - 5\text{in})^3 \right] + \left[ \frac{1}{3} \cdot 12\text{in} \cdot (15\text{in} - y_{\text{top}})^3 \right] + \left[ \left( \frac{1}{12} \cdot 3 \cdot 5\text{in} \right) \cdot (15\text{in} - y_{\text{top}})^3 \right]$$

$$\boxed{I_g = 5786.7\text{in}^4}$$

$$J := \left[ \frac{1}{3} \cdot 38\text{in} \cdot (5\text{in})^3 \cdot \left[ 1 - 0.63 \cdot \left( \frac{5\text{in}}{38\text{in}} \right) \right] \right] + \left[ 2 \cdot \frac{1}{3} \cdot 10\text{in} \cdot (6\text{in})^3 \cdot \left[ 1 - 0.63 \cdot \left( \frac{6\text{in}}{10\text{in}} \right) \right] \right]$$

$$\boxed{J = 2347.8\text{in}^4}$$

**Theoretical (AASHTO) One Lane and Two Lane Load Fractions:**One Lane

$$N_L := 1 \quad (\text{Number of Lanes})$$

$$K := \sqrt{(1 + \mu) \cdot \frac{I_{eg}}{J}} \quad \boxed{K = 1.705}$$

$$C := K \cdot \left( \frac{W}{L} \right) \quad \boxed{C = 1.784}$$

$$D(x) := \begin{cases} (5.75 - 0.5 \cdot N_L) + 0.7 \cdot N_L \cdot (1 - 0.2 \cdot C)^2 & \text{if } x \leq 5 \\ (5.75 - 0.5 \cdot N_L) & \text{if } x > 5 \end{cases} \quad \boxed{D(C) = 5.54}$$

$$LF_1 := \frac{S}{D(C) \cdot 1\text{ft}} \quad \boxed{LF_1 = 0.57}$$

Two Lanes

$$N_L := 2 \quad (\text{Number of Lanes})$$

$$K := \sqrt{(1 + \mu) \cdot \frac{I_{eg}}{J}} \quad \boxed{K = 1.705}$$

$$C := K \cdot \left( \frac{W}{L} \right) \quad \boxed{C = 1.784}$$

$$D(x) := \begin{cases} (5.75 - 0.5 \cdot N_L) + 0.7 \cdot N_L \cdot (1 - 0.2 \cdot C)^2 & \text{if } x \leq 5 \\ (5.75 - 0.5 \cdot N_L) & \text{if } x > 5 \end{cases} \quad \boxed{D(C) = 5.329}$$

$$LF_2 := \frac{S}{D(C) \cdot 1\text{ft}} \quad \boxed{LF_2 = 0.59}$$

**Section Flexural Capacity Based On J-10 Standards Material Properties:**

$$a := \frac{A_s \cdot f_y}{0.85 \cdot f_c' \cdot S} \quad \boxed{a = 1.98\text{in}}$$

$$M_n := A_s \cdot f_y \cdot \left( d - \frac{a}{2} \right) \quad \boxed{M_n = 306.9\text{ft}\cdot\text{kip}}$$

**Live Load Moment (Wheel Line):**

$$M_{HS20} := 133.5\text{ft}\cdot\text{kip} \quad (\text{Maximum Moment Due To HS20 Truck})$$

$$M_{Type3} := 106.8\text{ft}\cdot\text{kip} \quad (\text{Maximum Moment Due To Type 3 Rating Vehicle})$$

**Rating Calculation Based On J-10 Standard Material Properties and Theoretical Load Fraction:**

$\phi := 0.9$	(Strength Reduction Factor for Flexure)
$\gamma_D := 1.3$	(Dead Load Factor)
$\beta_L := 1.67$	(Coefficient)
$\gamma_L := 1.3$	(Live Load Factor)
$I := 0.3$	(Impact Factor)

**One Lane Inventory Rating Factors**

$$RF_{HS20} := \frac{\phi \cdot M_n - \gamma_D \cdot M_D}{\beta_L \cdot \gamma_L \cdot M_{HS20} \cdot LF_1 \cdot (1 + I)} \quad \boxed{RF_{HS20} = 1.06}$$

$$RF_{Type3} := \frac{\phi \cdot M_n - \gamma_D \cdot M_D}{\beta_L \cdot \gamma_L \cdot M_{Type3} \cdot LF_1 \cdot (1 + I)} \quad \boxed{RF_{Type3} = 1.33}$$

**One Lane Operating Rating Factors**

$$RF_{HS20} := \frac{\phi \cdot M_n - \gamma_D \cdot M_D}{\gamma_L \cdot M_{HS20} \cdot LF_1 \cdot (1 + I)} \quad \boxed{RF_{HS20} = 1.78}$$

$$RF_{Type3} := \frac{\phi \cdot M_n - \gamma_D \cdot M_D}{\gamma_L \cdot M_{Type3} \cdot LF_1 \cdot (1 + I)} \quad \boxed{RF_{Type3} = 2.22}$$

**Two Lane Inventory Rating Factors**

$$RF_{HS20} := \frac{\phi \cdot M_n - \gamma_D \cdot M_D}{\beta_L \cdot \gamma_L \cdot M_{HS20} \cdot LF_2 \cdot (1 + I)} \quad \boxed{RF_{HS20} = 1.02}$$

$$RF_{Type3} := \frac{\phi \cdot M_n - \gamma_D \cdot M_D}{\beta_L \cdot \gamma_L \cdot M_{Type3} \cdot LF_2 \cdot (1 + I)} \quad \boxed{RF_{Type3} = 1.28}$$

**Two Lane Operating Rating Factors**

$$RF_{HS20} := \frac{\phi \cdot M_n - \gamma_D \cdot M_D}{\gamma_L \cdot M_{HS20} \cdot LF_2 \cdot (1 + I)} \quad \boxed{RF_{HS20} = 1.71}$$

$$RF_{Type3} := \frac{\phi \cdot M_n - \gamma_D \cdot M_D}{\gamma_L \cdot M_{Type3} \cdot LF_2 \cdot (1 + I)} \quad \boxed{RF_{Type3} = 2.14}$$

**Revisions To Load Rating Using Test Data:****Actual Material Properties (If Known):**

$$f_c := 6200\text{psi} \quad (\text{Concrete Compression Strength})$$

$$f_y := 4725\text{psi} \quad (\text{Reinforcement Yield Strength})$$

**Section Flexural Capacity Based On Actual Material Properties:**

$$a := \frac{A_s \cdot f_y}{0.85 \cdot f_c \cdot S}$$

$$a = 1.89\text{in}$$

$$M_n := A_s \cdot f_y \cdot \left( d - \frac{a}{2} \right)$$

$$M_n = 364.0\text{ft}\cdot\text{kip}$$

**Experimental Load Fractions:**

$$LF_1 := 0.49$$

$$LF_2 := 0.54$$

**Rating Calculation Based On Actual Material Properties and Experimental Load Fractions:****One Lane Inventory Rating Factors**

$$RF_{HS20} := \frac{\phi \cdot M_n - \gamma_D \cdot M_D}{\beta_L \cdot \gamma_L \cdot M_{HS20} \cdot LF_1 \cdot (1 + I)}$$

$$RF_{HS20} = 1.52$$

$$RF_{Type3} := \frac{\phi \cdot M_n - \gamma_D \cdot M_D}{\beta_L \cdot \gamma_L \cdot M_{Type3} \cdot LF_1 \cdot (1 + I)}$$

$$RF_{Type3} = 1.90$$

**One Lane Operating Rating Factors**

$$RF_{HS20} := \frac{\phi \cdot M_n - \gamma_D \cdot M_D}{\gamma_L \cdot M_{HS20} \cdot LF_1 \cdot (1 + I)}$$

$$RF_{HS20} = 2.54$$

$$RF_{Type3} := \frac{\phi \cdot M_n - \gamma_D \cdot M_D}{\gamma_L \cdot M_{Type3} \cdot LF_1 \cdot (1 + I)}$$

$$RF_{Type3} = 3.17$$

**Two Lane Inventory Rating Factors**

$$RF_{HS20} := \frac{\phi \cdot M_n - \gamma_D \cdot M_D}{\beta_L \cdot \gamma_L \cdot M_{HS20} \cdot LF_2 \cdot (1 + I)}$$

$$RF_{HS20} = 1.38$$

$$RF_{Type3} := \frac{\phi \cdot M_n - \gamma_D \cdot M_D}{\beta_L \cdot \gamma_L \cdot M_{Type3} \cdot LF_2 \cdot (1 + I)}$$

$$RF_{Type3} = 1.72$$

**Two Lane Operating Rating Factors**

$$RF_{HS20} := \frac{\phi \cdot M_n - \gamma_D \cdot M_D}{\gamma_L \cdot M_{HS20} \cdot LF_2 \cdot (1 + I)}$$

$$RF_{HS20} = 2.30$$

$$RF_{Type3} := \frac{\phi \cdot M_n - \gamma_D \cdot M_D}{\gamma_L \cdot M_{Type3} \cdot LF_2 \cdot (1 + I)}$$

$$RF_{Type3} = 2.88$$



## Bridge 2 Rating Calculations:

### Bridge Properties:

$L := 30.5\text{ft}$  (Span Length of Bridge Measured Between Bearing Centers)

$N_b := 8$  (Number of PCDB Panels in Bridge)

$S := 38\text{in}$  (Width of Individual PCDB Panel)

$\text{surface} := 0 \frac{\text{lb}}{\text{ft}^2}$  (Weight of Wearing Surface per Square Foot)

### Panel Properties:

$A_s := 9.36\text{in}^2$  (Area of Primary Longitudinal Reinforcement)

$d := 12.45\text{in}$  (Distance To Reinforcement Centroid From Extreme Comp. Fiber)

$w := 344 \frac{\text{lb}}{\text{ft}}$  (PCDB Panel Weight per Foot)

### Material Properties According To J-10 Standards:

$f_c := 5000\text{psi}$  (Concrete Compression Strength)

$f_y := 40000\text{psi}$  (Nominal Reinforcement Yield Strength)

$\mu := 0.18$  (Poisson's Ratio)

### Units:

$\text{kip} := 1000\text{lb}$

### Curb to Curb Bridge Width:

$W := N_b \cdot S - 2 \cdot 8\text{in}$   $W = 24.00\text{ft}$

### Dead Load Moment:

$M_D := \frac{w \cdot L^2}{8} + \frac{\text{surface} \cdot S \cdot L^2}{8}$   $M_D = 40.0\text{ft} \cdot \text{kip}$

### Geometrical Properties:

$y_{\text{top}} := \frac{38\text{in} \cdot 5\text{in} \cdot 2.5\text{in} + 2 \cdot 6\text{in} \cdot 10\text{in} \cdot 10\text{in} + 2 \cdot 0.5 \cdot 2\text{in} \cdot 10\text{in} \cdot 8.33\text{in}}{38\text{in} \cdot 5\text{in} + 2 \cdot 6\text{in} \cdot 10\text{in} + 2 \cdot 0.5 \cdot 2\text{in} \cdot 10\text{in}}$  (Distance To Centroid From Panel Top)

$$y_{\text{top}} = 5.581\text{in}$$

$I_g := \left( \frac{1}{3} \cdot 38\text{in} \cdot y_{\text{top}}^3 \right) - \left[ \frac{1}{3} \cdot 22\text{in} \cdot (y_{\text{top}} - 5\text{in})^3 \right] + \left[ \frac{1}{3} \cdot 12\text{in} \cdot (15\text{in} - y_{\text{top}})^3 \right] + \left[ \left( \frac{1}{12} \cdot 3 \cdot 5\text{in} \right) \cdot (15\text{in} - y_{\text{top}})^3 \right]$

$$I_g = 5786.7\text{in}^4$$

$J := \left[ \frac{1}{3} \cdot 38\text{in} \cdot (5\text{in})^3 \cdot \left[ 1 - 0.63 \cdot \left( \frac{5\text{in}}{38\text{in}} \right) \right] \right] + \left[ 2 \cdot \frac{1}{3} \cdot 10\text{in} \cdot (6\text{in})^3 \cdot \left[ 1 - 0.63 \cdot \left( \frac{6\text{in}}{10\text{in}} \right) \right] \right]$

$$J = 2347.8\text{in}^4$$

**Theoretical (AASHTO) One Lane and Two Lane Load Fractions:**One Lane

$$N_L := 1 \quad (\text{Number of Lanes})$$

$$K := \sqrt{(1 + \mu) \cdot \frac{I_{eg}}{J}} \quad \boxed{K = 1.705}$$

$$C := K \cdot \left( \frac{W}{L} \right) \quad \boxed{C = 1.342}$$

$$D(x) := \begin{cases} (5.75 - 0.5 \cdot N_L) + 0.7 \cdot N_L \cdot (1 - 0.2 \cdot C)^2 & \text{if } x \leq 5 \\ (5.75 - 0.5 \cdot N_L) & \text{if } x > 5 \end{cases} \quad \boxed{D(C) = 5.625}$$

$$LF_1 := \frac{S}{D(C) \cdot 1\text{ft}} \quad \boxed{LF_1 = 0.56}$$

Two Lanes

$$N_L := 2 \quad (\text{Number of Lanes})$$

$$K := \sqrt{(1 + \mu) \cdot \frac{I_{eg}}{J}} \quad \boxed{K = 1.705}$$

$$C := K \cdot \left( \frac{W}{L} \right) \quad \boxed{C = 1.342}$$

$$D(x) := \begin{cases} (5.75 - 0.5 \cdot N_L) + 0.7 \cdot N_L \cdot (1 - 0.2 \cdot C)^2 & \text{if } x \leq 5 \\ (5.75 - 0.5 \cdot N_L) & \text{if } x > 5 \end{cases} \quad \boxed{D(C) = 5.499}$$

$$LF_2 := \frac{S}{D(C) \cdot 1\text{ft}} \quad \boxed{LF_2 = 0.58}$$

**Section Flexural Capacity Based On J-10 Standards Material Properties:**

$$a := \frac{A_s \cdot f_y}{0.85 \cdot f_c' \cdot S} \quad \boxed{a = 2.32\text{in}}$$

$$M_n := A_s \cdot f_y \cdot \left( d - \frac{a}{2} \right) \quad \boxed{M_n = 352.3\text{ft}\cdot\text{kip}}$$

**Live Load Moment (Wheel Line):**

$$M_{HS20} := 144.9\text{ft}\cdot\text{kip} \quad (\text{Maximum Moment Due To HS20 Truck})$$

$$M_{Type3} := 116.4\text{ft}\cdot\text{kip} \quad (\text{Maximum Moment Due To Type 3 Rating Vehicle})$$

**Rating Calculation Based On J-10 Standard Material Properties and Theoretical Load Fraction:**

$\phi := 0.9$	(Strength Reduction Factor for Flexure)
$\gamma_D := 1.3$	(Dead Load Factor)
$\beta_L := 1.67$	(Coefficient)
$\gamma_L := 1.3$	(Live Load Factor)
$I := 0.3$	(Impact Factor)

**One Lane Inventory Rating Factors**

$$RF_{HS20} := \frac{\phi \cdot M_n - \gamma_D \cdot M_D}{\beta_L \cdot \gamma_L \cdot M_{HS20} \cdot LF_1 \cdot (1 + I)} \quad \boxed{RF_{HS20} = 1.15}$$

$$RF_{Type3} := \frac{\phi \cdot M_n - \gamma_D \cdot M_D}{\beta_L \cdot \gamma_L \cdot M_{Type3} \cdot LF_1 \cdot (1 + I)} \quad \boxed{RF_{Type3} = 1.43}$$

**One Lane Operating Rating Factors**

$$RF_{HS20} := \frac{\phi \cdot M_n - \gamma_D \cdot M_D}{\gamma_L \cdot M_{HS20} \cdot LF_1 \cdot (1 + I)} \quad \boxed{RF_{HS20} = 1.92}$$

$$RF_{Type3} := \frac{\phi \cdot M_n - \gamma_D \cdot M_D}{\gamma_L \cdot M_{Type3} \cdot LF_1 \cdot (1 + I)} \quad \boxed{RF_{Type3} = 2.39}$$

**Two Lane Inventory Rating Factors**

$$RF_{HS20} := \frac{\phi \cdot M_n - \gamma_D \cdot M_D}{\beta_L \cdot \gamma_L \cdot M_{HS20} \cdot LF_2 \cdot (1 + I)} \quad \boxed{RF_{HS20} = 1.13}$$

$$RF_{Type3} := \frac{\phi \cdot M_n - \gamma_D \cdot M_D}{\beta_L \cdot \gamma_L \cdot M_{Type3} \cdot LF_2 \cdot (1 + I)} \quad \boxed{RF_{Type3} = 1.40}$$

**Two Lane Operating Rating Factors**

$$RF_{HS20} := \frac{\phi \cdot M_n - \gamma_D \cdot M_D}{\gamma_L \cdot M_{HS20} \cdot LF_2 \cdot (1 + I)} \quad \boxed{RF_{HS20} = 1.88}$$

$$RF_{Type3} := \frac{\phi \cdot M_n - \gamma_D \cdot M_D}{\gamma_L \cdot M_{Type3} \cdot LF_2 \cdot (1 + I)} \quad \boxed{RF_{Type3} = 2.34}$$

**Revisions To Load Rating Using Test Data:****Actual Material Properties (If Known):**

$$f_c := 5000\text{psi} \quad (\text{Concrete Compression Strength})$$

$$f_y := 4000\text{psi} \quad (\text{Reinforcement Yield Strength})$$

**Section Flexural Capacity Based On Actual Material Properties:**

$$a := \frac{A_s \cdot f_y}{0.85 \cdot f_c \cdot S}$$

$$a = 2.32\text{in}$$

$$M_n := A_s \cdot f_y \cdot \left( d - \frac{a}{2} \right)$$

$$M_n = 352.3\text{ft}\cdot\text{kip}$$

**Experimental Load Fractions:**

$$LF_1 := 0.68$$

$$LF_2 := 0.97$$

**Rating Calculation Based On Actual Material Properties and Experimental Load Fractions:****One Lane Inventory Rating Factors**

$$RF_{HS20} := \frac{\phi \cdot M_n - \gamma_D \cdot M_D}{\beta_L \cdot \gamma_L \cdot M_{HS20} \cdot LF_1 \cdot (1 + I)}$$

$$RF_{HS20} = 0.95$$

$$RF_{Type3} := \frac{\phi \cdot M_n - \gamma_D \cdot M_D}{\beta_L \cdot \gamma_L \cdot M_{Type3} \cdot LF_1 \cdot (1 + I)}$$

$$RF_{Type3} = 1.19$$

**One Lane Operating Rating Factors**

$$RF_{HS20} := \frac{\phi \cdot M_n - \gamma_D \cdot M_D}{\gamma_L \cdot M_{HS20} \cdot LF_1 \cdot (1 + I)}$$

$$RF_{HS20} = 1.59$$

$$RF_{Type3} := \frac{\phi \cdot M_n - \gamma_D \cdot M_D}{\gamma_L \cdot M_{Type3} \cdot LF_1 \cdot (1 + I)}$$

$$RF_{Type3} = 1.98$$

**Two Lane Inventory Rating Factors**

$$RF_{HS20} := \frac{\phi \cdot M_n - \gamma_D \cdot M_D}{\beta_L \cdot \gamma_L \cdot M_{HS20} \cdot LF_2 \cdot (1 + I)}$$

$$RF_{HS20} = 0.67$$

$$RF_{Type3} := \frac{\phi \cdot M_n - \gamma_D \cdot M_D}{\beta_L \cdot \gamma_L \cdot M_{Type3} \cdot LF_2 \cdot (1 + I)}$$

$$RF_{Type3} = 0.83$$

**Two Lane Operating Rating Factors**

$$RF_{HS20} := \frac{\phi \cdot M_n - \gamma_D \cdot M_D}{\gamma_L \cdot M_{HS20} \cdot LF_2 \cdot (1 + I)}$$

$$RF_{HS20} = 1.12$$

$$RF_{Type3} := \frac{\phi \cdot M_n - \gamma_D \cdot M_D}{\gamma_L \cdot M_{Type3} \cdot LF_2 \cdot (1 + I)}$$

$$RF_{Type3} = 1.39$$



### Bridge 3 Rating Calculations:

#### Bridge Properties:

$L := 29.5\text{ft}$  (Span Length of Bridge Measured Between Bearing Centers)

$N_b := 9$  (Number of PCDB Panels in Bridge)

$S := 39\text{in}$  (Width of Individual PCDB Panel)

$\text{surface} := 0 \frac{\text{lb}}{\text{ft}^2}$  (Weight of Wearing Surface per Square Foot)

#### Panel Properties:

$A_s := 7.20\text{in}^2$  (Area of Primary Longitudinal Reinforcement)

$d := 11.58\text{in}$  (Distance To Reinforcement Centroid From Extreme Comp. Fiber)

$w := 318.4 \frac{\text{lb}}{\text{ft}}$  (PCDB Panel Weight per Foot)

#### Material Properties According To J-10 Standards:

$f_c := 5000\text{psi}$  (Concrete Compression Strength)

$f_y := 40000\text{psi}$  (Nominal Reinforcement Yield Strength)

$\mu := 0.18$  (Poisson's Ratio)

#### Units:

$\text{kip} := 1000\text{lb}$

#### Curb to Curb Bridge Width:

$W := N_b \cdot S - 2 \cdot 12\text{in}$   $W = 27.25\text{ft}$

#### Dead Load Moment:

$M_D := \frac{w \cdot L^2}{8} + \frac{\text{surface} \cdot S \cdot L^2}{8}$   $M_D = 34.6\text{ft} \cdot \text{kip}$

#### Geometrical Properties:

$y_{\text{top}} := \frac{39\text{in} \cdot 5\text{in} \cdot 2.5\text{in} + 2 \cdot 5.5\text{in} \cdot 9\text{in} \cdot 9.5\text{in} + 2 \cdot 0.5 \cdot 1.5\text{in} \cdot 9\text{in} \cdot 8\text{in}}{39\text{in} \cdot 5\text{in} + 2 \cdot 5.5\text{in} \cdot 9\text{in} + 2 \cdot 0.5 \cdot 1.5\text{in} \cdot 9\text{in}}$  (Distance To Centroid From Panel Top)

$$y_{\text{top}} = 4.995\text{in}$$

$I_g := \left( \frac{1}{3} \cdot 39\text{in} \cdot y_{\text{top}}^3 \right) + \left[ \frac{1}{3} \cdot 11\text{in} \cdot (14\text{in} - y_{\text{top}})^3 \right] + \left[ \left( \frac{1}{12} \cdot 3\text{in} \right) \cdot (14\text{in} - y_{\text{top}})^3 \right]$   $I_g = 4480.1\text{in}^4$

$J := \left[ \frac{1}{3} \cdot 39\text{in} \cdot (5\text{in})^3 \cdot \left[ 1 - 0.63 \cdot \left( \frac{5\text{in}}{39\text{in}} \right) \right] \right] + \left[ 2 \cdot \frac{1}{3} \cdot 9\text{in} \cdot (5.5\text{in})^3 \cdot \left[ 1 - 0.63 \cdot \left( \frac{5.5\text{in}}{9\text{in}} \right) \right] \right]$   $J = 2107.7\text{in}^4$

**Theoretical (AASHTO) One Lane and Two Lane Load Fractions:**One Lane

$$N_L := 1 \quad (\text{Number of Lanes})$$

$$K := \sqrt{(1 + \mu) \cdot \frac{I_{eg}}{J}} \quad \boxed{K = 1.584}$$

$$C := K \cdot \left( \frac{W}{L} \right) \quad \boxed{C = 1.463}$$

$$D(x) := \begin{cases} (5.75 - 0.5 \cdot N_L) + 0.7 \cdot N_L \cdot (1 - 0.2 \cdot C)^2 & \text{if } x \leq 5 \\ (5.75 - 0.5 \cdot N_L) & \text{if } x > 5 \end{cases} \quad \boxed{D(C) = 5.6}$$

$$LF_1 := \frac{S}{D(C) \cdot 1\text{ft}} \quad \boxed{LF_1 = 0.58}$$

Two Lanes

$$N_L := 2 \quad (\text{Number of Lanes})$$

$$K := \sqrt{(1 + \mu) \cdot \frac{I_{eg}}{J}} \quad \boxed{K = 1.584}$$

$$C := K \cdot \left( \frac{W}{L} \right) \quad \boxed{C = 1.463}$$

$$D(x) := \begin{cases} (5.75 - 0.5 \cdot N_L) + 0.7 \cdot N_L \cdot (1 - 0.2 \cdot C)^2 & \text{if } x \leq 5 \\ (5.75 - 0.5 \cdot N_L) & \text{if } x > 5 \end{cases} \quad \boxed{D(C) = 5.451}$$

$$LF_2 := \frac{S}{D(C) \cdot 1\text{ft}} \quad \boxed{LF_2 = 0.60}$$

**Section Flexural Capacity Based On J-10 Standards Material Properties:**

$$a := \frac{A_s \cdot f_y}{0.85 \cdot f_c' \cdot S} \quad \boxed{a = 1.74\text{in}}$$

$$M_n := A_s \cdot f_y \cdot \left( d - \frac{a}{2} \right) \quad \boxed{M_n = 257.1\text{ft}\cdot\text{kip}}$$

**Live Load Moment (Wheel Line):**

$$M_{HS20} := 137.3\text{ft}\cdot\text{kip} \quad (\text{Maximum Moment Due To HS20 Truck})$$

$$M_{Type3} := 109.9\text{ft}\cdot\text{kip} \quad (\text{Maximum Moment Due To Type 3 Rating Vehicle})$$

**Rating Calculation Based On J-10 Standard Material Properties and Theoretical Load Fraction:**

$\phi := 0.9$	(Strength Reduction Factor for Flexure)
$\gamma_D := 1.3$	(Dead Load Factor)
$\beta_L := 1.67$	(Coefficient)
$\gamma_L := 1.3$	(Live Load Factor)
$I := 0.3$	(Impact Factor)

**One Lane Inventory Rating Factors**

$$RF_{HS20} := \frac{\phi \cdot M_n - \gamma_D \cdot M_D}{\beta_L \cdot \gamma_L \cdot M_{HS20} \cdot LF_1 \cdot (1 + I)} \quad \boxed{RF_{HS20} = 0.83}$$

$$RF_{Type3} := \frac{\phi \cdot M_n - \gamma_D \cdot M_D}{\beta_L \cdot \gamma_L \cdot M_{Type3} \cdot LF_1 \cdot (1 + I)} \quad \boxed{RF_{Type3} = 1.04}$$

**One Lane Operating Rating Factors**

$$RF_{HS20} := \frac{\phi \cdot M_n - \gamma_D \cdot M_D}{\gamma_L \cdot M_{HS20} \cdot LF_1 \cdot (1 + I)} \quad \boxed{RF_{HS20} = 1.38}$$

$$RF_{Type3} := \frac{\phi \cdot M_n - \gamma_D \cdot M_D}{\gamma_L \cdot M_{Type3} \cdot LF_1 \cdot (1 + I)} \quad \boxed{RF_{Type3} = 1.73}$$

**Two Lane Inventory Rating Factors**

$$RF_{HS20} := \frac{\phi \cdot M_n - \gamma_D \cdot M_D}{\beta_L \cdot \gamma_L \cdot M_{HS20} \cdot LF_2 \cdot (1 + I)} \quad \boxed{RF_{HS20} = 0.81}$$

$$RF_{Type3} := \frac{\phi \cdot M_n - \gamma_D \cdot M_D}{\beta_L \cdot \gamma_L \cdot M_{Type3} \cdot LF_2 \cdot (1 + I)} \quad \boxed{RF_{Type3} = 1.01}$$

**Two Lane Operating Rating Factors**

$$RF_{HS20} := \frac{\phi \cdot M_n - \gamma_D \cdot M_D}{\gamma_L \cdot M_{HS20} \cdot LF_2 \cdot (1 + I)} \quad \boxed{RF_{HS20} = 1.35}$$

$$RF_{Type3} := \frac{\phi \cdot M_n - \gamma_D \cdot M_D}{\gamma_L \cdot M_{Type3} \cdot LF_2 \cdot (1 + I)} \quad \boxed{RF_{Type3} = 1.68}$$

**Revisions To Load Rating Using Test Data:****Actual Material Properties (If Known):**

$$f_c := 5000\text{psi} \quad (\text{Concrete Compression Strength})$$

$$f_y := 4000\text{psi} \quad (\text{Reinforcement Yield Strength})$$

**Section Flexural Capacity Based On Actual Material Properties:**

$$a := \frac{A_s \cdot f_y}{0.85 \cdot f_c \cdot S}$$

$$a = 1.74\text{in}$$

$$M_n := A_s \cdot f_y \cdot \left( d - \frac{a}{2} \right)$$

$$M_n = 257.1\text{ft}\cdot\text{kip}$$

**Experimental Load Fractions:**

$$LF_1 := 0.42$$

$$LF_2 := 0.56$$

**Rating Calculation Based On Actual Material Properties and Experimental Load Fractions:****One Lane Inventory Rating Factors**

$$RF_{HS20} := \frac{\phi \cdot M_n - \gamma_D \cdot M_D}{\beta_L \cdot \gamma_L \cdot M_{HS20} \cdot LF_1 \cdot (1 + I)}$$

$$RF_{HS20} = 1.14$$

$$RF_{Type3} := \frac{\phi \cdot M_n - \gamma_D \cdot M_D}{\beta_L \cdot \gamma_L \cdot M_{Type3} \cdot LF_1 \cdot (1 + I)}$$

$$RF_{Type3} = 1.43$$

**One Lane Operating Rating Factors**

$$RF_{HS20} := \frac{\phi \cdot M_n - \gamma_D \cdot M_D}{\gamma_L \cdot M_{HS20} \cdot LF_1 \cdot (1 + I)}$$

$$RF_{HS20} = 1.91$$

$$RF_{Type3} := \frac{\phi \cdot M_n - \gamma_D \cdot M_D}{\gamma_L \cdot M_{Type3} \cdot LF_1 \cdot (1 + I)}$$

$$RF_{Type3} = 2.39$$

**Two Lane Inventory Rating Factors**

$$RF_{HS20} := \frac{\phi \cdot M_n - \gamma_D \cdot M_D}{\beta_L \cdot \gamma_L \cdot M_{HS20} \cdot LF_2 \cdot (1 + I)}$$

$$RF_{HS20} = 0.86$$

$$RF_{Type3} := \frac{\phi \cdot M_n - \gamma_D \cdot M_D}{\beta_L \cdot \gamma_L \cdot M_{Type3} \cdot LF_2 \cdot (1 + I)}$$

$$RF_{Type3} = 1.07$$

**Two Lane Operating Rating Factors**

$$RF_{HS20} := \frac{\phi \cdot M_n - \gamma_D \cdot M_D}{\gamma_L \cdot M_{HS20} \cdot LF_2 \cdot (1 + I)}$$

$$RF_{HS20} = 1.43$$

$$RF_{Type3} := \frac{\phi \cdot M_n - \gamma_D \cdot M_D}{\gamma_L \cdot M_{Type3} \cdot LF_2 \cdot (1 + I)}$$

$$RF_{Type3} = 1.79$$



## Bridge 4 Rating Calculations:

### Bridge Properties:

$L := 23.5\text{ft}$  (Span Length of Bridge Measured Between Bearing Centers)

$N_b := 9$  (Number of PCDB Panels in Bridge)

$S := 39\text{in}$  (Width of Individual PCDB Panel)

$\text{surface} := 60 \frac{\text{lbf}}{\text{ft}^2}$  (Weight of Wearing Surface per Square Foot)

### Panel Properties:

$A_s := 5.56\text{in}^2$  (Area of Primary Longitudinal Reinforcement)

$d := 11.85\text{in}$  (Distance To Reinforcement Centroid From Extreme Comp. Fiber)

$w := 318.4 \frac{\text{lbf}}{\text{ft}}$  (PCDB Panel Weight per Foot)

### Material Properties According To J-10 Standards:

$f_c := 5000\text{psi}$  (Concrete Compression Strength)

$f_y := 40000\text{psi}$  (Nominal Reinforcement Yield Strength)

$\mu := 0.18$  (Poisson's Ratio)

### Units:

$\text{kip} := 1000\text{lbf}$

### Curb to Curb Bridge Width:

$W := N_b \cdot S - 2 \cdot 12\text{in}$   $W = 27.25\text{ft}$

### Dead Load Moment:

$M_D := \frac{w \cdot L^2}{8} + \frac{\text{surface} \cdot S \cdot L^2}{8}$   $M_D = 35.4\text{ft} \cdot \text{kip}$

### Geometrical Properties:

$y_{\text{top}} := \frac{39\text{in} \cdot 5\text{in} \cdot 2.5\text{in} + 2 \cdot 5.5\text{in} \cdot 9\text{in} \cdot 9.5\text{in} + 2 \cdot 0.5 \cdot 1.5\text{in} \cdot 9\text{in} \cdot 8\text{in}}{39\text{in} \cdot 5\text{in} + 2 \cdot 5.5\text{in} \cdot 9\text{in} + 2 \cdot 0.5 \cdot 1.5\text{in} \cdot 9\text{in}}$  (Distance To Centroid From Panel Top)

$$y_{\text{top}} = 4.995\text{in}$$

$I_g := \left( \frac{1}{3} \cdot 39\text{in} \cdot y_{\text{top}}^3 \right) + \left[ \frac{1}{3} \cdot 11\text{in} \cdot (14\text{in} - y_{\text{top}})^3 \right] + \left[ \left( \frac{1}{12} \cdot 3\text{in} \right) \cdot (14\text{in} - y_{\text{top}})^3 \right]$   $I_g = 4480.1\text{in}^4$

$J := \left[ \frac{1}{3} \cdot 39\text{in} \cdot (5\text{in})^3 \cdot \left[ 1 - 0.63 \cdot \left( \frac{5\text{in}}{39\text{in}} \right) \right] \right] + \left[ 2 \cdot \frac{1}{3} \cdot 9\text{in} \cdot (5.5\text{in})^3 \cdot \left[ 1 - 0.63 \cdot \left( \frac{5.5\text{in}}{9\text{in}} \right) \right] \right]$   $J = 2107.7\text{in}^4$

**Theoretical (AASHTO) One Lane and Two Lane Load Fractions:**One Lane

$$N_L := 1 \quad (\text{Number of Lanes})$$

$$K := \sqrt{(1 + \mu) \cdot \frac{I_{eg}}{J}} \quad \boxed{K = 1.584}$$

$$C := K \cdot \left( \frac{W}{L} \right) \quad \boxed{C = 1.836}$$

$$D(x) := \begin{cases} (5.75 - 0.5 \cdot N_L) + 0.7 \cdot N_L \cdot (1 - 0.2 \cdot C)^2 & \text{if } x \leq 5 \\ (5.75 - 0.5 \cdot N_L) & \text{if } x > 5 \end{cases} \quad \boxed{D(C) = 5.53}$$

$$LF_1 := \frac{S}{D(C) \cdot 1\text{ft}} \quad \boxed{LF_1 = 0.59}$$

Two Lanes

$$N_L := 2 \quad (\text{Number of Lanes})$$

$$K := \sqrt{(1 + \mu) \cdot \frac{I_{eg}}{J}} \quad \boxed{K = 1.584}$$

$$C := K \cdot \left( \frac{W}{L} \right) \quad \boxed{C = 1.836}$$

$$D(x) := \begin{cases} (5.75 - 0.5 \cdot N_L) + 0.7 \cdot N_L \cdot (1 - 0.2 \cdot C)^2 & \text{if } x \leq 5 \\ (5.75 - 0.5 \cdot N_L) & \text{if } x > 5 \end{cases} \quad \boxed{D(C) = 5.31}$$

$$LF_2 := \frac{S}{D(C) \cdot 1\text{ft}} \quad \boxed{LF_2 = 0.61}$$

**Section Flexural Capacity Based On J-10 Standards Material Properties:**

$$a := \frac{A_s \cdot f_y}{0.85 \cdot f_c' \cdot S} \quad \boxed{a = 1.34\text{in}}$$

$$M_n := A_s \cdot f_y \cdot \left( d - \frac{a}{2} \right) \quad \boxed{M_n = 207.2\text{ft}\cdot\text{kip}}$$

**Live Load Moment (Wheel Line):**

$$M_{HS20} := 94.2\text{ft}\cdot\text{kip} \quad (\text{Maximum Moment Due To HS20 Truck})$$

$$M_{Type3} := 82.9\text{ft}\cdot\text{kip} \quad (\text{Maximum Moment Due To Type 3 Rating Vehicle})$$

**Rating Calculation Based On J-10 Standard Material Properties and Theoretical Load Fraction:**

$\phi := 0.9$	(Strength Reduction Factor for Flexure)
$\gamma_D := 1.3$	(Dead Load Factor)
$\beta_L := 1.67$	(Coefficient)
$\gamma_L := 1.3$	(Live Load Factor)
$I := 0.3$	(Impact Factor)

**One Lane Inventory Rating Factors**

$$RF_{HS20} := \frac{\phi \cdot M_n - \gamma_D \cdot M_D}{\beta_L \cdot \gamma_L \cdot M_{HS20} \cdot LF_1 \cdot (1 + I)} \quad \boxed{RF_{HS20} = 0.90}$$

$$RF_{Type3} := \frac{\phi \cdot M_n - \gamma_D \cdot M_D}{\beta_L \cdot \gamma_L \cdot M_{Type3} \cdot LF_1 \cdot (1 + I)} \quad \boxed{RF_{Type3} = 1.02}$$

**One Lane Operating Rating Factors**

$$RF_{HS20} := \frac{\phi \cdot M_n - \gamma_D \cdot M_D}{\gamma_L \cdot M_{HS20} \cdot LF_1 \cdot (1 + I)} \quad \boxed{RF_{HS20} = 1.50}$$

$$RF_{Type3} := \frac{\phi \cdot M_n - \gamma_D \cdot M_D}{\gamma_L \cdot M_{Type3} \cdot LF_1 \cdot (1 + I)} \quad \boxed{RF_{Type3} = 1.71}$$

**Two Lane Inventory Rating Factors**

$$RF_{HS20} := \frac{\phi \cdot M_n - \gamma_D \cdot M_D}{\beta_L \cdot \gamma_L \cdot M_{HS20} \cdot LF_2 \cdot (1 + I)} \quad \boxed{RF_{HS20} = 0.86}$$

$$RF_{Type3} := \frac{\phi \cdot M_n - \gamma_D \cdot M_D}{\beta_L \cdot \gamma_L \cdot M_{Type3} \cdot LF_2 \cdot (1 + I)} \quad \boxed{RF_{Type3} = 0.98}$$

**Two Lane Operating Rating Factors**

$$RF_{HS20} := \frac{\phi \cdot M_n - \gamma_D \cdot M_D}{\gamma_L \cdot M_{HS20} \cdot LF_2 \cdot (1 + I)} \quad \boxed{RF_{HS20} = 1.44}$$

$$RF_{Type3} := \frac{\phi \cdot M_n - \gamma_D \cdot M_D}{\gamma_L \cdot M_{Type3} \cdot LF_2 \cdot (1 + I)} \quad \boxed{RF_{Type3} = 1.64}$$

**Revisions To Load Rating Using Test Data:****Actual Material Properties (If Known):**

$$f_c := 5000\text{psi} \quad (\text{Concrete Compression Strength})$$

$$f_y := 4000\text{psi} \quad (\text{Reinforcement Yield Strength})$$

**Section Flexural Capacity Based On Actual Material Properties:**

$$a := \frac{A_s \cdot f_y}{0.85 \cdot f_c \cdot S}$$

$$a = 1.34\text{in}$$

$$M_n := A_s \cdot f_y \cdot \left( d - \frac{a}{2} \right)$$

$$M_n = 207.2\text{ft}\cdot\text{kip}$$

**Experimental Load Fractions:**

$$LF_1 := 0.61$$

$$LF_2 := 0.63$$

**Rating Calculation Based On Actual Material Properties and Experimental Load Fractions:****One Lane Inventory Rating Factors**

$$RF_{HS20} := \frac{\phi \cdot M_n - \gamma_D \cdot M_D}{\beta_L \cdot \gamma_L \cdot M_{HS20} \cdot LF_1 \cdot (1 + I)}$$

$$RF_{HS20} = 0.87$$

$$RF_{Type3} := \frac{\phi \cdot M_n - \gamma_D \cdot M_D}{\beta_L \cdot \gamma_L \cdot M_{Type3} \cdot LF_1 \cdot (1 + I)}$$

$$RF_{Type3} = 0.98$$

**One Lane Operating Rating Factors**

$$RF_{HS20} := \frac{\phi \cdot M_n - \gamma_D \cdot M_D}{\gamma_L \cdot M_{HS20} \cdot LF_1 \cdot (1 + I)}$$

$$RF_{HS20} = 1.45$$

$$RF_{Type3} := \frac{\phi \cdot M_n - \gamma_D \cdot M_D}{\gamma_L \cdot M_{Type3} \cdot LF_1 \cdot (1 + I)}$$

$$RF_{Type3} = 1.64$$

**Two Lane Inventory Rating Factors**

$$RF_{HS20} := \frac{\phi \cdot M_n - \gamma_D \cdot M_D}{\beta_L \cdot \gamma_L \cdot M_{HS20} \cdot LF_2 \cdot (1 + I)}$$

$$RF_{HS20} = 0.84$$

$$RF_{Type3} := \frac{\phi \cdot M_n - \gamma_D \cdot M_D}{\beta_L \cdot \gamma_L \cdot M_{Type3} \cdot LF_2 \cdot (1 + I)}$$

$$RF_{Type3} = 0.95$$

**Two Lane Operating Rating Factors**

$$RF_{HS20} := \frac{\phi \cdot M_n - \gamma_D \cdot M_D}{\gamma_L \cdot M_{HS20} \cdot LF_2 \cdot (1 + I)}$$

$$RF_{HS20} = 1.40$$

$$RF_{Type3} := \frac{\phi \cdot M_n - \gamma_D \cdot M_D}{\gamma_L \cdot M_{Type3} \cdot LF_2 \cdot (1 + I)}$$

$$RF_{Type3} = 1.59$$